Development and Validation of a Novel Framework for Designing and Optimizing Passive Prosthetic Feet Using Lower Leg Trajectory

by

Kathryn M. Olesnavage

B.S., Massachusetts Institute of Technology (2012)
S.M., Massachusetts Institute of Technology (2014)

Submitted to the Department of Mechanical Engineering
in partial fulfillment of the requirements for the degree of

Doctor of Philosophy in Mechanical Engineering

at the

MASSACHUSETTS INSTITUTE OF TECHNOLOGY

February 2018

Author ..... Signature redacted ...
Department of Mechanical Engineering
September 22, 2017

Certified by ..... Signature redacted
Amos G. Winter, V
Associate Professor
Thesis Supervisor

Accepted by ..... Signature redacted
Rohan Abeyaratne
Chairman, Department Committee on Graduate Theses

Development and Validation of a Novel Framework for Designing and Optimizing Passive Prosthetic Feet Using Lower Leg Trajectory

by

Kathryn M. Olesnavage

Submitted to the Department of Mechanical Engineering
on September 22, 2017, in partial fulfillment of the
requirements for the degree of
Doctor of Philosophy in Mechanical Engineering

Abstract

This thesis presents a novel framework to optimize the design of passive prosthetic feet to best replicate physiological lower leg trajectory under typical ground reaction forces. The goal of developing this framework is ultimately to design a low cost, mass-manufacturable prosthetic foot for persons with amputations living in the developing world.

Despite a vast body of literature on prosthetic foot design, there is a dearth of knowledge regarding how the mechanical characteristics of passive prosthetic feet affect their biomechanical performance. Without understanding this relationship, the design of a prosthetic foot cannot be optimized for peak performance as measured by gait symmetry, metabolic cost of walking, or subjective feedback.

The approach to designing prosthetic feet introduced here involves predicting the lower leg trajectory for a given prosthetic foot under typical loading and comparing this modeled trajectory to target physiological gait kinematics with a novel metric called the Lower Leg Trajectory Error (LLTE). The usefulness of this design approach was demonstrated by optimizing three simple conceptual models of prosthetic feet, each with two degrees of freedom. An experimental prosthetic foot with variable ankle stiffness was built based on one of these analytical models and tested by a subject with unilateral transtibial amputation in a gait lab under five different ankle stiffness conditions. Across five prosthetic-side steps with each of the five ankle stiffness conditions, the constitutive model used in the optimization process accurately predicted the horizontal and vertical position of the knee throughout stance phase to within an average of 1.0 cm and 0.3 cm, respectively, and the orientation of the lower leg segment to within 1.5°.

After validating the theory behind this approach with the simple conceptual foot models, a method was developed to implement the same approach in optimizing the shape and size of a single-part compliant foot, resulting in a lightweight, easy to manufacture, low cost prosthetic foot. The optimal prosthetic foot design was built and

tested qualitatively on six subjects in India with unilateral transtibial amputations with promising preliminary results.

Thesis Supervisor: Amos G. Winter, V
Title: Associate Professor

Acknowledgments

I wasn't always sure that pursuing a PhD was the right decision for me, but looking back now on all of the experiences I've had and the people I've met along the way, I'm filled with immense gratitude for having had this opportunity. There are a few people in particular who were instrumental in supporting me through this dissertation:

My mom, my dad, and my brother, Jason - I never had any doubt that wherever life took me, you'd all be there for me. You've proven that quite literally by following me to Boston, England, India, Cyprus, and now Los Angeles. Thank you for instilling in me a desire to constantly strive for improvement, while also teaching me to value the important things in life.

All of the close friends I've had during my time in grad school, especially Emma Edwards, Victor Prost, Sahil Shah, Katie Taylor, Yash Narang, Will Sorensen, and Liz Adair - thank you all for accompanying me on afteroon Verde's runs, grabbing drinks with me at the Muddy, and letting me drag you on bike adventures. Most importantly, thank you for keeping me laughing even when things were tough.

The MIT Cycling team - you guys have taught me what it means to always put the team before yourself. Anytime I think about grad school, my experiences with the cycling team will be central to this time in my life.

My committee members, Caroline Hargrove, Hugh Herr, and Sangbae Kim - your insight and support pushed my research to a higher caliber. I've enjoyed working with each of you the past several years. A special thanks to Caroline and everyone at McLaren Applied Technologies for allowing me to spend a few months learning from their expertise.

Matty Major, Rebecca Stine, and everyone at Northwestern University Prosthetics-Orthotics Center - this work would not have made it nearly as far without your knowledge of the clinical side of prosthetics. Thank you for collaborating with us!

Rob Stoner, Chintan Vaishnav, and the MIT Tata Center for Technology and Design - without you, none of this would have been possible. Thank you for your support!

Mr. Mehta, Dr. Mathur, Dr. Pooja, and the entire BMVSS organization - thank you for inspiring this work and for helping me make the most of every trip to India.

A very special thanks to Paul, my driver/ tour guide/ translator on nearly every trip to Jaipur - nothing has made me feel more at home in India than you and your family taking me in and cooking me dinner on four consecutive birthdays. I look forward to maintaining our friendship for years to come!

And finally, my advisor, Amos - I can't possibly capture the past five years of experiences in a few short sentences. Listening to Freeze Frame in research meetings, taking red bull-fueled road trips across the UK, pushing each other to always order dessert (no matter how full we may think we are) - the memories go on and on. I can't imagine having done a PhD under anyone else's guidance. Thank you for being a role model for me as an engineer, a leader, and a person.

Contents

1 Introduction **17**

1.1 Mechanical Design of Prosthetic Feet Described in Literature 18

1.2 Outline of Thesis 19

2 A Novel Framework for Quantitatively Connecting the Mechanical Design of Passive Prosthetic Feet to Lower Leg Trajectory **23**

2.1 Introduction 23

2.2 Roll-Over Geometry and Leg Orientation 25

2.3 Framework for Replicating Lower Leg Trajectory Under Input Loads 28

2.4 Design Optimization 32

2.4.1 Model Foot Architecture 32

2.4.2 Lower Leg Trajectory Error Calculation and Optimization . . 33

2.4.3 Roll-Over Geometry Calculation and Optimization 40

2.4.4 LLTE Optimization Results 40

2.5 Discussion 44

2.6 Conclusions 47

3 Clinical Validation of Predicting Lower Leg Trajectory for Passive Prosthetic Feet Using Physiological Data as Inputs **51**

3.1 Introduction 51

3.1.1 Lower Leg Trajectory Error 52

3.2 Methods 53

3.2.1 Experimental Prosthetic Foot Design 53

3.2.2 Data Collection 56
3.2.3 Data Analysis 58
3.3 Results 62
3.4 Discussion 65
3.4.1 Accuracy of Constitutive Model 65
3.4.2 Physiological Data as Model Inputs and Target Outputs . . . 68
3.4.3 Effect of LLTE values on gait symmetry 72
3.5 Conclusions 73

4 Passive Single-Part Prosthetic Foot Shape and Size Optimization Using Lower Leg Trajectory Error 79
4.1 Introduction 79
4.2 Method 83
4.2.1 Size and Shape Parameterization 83
4.2.2 Materials 86
4.2.3 Constraints 86
4.2.4 Evaluating LLTE 88
4.2.5 Optimization Problem Formulation 93
4.2.6 Prototype Fabrication and Finite Element Model Validation . 95
4.2.7 Preliminary Testing in India 97
4.3 Results 97
4.4 Discussion 101
4.5 Conclusions 104

5 Conclusion 111

A Considerations in Selecting Particular Variables and Normalization Factors in LLTE Definition 113

B Design and Qualitative Testing of a Prosthetic Foot with Rotational Ankle and Metatarsal Joints to Mimic Physiological Roll-Over

Shape **121**

B.1 Introduction 122

B.1.1 Biomechanical Gait Data 124

B.2 Prototype Concept and Optimization 125

B.2.1 Rotational Stiffness Optimization for Roll-Over Shape 127

B.3 Mechanical Design 132

B.4 Preliminary Testing Results and Discussion 134

B.5 Conclusion 136

C Design and Preliminary Testing of a Prototype for Evaluating Lower Leg Trajectory Error as an Optimization Metric for Prosthetic Feet 143

C.1 Introduction 144

C.2 Prototype Concept and Optimization 145

C.2.1 Calculation of LLTE† 146

C.2.2 Design Optimization 150

C.3 Mechanical Design 151

C.3.1 Spring Selection and Considerations 152

C.3.2 Cantilever Beam Forefoot Design 153

C.3.3 Preliminary Testing 154

C.4 Discussion and Conclusion 156

THIS PAGE INTENTIONALLY LEFT BLANK

List of Figures

2-1 Illustration of multiple possible orientations of the lower leg relative to the ground for a foot with known roll-over geometry 26

2-2 Free-body diagram of a foot-ankle-knee system in the saggital plane . 27

2-3 Lower leg kinematics of a physiological foot-ankle-knee system and a rigid foot shaped such that the roll-over geometry is identical to that of the physiological system 28

2-4 Three analytical prosthetic foot architectures optimized and compared using LLTE: (a) rigid model, (b) rotational ankle and metatarsal model, and (c) rotational ankle, beam forefoot model. 33

2-5 Free-body diagrams of the three architectures of feet considered . . . 36

2-6 LLTE values calculated for each conceptual model foot over the prescribed ranges of the design variables 41

2-7 Lower leg trajectories for LLTE-optimal foot designs from foot flat to late stance. 42

2-8 Individual parameters that make up the LLTE for LLTE-optimal designs 43

2-9 Roll-over geometries of the LLTE-optimal and the RO-optimal foot designs 44

3-1 The conceptual architecture of the rotational ankle, beam forefoot foot optimized for Lower Leg Trajectory Error along with the prototype designed and built based on this concept 54

3-2 LLTE values calculated for the rotational ankle, beam forefoot foot architecture while varying each design variable independently 55

3-3 Instron-measured and linear fit rotational stiffness of the experimental prosthetic ankle with each of five different sets of U-shaped flexures . 56

3-4 Graphical definition of variables used in Eqns. (3.1)-(3.3) to calculate the position of the lower leg segment under a particular set of ground reaction forces and center of pressure position. 59

3-5 Lower leg trajectory as predicted by the constitutive model compared to corresponding measured kinematic data during *in vivo* testing . . . 62

3-6 Prosthetic-side ankle moment versus ankle angle measured during *in vivo* testing for each of the five ankle conditions 63

3-7 Average kinetic and kinematic variables over stance phase measured during *in vivo* testing for each of the five ankle stiffness conditions compared to the corresponding physiological data used in initial optimization 65

3-8 Average ankle, knee, and hip angles over stance phase for each ankle stiffness condition 67

3-9 Average ankle, knee, and hip moments over stance phase for each ankle stiffness condition 68

3-10 Average ankle, knee and hip powers over stance phase for each ankle stiffness condition 69

4-1 Lower leg position for modeled prosthetic foot and target physiological gait data at one particular time interval during a step, with variables used in Eqn. (2.1) shown 81

4-2 Parameterization of the keel of the foot 85

4-3 Various possible keel designs that fall within the defined design space 86

4-4 Examples of keel shapes that fall within the bounded design space, but are not physically meaningful 87

4-5 Five data points out of 26 total that were used as representative of stance phase in the single part foot optimization 89

4-6 Free body diagrams of the ground reaction forces on the feet and the lower leg position during three of the five time intervals used in the finite element LLTE evaluation 90

4-7 Example of a deformed foot result from the FE model in the ankle-knee reference frame with the variables used in Eqn. (4.8) - (4.10) labeled . 91

4-8 Deformed foot finite element results from Fig. 4-7 rotated into the global reference frame 92

4-9 Experimental set up used to validate finite element model of foot . . 96

4-10 Optimal keel designs found through the wide Bézier curve optimization method 99

4-11 Lower leg trajectory for the optimal compliant foot compared to the target physiological lower leg trajectory for each of the five loading scenarios considered 100

4-12 Solid model of foot based on optimal design, with added heel and male pyramid adapter to attach the foot to the rest of the prosthesis . . . 100

4-13 Comparison of Instron-measured and FEA-calculated vertical displacements of the foot prototype 101

A-1 Comparison of optimization results using alternative normalization factors for cost function definition 117

B-1 Subject squatting with the Jaipur Foot 124

B-2 Conceptual architecture of the prototype with rotational ankle and metatarsal joints 126

B-3 Free body diagram of loading applied analytically to prototype corresponding to a particular instantaneous time during the step 127

B-4 Deformed shape of the foot corresponding to a particular instantaneous time during the step 128

B-5 Best fit roll-over shape for the roll-over-optimal prototype 129

B-6 Kinematic limitations of roll-over-optimal prototype 130

B-7 R-squared values comparing roll-over geometries of physiological foot to prototype feet with metatarsal stiffness 2.0 N·m/deg for a range of ankle stiffness values 131
B-8 Roll-over shape for prototype adjusted for natural metatarsal motion 132
B-9 Solid model of the foot prototype 133
B-10 Picture of the final prototype as tested 134

C-1 Conceptual prosthetic foot architecture 146
C-2 Free body diagram showing calculation of ankle moment from ground reaction forces when center of pressure acts on rigid structure 148
C-3 Free body diagram for ground reaction forces acting on compliant beam forefoot 149
C-4 LLTE† values for slice of design space for which d_{rigid} is held constant at $d_{rigid} = 0.08$ m 151
C-5 Graphical comparison of optimal foot design lower leg trajectory with physiological lower leg trajectory 152
C-6 Individual spatial coordinates of optimal foot design compared to physiological target values throughout stance phase 153
C-7 Solid model of prototype designed based on LLTE† optimization . . . 154
C-8 Linear extension spring configuration used to produce constant ankle joint rotational stiffness of $k_{ank} = 6.1$ N· m/deg 155

List of Tables

2.1 Optimal design variables and LLTE values for the LLTE-optimal designs for all three prosthetic foot architectures 41

2.2 Optimal design variables and LLTE values for the roll-over-optimal designs for all three prosthetic foot architectures 41

3.1 Number of instances each ankle stiffness condition was found to be the most and least symmetric, as calculated by the difference between the sound side and prosthetic side data values at each of 21 local maxima and minima identified in the ankle, knee, and hip joint angle, moment and power data. 66

THIS PAGE INTENTIONALLY LEFT BLANK

Chapter 1

Introduction

The goal of this thesis was to (1) develop a method to connect the mechanical design of a passive prosthetic foot to its biomechanical functionality using fundamental physics, and (2) to implement this method to design and build a low cost, mass-manufacturable foot to meet the needs of persons with lower limb amputations living in India. This work was motivated by our parter organization in Jaipur, India, Bhagwan Mahaveer Viklang Sahayata Samiti (BMVSS). BMVSS is one of the world's largest distributors of assistive devices. In 2016, they distributed over 26,000 prosthetic limbs across the developing world [2]. Since its founding in 1975, BMVSS have fitted nearly 514,000 limbs. The organization provides limbs free of charge, but continues to grow steadily funded only by donations and government subsidies.

The prosthetic foot developed by BMVSS, also the organization's most widely known product, is the Jaipur Foot. The Jaipur Foot was originally designed in response to the solid ankle, cushion heel (SACH) foot [9]. While common in developing countries due to its low cost and durability, the solid ankle of the SACH foot does not allow users to squat, an important activity for many living in India. The Jaipur Foot was developed explicitly to permit squatting. It is handmade from wood, rubber, and foam, looks like a biological foot, and is designed to be used either barefoot or with shoes. The Jaipur Foot costs approximately $5 - $10 USD, and typically lasts three to five years in the field. It is regarded as a relatively high-performing prosthetic foot, even compared to feet that are orders of magnitude more expensive. One study

found that the Jaipur Foot allowed a more natural gait than either a SACH foot or a Seattle foot [1].

However, because the Jaipur Foot is handmade, quality varies from foot to foot. Aditionally, the fabrication process is relatively slow and expensive. BMVSS has worked with industrial partners to produce injection moldable feet, but these designs lasted only one to six months in the field.

This project began as a collaboration between the Global Engineering and Research (GEAR) Lab at MIT and BMVSS to produce a prosthetic foot that meets the needs of the current Jaipur Foot users. The new foot must meet or exceed the performance of the Jaipur Foot, be mass-manufacturable, and cost no more than $10 USD to make.

1.1 Mechanical Design of Prosthetic Feet Described in Literature

In order to design a foot that performs as well as, if not better than, the Jaipur Foot, it was necessary to first understand how the mechanical design of a prosthetic foot affects its biomechanical functionality. It is well-established that the mechanical design of a prosthetic foot affects how people walk with it, but there is a gap in understanding exactly how the mechanical characteristics of a foot affect its biomechanical performance. Five different literature reviews of studies investigating the effects of different prosthetic feet on various aspects of gait all reached the same conclusion, that we have a poor understanding of the relationship between the mechanical design of a prosthetic foot and its performance [3–5, 7, 10]. In a literature review performed and published as part of the author's masters thesis [8], the types of metrics used to design and/or evaluate prosthetic feet were categorized into one of four categories: (1) purely mechanical characteristics, also referred to as Amputee Independent Prosthesis Properties [6], (2) biomechanical gait analysis, (3) metabolic cost of walking, and (4) subjective user preference [8]. An engineer designing a prosthetic foot can

only dictate the mechanical characteristics, such as the materials, shape, size, and articulation. However, from a clinical perspective, the most important aspect of a prosthetic foot is how it affects gait symmetry, metabolic cost of walking, and subjective user preference. Thus to improve on prosthetic foot mechanical design, it is critical that the connection between the mechanical characteristics of a prosthetic foot and its clinical performance, as measured through gait symmetry, metabolic cost of walking and subjective user preference, be understood.

1.2 Outline of Thesis

This work describes the development of a novel approach to connecting the mechanical design of a prosthetic foot to its biomechanical functionality by predicting the lower leg trajectory for the foot under an assumed set of ground reaction force and center of pressure data. This lower leg trajectory is then compared with a target lower leg trajectory using a root-mean-square error function which the author has called the Lower Leg Trajectory Error (LLTE). To demonstrate this approach to prosthetic foot design optimization, three analytical prosthetic foot conceptual designs, each with three degrees of freedom, were optimized (Chapter 2). To validate these theoretical results in a clinical context, an experimental prosthetic foot was designed and built based on one of these models. A subject with a unilateral transtibial amputation tested this foot with five different values of ankle rotational stiffness, one of the design variables included in the optimization, such that the conditions tested spanned a range of LLTE values. The kinematics measured during *in vivo* testing were compared to the kinematic data predicted by the constitutive model. Both the kinematic and kinetic data from *in vivo* testing were compared to the target physiological data used to optimize the foot (Chapter 3). Once the theoretical approach was validated with the simple prosthetic foot models, a framework was developed to apply the same optimization process to a single-part compliant prosthetic foot, which was made out of nylon to produce a low-cost, mass-manufacturable prosthetic foot. This foot was tested qualitatively in India at BMVSS (Chapter 4).

Appendix A discusses in detail how the particular definition of LLTE used throughout this dissertation was selected. Appendices B and C describe two additional prosthetic foot prototypes that were designed and tested before the approach of replicating lower leg trajectory was established. Both are examples of the conceptual feet optimized for LLTE in Chapter 2, but the prototype in Appendix B was optimized for roll-over geometry and then adjusted to improve kinematics, while the prototype in Appendix C was optimized for an alternative definition of Lower Leg Trajectory Error using the position of the ankle to define the lower leg trajectory rather than the position of the knee. While these prototypes are not directly necessary to understand the approach of optimizing feet for lower leg trajectory, they were instrumental in arriving at the definition of Lower Leg Trajectory Error used throughout this thesis and provide further examples of how the mechanical design of prosthetic feet can be optimized for different objectives. Qualitative testing with these feet was also useful in elucidating design requirements, such as weight, size, and features for attachment to the rest of the prosthesis, that influenced the method for producing the single part foot presented in Chapter 4.

Bibliography

[1] A. P. Arya, A. Lees, H.C. Nirula, and L. Klenerman. A biomechanical comparison of the SACH, Seattle and Jaipur feet using ground reaction forces. *Prosthetics and Orthotics International*, 19:37–45, 1995.

[2] Bhagwan Mahaveer Viklang Sahayata Samiti. Jaipurfoot.org. `http://www.jaipurfoot.org`.

[3] Brian J. Hafner. Clinical Prescription and Use of Prosthetic Foot and Ankle Mechanisms: A Review of the Literature. *Journal of Prosthetics and Orthotics*, 17(4):S5–S11, 2005.

[4] Brian J. Hafner, Joan E. Sanders, Joseph Czerniecki, and John Fergason. Energy storage and return prostheses: does patient perception correlate with biomechanical analaysis? *Clinical Biomechanics*, 17(5):325–344, 2002.

[5] Cheriel J Hofstad, Harmen van der Linde, Jacques van Limbeek, and Klaas Postema. Prescription of prosthetic ankle-foot mechanisms after lower limb amputation. *The Cochrane Library*, 2004.

[6] Matthew J Major, Martin Twiste, Laurence P J Kenney, and David Howard. Amputee Independent Prosthesis Properties — A new model for description and measurement. *Journal of Biomechanics*, 44(14):2572–2575, 2011.

[7] Matthew J Major, Martin Twiste, Laurence PJ Kenney, and David Howard. The effects of prosthetic ankle stiffness on ankle and knee kinematics, prosthetic limb loading, and net metabolic cost of trans-tibial amputee gait. *Clin. Biomech.*, 29(1):98–104, 2014.

[8] Kathryn M. Olesnavage. Design and evaluation of a cantilever beam-type prosthetic foot for indian persons with amputations. Master's thesis, Massachusetts Institute of Technology, Cambridge, 2014.

[9] P. K. Sethi, M. P. Udawat, S. C. Kasliwal, and R. Chandra. Vulcanized rubber foot for lower limb amputees. *Prosthetics and Orthotics International*, 2:125–136, 1978.

[10] Harmen van der Linde, Cheriel J Hofstad, Alexander CH Geurts, Klaas Postema, Jan HB Geertzen, Jacques van Limbeek, et al. A systematic literature review

of the effect of different prosthetic components on human functioning with a lower-limb prosthesis. *J. Rehabil. Res. Develop.*, 41(4):555–570, 2004.

Chapter 2

A Novel Framework for Quantitatively Connecting the Mechanical Design of Passive Prosthetic Feet to Lower Leg Trajectory

2.1 Introduction

As discussed in Chapter 1, there is substantial evidence to suggest that the mechanical function of passive below-knee prostheses affects walking mechanics and efficiency of users [3–5, 11, 13, 14, 16, 18, 22]. However, multiple reviews of the literature have concluded that *how* the mechanical features of a passive prosthesis affect the functionality is not fully understood [7, 11, 15, 19]. Without this knowledge, passive prosthetic feet cannot be quantitatively optimized for peak performance and desired behaviors.

The most recent of the aforementioned literature reviews categorized the mechanical characterization of prosthetic feet into two approaches: lumped parameter models and roll-over models [15]. Lumped parameter models use discrete viscoelastic proper-

ties, such as stiffness and damping coefficients, to represent the foot. These properties are measured at particular locations on the foot and under specified loading scenarios. There is no consensus on which viscoelastic properties should be measured or how many different discrete load scenarios should be considered. Typically only one or two are presented, often for a load applied to the forefoot, the heel, or both, but these are inadequate to capture the behavior of the foot across all of stance phase [15]. One study addressed this by using 66 independent, one degree-of-freedom spring and damper models to represent the full behavior of the foot, but doing so loses the simplicity that makes the lumped parameter approach desirable [20]. Because the viscoelastic properties of a biological foot/ankle complex cannot be measured in a meaningful way, there is no way to determine target values that a prosthetic foot designer can use to optimize the mechanical properties of a mechanical foot. Instead, most studies measure these properties of existing commercially available feet, and either replicate and vary those properties with experimental prototypes for clinical testing, or simply test a variety of commercially available feet after having measured these properties, and empirically draw conclusions about the affect of the lumped parameter values on the biomechanical performance. However, these results cannot be assumed to be generally applicable until it is shown that the lumped parameters used are sufficient to fully capture the behavior of any prosthetic foot.

Roll-over geometry models are more comprehensive, as they incorporate the behavior of the foot throughout all of stance phase rather than at a few discrete instants. The roll-over geometry of a foot is defined as the path of the center of pressure along the foot in the ankle-knee reference frame during the single-limb stance phase [9]. Studies have suggested that prosthetic feet that replicate roll-over geometry result in increased metabolic efficiency, more symmetric gait, and higher subjective preference [1, 2, 9, 13, 14]. However, as will be discussed in the following section, roll-over geometry has limitations that make it insufficient as a design objective in optimizing the mechanical properties of prosthetic feet.

This work proposes a novel framework that connects the mechanical design of a prosthetic foot to its biomechanical functionality by applying an assumed set of

loads on an analytical model of a prosthetic foot and calculating the deformation under those loads. Then the deformed shape of the foot at each time interval during stance is used to obtain the trajectory of the lower leg segment under those assumed loads. A cost function, which we have called the Lower Leg Trajectory Error (LLTE), quantifies how far this calculated lower leg trajectory is from a target trajectory. The cost function can be used to optimize the mechanical design of a prosthetic foot to best replicate the target lower leg trajectory under the applied loads. This framework provides an advantage over lumped parameter models by incorporating all of stance phase, and by directly connecting the mechanical properties of a prosthetic foot to its biomechanical performance using fundamental physics. This approach to prosthetic foot design also provides advantages over roll-over geometry by accounting for the deformation within the foot at each time interval during stance and the foot's kinematic constraints with the ground, which are necessary factors to determine the relative orientation between the lab reference frame and the ankle-knee reference frame.

2.2 Roll-Over Geometry and Leg Orientation

The goal of a passive prosthesis is to replicate biological limb functionality with a relatively simple mechanical structure. For a passive mechanical prosthesis, a given loading scenario will produce a specific deformed shape. The relationship between the loading and the deformation, or the stiffness, can be non-linear and/or vary in different parts of the structure, but even in these complex situations, the deformation resulting from a specific load can always be calculated.

Similar to stiffness, the roll-over geometry of a prosthetic foot is a measure of the shape of the foot in response to loading. When the center of pressure is at a certain position along the foot, the roll-over geometry shows the vertical deflection of that point in response to the corresponding ground reaction forces. The roll-over geometry also serves to simplify the many variables that can be measured during a biological step into a single curve that can be used as a design objective.

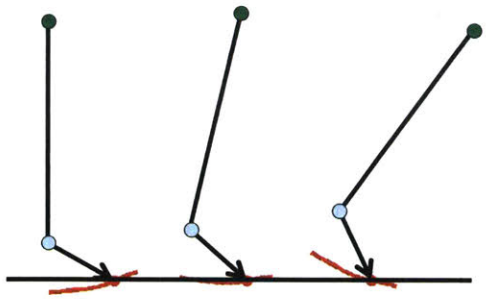

Figure 2-1: For a below-knee prosthesis (shown here with the green dot representing the user's knee, blue dot representing the ankle) for which all that is known is the roll-over geometry (red curve), when the center of pressure is at a particular location (red dot), the orientation of the lower leg segment is indeterminable.

While the roll-over geometry compiles a lot of information into a single curve, it does not provide any information regarding the orientation of the lower leg segment in the laboratory reference frame (Fig. 2-1). When the center of pressure is located at a particular point along the roll-over geometry, that single point does not constrain the angular orientation of the foot-ankle-knee complex. More information is needed about the physical construction of the foot and how it interacts with the ground to fully define the orientation of the system.

A person with a transtibial amputation interfaces with the prosthesis through the socket. Throughout this work, it is assumed that there is no relative motion between the user and the socket, and that the socket and pylon are perfectly rigid. Under these assumptions, the position and orientation of the socket dictates the position and orientation of the user's residual limb. Both the socket and the residual limb make up the lower leg. In reality, there will be some motion between the residual limb and the socket primarily along the direction of the ankle-knee axis, but this motion is negligible relative to the motion of the lower leg as a whole during stance phase. The socket also transmits forces and moments to the user (Fig. 2-2). The orientation of the socket defines the moment arm from the ground reaction forces to the user's residual limb and knee. Therefore any variation in the orientation of the lower leg affects both the gait kinematics and the loading at the user's knee.

The physical geometry of a prosthetic foot introduces additional constraints. Typically, the foot and ground must be in contact at the instantaneous center of pressure,

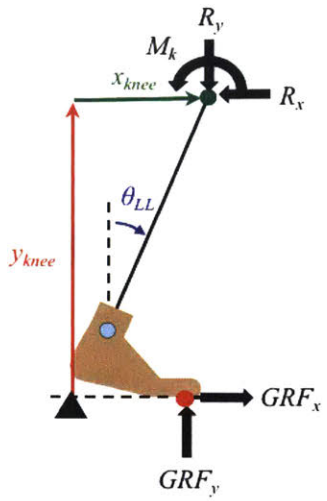

Figure 2-2: Free-body diagram of a foot-ankle-knee system in the saggital plane. The system is acted on by the ground reaction forces (GRF_x and GRF_y) and the reaction loads (R_x and R_y) and moment (M_k) at the knee. The position and orientation of the lower leg segment is fully defined by three variables: the horizontal and vertical position of the knee (x_{knee} and y_{knee}, respectively) and the angle of the lower leg with respect to vertical (θ_{LL}). The orientation of the lower limb affects not only the gait kinematics of the user, but also the reaction loading on his or her residual limb and at the knee.

and no part of the foot can ever intersect the ground. For a particular foot geometry with known mechanical behavior, these constraints fully define the orientation of the lower limb. For example, consider a rigid foot, such as cut from a block of wood, shaped so that it exactly replicates the roll-over geometry of a physiological foot-ankle complex as obtained from published gait data [21]. Because no deformation occurs within the foot, the shape of the bottom of the foot determines the roll-over geometry, which makes rigid feet a useful tool to investigate different roll-over geometries [1, 2]. During stance phase, the ground must be tangent to the foot at the instantaneous center of pressure. Any other orientation would result in the foot intersecting the ground. If the center of pressure progresses forward along the ground at the same rate as in the physiological step, and if no slipping occurs between the foot and the ground, the trajectory of the foot-ankle-knee system can be found from simple geometry and compared to physiological lower leg kinematics (Fig. 2-3). Even though the feet in Fig. 2-3 have identical roll-over geometries, the resulting lower leg

(a) (b)

Figure 2-3: Lower leg kinematics of (a) a physiological foot-ankle-knee system [21], and (b) a rigid foot shaped such that the roll-over geometry is identical to that of the physiological system. While the roll-over geometries match exactly, the orientations of the roll-over geometries with respect to the ground do not, resulting in different kinematics.

kinematics differ due to the articulation inherent to the physiological foot as opposed to the rigid foot. The roll-over geometries match exactly, but the orientations of the roll-over geometries differ, resulting in different kinematics.

The additional constraints imposed by the physical embodiment of a prosthetic foot can be included in modeling to optimize the design of a given foot not only for roll-over geometry, but also for the orientation of the roll-over geometry in the laboratory reference frame, and thus the trajectory of the lower leg.

2.3 Framework for Replicating Lower Leg Trajectory Under Input Loads

The framework presented here consists of predicting the lower leg trajectory for a model prosthetic foot under an input set of loading data, then comparing that trajectory to a target set of lower leg trajectory data. By defining a cost function that quantifies the net difference between the model and target trajectories, the Lower Leg Trajectory Error, this approach can be used to optimize the mechanical design of a prosthetic foot to best replicate the target lower leg trajectory under the input set of loads. This concept can be described by thinking of a below-knee prosthesis as a black box attached to the user's residual limb. If this black box moves through space

in such a way as to position the user's knee and lower leg correctly, it will enable natural gait kinematics for the lower leg segment, which in turn allows all body segments proximal to the lower leg to also follow natural trajectories. In reality, a passive prosthesis is a compliant structure. Given the loads on a particular structure, the resulting deformed shape of that structure can be calculated analytically for simple structures, or with finite element analysis for more complex structures. The author proposes that a goal of passive prosthetic foot design should be to create a structure that, when acted upon by typical loads as measured during gait analysis, deforms in such a way as to replicate target kinematics. The LLTE provides a measurement of how well a particular prosthesis accomplishes this goal. The idealized black box that produces exactly the target kinematics under the input loading would have an LLTE $= 0$. A passive prosthesis will never be able to exactly reproduce physiological lower leg trajectory because it cannot output more energy than it stores (as a physiological ankle does); but using physiological kinematics as a target and optimizing for minimal LLTE may produce a foot design that comes closest.

To calculate the lower leg trajectory for a particular prosthetic foot model, an input set of kinetic data, that is, ground reaction forces and center of pressure progression along the ground, is required, as well as a set of target kinematic data to which the simulated kinematic results can be compared. Throughout this work, a set of published gait data for a single step from an able-bodied subject provides both the input kinetic data and the target output kinematic data [21].

In using able-bodied gait data for the target kinematics as is done in this work, it is implicitly assumed that symmetric gait and physiological ground reaction forces are optimal. Some recent work suggests that symmetric gait kinematics may not be metabolically optimal for persons with unilateral transtibial amputations [8]. According to these studies, the objective of prosthetic foot design should not be to reproduce symmetric, able-bodied gait kinematics if the clinical goal is to minimize the metabolic cost of walking. However, there are both social and biomechanical reasons to target symmetric gait. From a social standpoint, gait asymmetries may draw unwanted attention to the fact that someone uses a prosthesis. From the author's

experience working with Bhagwan Mahaveer Viklang Sahayata Samiti (BMVSS) of Jaipur, India, the largest distributor of prosthetic limbs in the world, amputees in poor countries want to appear as able-bodied as possible to avoid stigmas against disability. Many of BMVSS's patients with above-knee amputations choose to use a heavy cosmesis over their endoskeletal pylon to better hide their prosthesis, despite the fact that the added mass decreases the metabolic efficiency of walking. Another argument for targeting symmetric gait kinematics and ground loading is to minimize the risk of injuries related to long-term prosthesis use [6]. To the author's knowledge, no studies advocating for targeting asymmetric gait have investigated these long-term consequences.

To define the position of the lower leg in the saggital plane for a kinematic simulation of a given prosthesis model, three variables, x_{knee}^{model}, y_{knee}^{model}, and θ_{LL}^{model}, are needed (Fig. 2-2). These can then be compared to target kinematic values taken from published physiological gait data, x_{knee}^{phys}, y_{knee}^{phys}, and θ_{LL}^{phys}. Because the lower leg moves throughout a step, each of these variables are functions of time. The cost function, or Lower Leg Trajectory Error (LLTE), is defined as a root-mean-square error between the predicted lower leg trajectory for a modeled prosthetic foot and the target lower leg trajectory data, where each component is normalized by the mean value of that component in the physiological data set. That is,

$$LLTE \equiv \left[\frac{1}{N}\sum_{n=1}^{N}\left\{\left(\frac{x_{knee,n}^{model}-x_{knee,n}^{phys}}{\bar{x}_{knee}^{phys}}\right)^2+\left(\frac{y_{knee,n}^{model}-y_{knee,n}^{phys}}{\bar{y}_{knee}^{phys}}\right)^2+\left(\frac{\theta_{LL,n}^{model}-\theta_{LL,n}^{phys}}{\bar{\theta}_{LL}^{phys}}\right)^2\right\}\right]^{\frac{1}{2}}, \tag{2.1}$$

where the subscript n refers to the n^{th} time interval and N is the total number of time intervals considered. The variables $\bar{x}_{knee}^{phys}$, $\bar{y}_{knee}^{phys}$, and $\bar{\theta}_{LL}^{phys}$ are the average values of each of the physiological parameters over the portion of the step included in the optimization and serve to normalize the error in each parameter. Smaller LLTE values signify a better fit with the able-bodied ankle-knee trajectory; a model that

fit the data exactly would result in an LLTE value of zero. A detailed explanation of the rationale for this particular cost function definition is provided in Appendix A. However, the emphasis of this work is the framework to connect the mechanical design of a prosthetic foot to its biomechanical performance and a means of optimizing feet to replicate a target lower leg trajectory under given loads, rather than on the definition of the cost function or the resulting specific optimal designs presented herein.

It is important to note that a compliant structure, such as a prosthetic foot, defines a relationship between loads and motion. Within the framework presented here, forces are used as inputs to calcuate the output motion. Similarly, the physiological motion could be used as inputs to calculate the output loading. Even though the loading on the foot is assumed and the motion calculated, this framework produces a prosthetic foot that comes as close as possible to enabling the user to replicate both physiological loading and motion, within the limitations of a specific foot's mechanical design (such as degrees of freedom, joint stiffness, etc.). The assumed loading, which is necessary to calculate the LLTE value for the foot, does not mean that a person with a transtibial amputation is expected to exert this exact loading on any foot he or she uses. In fact, this will almost certainly not be the case. But it can be said that if, under physiological loading, a prosthetic foot deforms such that the lower leg follows a trajectory far from physiological (i.e. the foot has a high LLTE value), then the only way the user will be able to walk with typical kinematics while using that foot would be to diverge from physiological loading. With that same foot, the user could only walk with physiological loading if the lower leg kinematics diverged from physiological. In reality, it is expected that the user would compensate using such a foot with changes in both loading and kinematics. Optimizing a foot for minimal LLTE value is intended to find the foot that is the least disruptive to what the rest of the user's body was designed to do during walking, in terms of both loading and motion.

2.4 Design Optimization

2.4.1 Model Foot Architecture

To demonstrate the usefulness of the LLTE as a design objective, three different conceptual foot models were optimized for lower leg trajectory. The first model was a rigid foot with a circular arc forming the bottom (Fig. 2-4a), as used in Adamczyk's roll-over geometry studies [1,2]. The design variables that could be varied to minimize the LLTE were the radius of the circular arc, R, and the horizontal position of the center of the circle, x_c. The vertical position of the center of the circle was determined by the length of the prosthesis from floor to knee when the lower leg segment is vertical.

The second model had rotational joints at the ankle and metatarsal, which replicated the articulated joints of biological feet (Fig. 2-4b). The design variables were the rotational stiffnesses of the ankle and metatarsal joints, k_{ank} and k_{met}, respectively. The links connecting these joints were modeled as perfectly rigid. The geometry of the foot, defined by the height of the center of rotation of the ankle joint, h, and the horizontal distance from the ankle to the metatarsal joint, d_{met}, was based on physiological data and held constant throughout the optimization [21].

The third model consisted of a rotational joint at the ankle, but rather than a rotational metatarsal joint, it had a cantilever beam forefoot (Fig. 2-4c). For this model, the design variables were the ankle stiffness, k_{ank}, and the forefoot beam bending stiffness, EI. The beam bending stiffness is the product of the elastic modulus of the beam material, E, and the second area moment of inertia of the beam cross-section, I. By considering the product as a whole rather than the components individually, the mechanical behavior of the beam can be optimized without constraining the design to any particular material. As with the jointed ankle and metatarsal model, the geometry of the foot, that is, the height of the ankle joint, h, and the horizontal length of the rigid structure from the ankle joint, d_{rigid}, was based on the location of the ankle and metatarsal joints in the physiological data and was held fixed throughout the optimization.

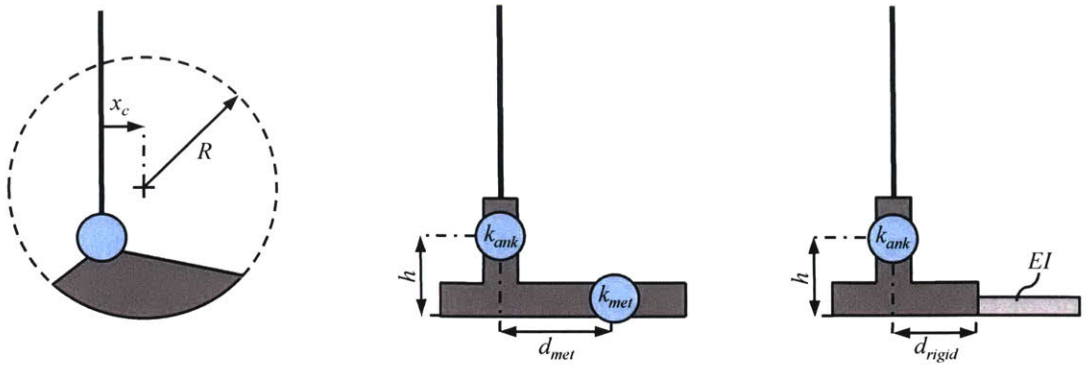

(a) (b) (c)

Figure 2-4: Three analytical prosthetic foot architectures optimized and compared using LLTE: (a) rigid model, (b) rotational ankle and metatarsal model, and (c) rotational ankle, beam forefoot model.

2.4.2 Lower Leg Trajectory Error Calculation and Optimization

To find the predicted lower leg trajectory for each foot architecture, the horizontal and vertical components of the ground reaction forces and the position of the center of pressure along the ground were used as inputs. The published gait data from which these inputs were obtained for this study were collected during a single step for a subject of body mass 56.7 kg [21]. Consequently, all results are specific to these particular data, but the method could similarly be applied to normative data. Because the purpose of this exercise is to demonstrate the usefulness of the LLTE in evaluating and comparing prosthetic foot models rather than to actually design a prosthetic foot, this does not affect the merit of the work. Using the published ground reaction forces and position of center of pressure as inputs, the resulting deformed shape of the foot-ankle complex and subsequent lower leg trajectory was calculated for each foot model for the portion of stance starting when the orientation of the lower leg segment relative to vertical in the physiological data set, θ_{LL}^{phys}, becomes greater than zero, and ending when the metatarsal joint marker in the published data set lifts off the ground at the end of stance. Before and after these times, the two articulated foot models are in point contact with the ground either at the very end of the heel or the toe, and can rotate about these contact points. As such, the position of the lower

leg segment at these points cannot be calculated from the ground reaction force and center of pressure data without making additional assumptions. The position of the lower leg segment could be calculated for the rigid circular foot during early stance, when $\theta_{LL}^{phys} < 0$, but for the sake of comparison with the other two models, this was not included here. The following subsections describe the calculation of the deformed shape of the foot-ankle complex and lower leg trajectory for each foot model.

Rigid Foot

By definition, the shape of the rigid foot does not change under any applied load. Thus the only input required to calculate the lower leg trajectory for the rigid foot is the location of the center of pressure along the ground throughout the step. If no slipping occurs between the foot and the ground, then the progression of the center of pressure along the ground, $x_{cp,g}$, must be equal to the progression of the center of pressure along the bottom arc of the foot (Fig. 2-5a). The orientation of the lower leg, θ_{LL}, was calculated for each time interval during the step as

$$\theta_{LL} = \frac{x_{cp,g} - x_c}{R}. \tag{2.2}$$

The corresponding position of the instantaneous center of pressure on the foot in the ankle-knee reference frame with the origin at the intersection of the ankle-knee axis and the ground when $\theta_{LL} = 0$ is defined as $(x_{cp,f}, y_{cp,f})$, where

$$x_{cp,f} = x_c + R \sin \theta_{LL} \tag{2.3}$$

and

$$y_{cp,f} = R(1 - \cos \theta_{LL}). \tag{2.4}$$

In the actual orientation, the instantaneous center of pressure on the ground and on the foot must coincide. Further, the ground must be tangent to the foot at this instantaneous center of pressure (Fig. 2-5b). The x_{knee} and y_{knee} position of the knee

in the laboratory reference frame was determined for each time interval by calculating θ_{LL} from Eq. (2.2), rotating the foot-ankle-knee system by θ_{LL} by multiplying the array of coordinate points of the model in the ankle-knee reference frame by the rotation matrix, then translating the rotated system such that the instantaneous center of pressure on the foot was coincident with the instantaneous center of pressure on the ground. Once the lower leg position and orientation coordinates were found for each time interval from midstance to toe off, the LLTE value was calculated using Eq. (2.1) for the particular selection of design variables, x_c and R. This was repeated for a range of design variable values to find the set with the lowest LLTE value. The range of values for each design variable was selected by sampling the feasible design space, that is, $R > 0$ and $-R \leq x_c \leq R$, at a course resolution, then reducing the range and increasing the resolution in the vicinity of the design variable values yielding the mimimum LLTE value. The resulting ranges of design variable values sampled at high resolution were -0.07 m $\leq x_c \leq$ 0.08 m and 0.1 m $\leq R \leq$ 0.9 m.

Rotational Ankle and Metatarsal Foot

The geometry of this foot was selected to approximately match the locations of the joint center of rotations of the subject of Winter's gait data, with $h = 8\,\text{cm}$ and $d_{met} = 10.5\,\text{cm}$ (Fig. 2-4b) [21].

A free body diagram for a particular instant during a step is depicted in Fig. 2-5c. It can be shown geometrically that

$$\theta_{LL} = \theta_{ank} + \theta_{met}, \tag{2.5}$$

where θ_{LL} is the angle of the lower leg segment as previously defined and θ_{ank} and θ_{met} are the angles of the ankle and metatarsal joints, respectively. For constant rotational joint stiffnesses k_{ank} and k_{met}, the joint angles are given by

$$\theta_{ank} = \frac{M_{ank}}{k_{ank}} \tag{2.6}$$

and

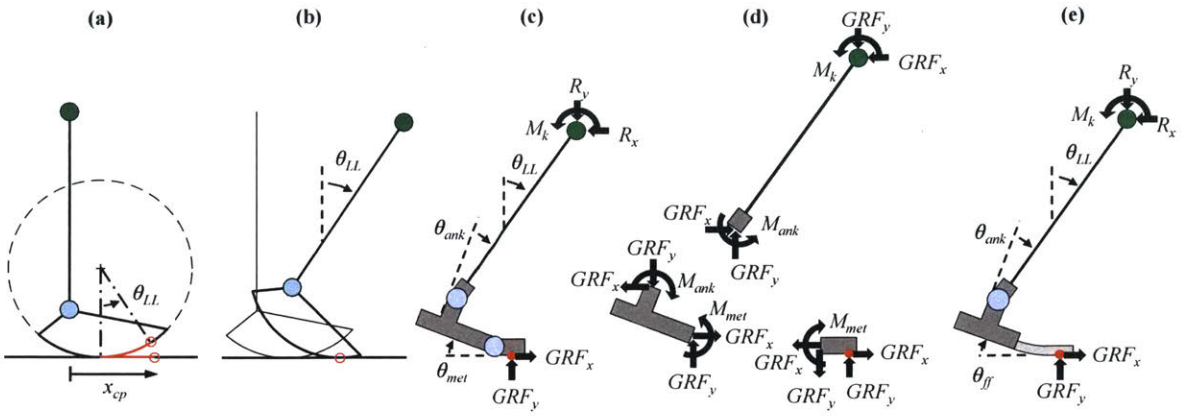

Figure 2-5: Free-body diagrams of the foot models considered. (a) For the rigid foot, under a no-slip assumption the distance progressed by the center of pressure along the ground and along the bottom of the foot, shown here in red, must be equal. The instantaneous position of the center of pressure, x_{cp}, was obtained from published gait data and used as an input to calculate the lower leg trajectory [21]. (b) The orientation of the lower leg was calculated by rotating the foot-ankle-knee model by θ_{LL}, then translating the rotated model such that the location of the center of pressure on the foot and on the ground were coincident. (c) Free body diagram of the rotational ankle and metatarsal foot's knee-ankle-foot system at a particular instant during stance. (d) Free body diagrams showing reaction loads and moments at the metatarsal and ankle joints when the center of pressure is distal to the metatarsal joint. Under the quasistatic assumption, the joint moments and angles can be calculated from the ground reaction forces and position of the center of pressure for a given set of joint stiffnesses. (e) Free body diagram of the knee-ankle-foot system for the rotational ankle, beam forefoot model at a particular instant during stance.

$$\theta_{met} = \frac{M_{met}}{k_{met}}, \tag{2.7}$$

where M_{ank} and M_{met} are the moments at each of the joints produced by the ground reaction forces.

Assuming quasistatic loading and neglecting the mass of the prosthesis, equilibrium equations were used to find the joint moments as functions of the ground reaction forces and foot geometry. When the center of pressure is proximal to the metatarsal joint, the moments are

$$M_{met} = 0\,\mathrm{N}\cdot\mathrm{m} \tag{2.8}$$

and

$$M_{ank} = GRF_y \cdot x_{cp} + GRF_x \cdot h. \tag{2.9}$$

When the center of pressure is distal to the metatarsal (Fig. 2-5d), these equations become

$$M_{met} = GRF_y \cdot \left(x_{cp} - d_{met}\right) \tag{2.10}$$

and

$$\begin{aligned} M_{ank} = M_{met} &+ GRF_y \cdot \left(d_{met}\cos\theta_{met} - h\sin\theta_{met}\right) \\ &+ GRF_x \cdot \left(d_{met}\sin\theta_{met} + h\cos\theta_{met}\right). \end{aligned} \tag{2.11}$$

Using equations (2.5) through (2.11) and the inputs from typical walking as previously described, the angle of the lower leg segment was calculated for a particular set of joint stiffness values to obtain θ_{LL} for each time interval. The position of the knee at each time, given by x_{knee} and y_{knee}, was found geometrically from the deformed shape of the prosthesis and the instantaneous location of the center of pressure in the global reference frame, and by assuming no slipping occured between the bottom of the foot and the ground.

For each set of joint stiffnesses, k_{ank} and k_{met}, from a range of feasible values, $x_{knee,n}$, $y_{knee,n}$ and $\theta_{LL,n}$ were found using the above equations and then used to calculate the LLTE value. This was repeated for each set of joint stiffnesses in the range 2.0 N·m/deg $\leq k_{ank} \leq$12.0 N·m/deg and 1.2 N·m/deg $\leq k_{met} \leq$12.0 N·m/deg to find optimal stiffness values to minimize the LLTE. As was done for the rigid foot, the ranges of values were selected to encompass the set of feasible design variable values with the minimum LLTE, where feasible values in this case were $k_{ank} > 0$ and $k_{met} > 0$.

Rotational Ankle, Beam Forefoot Foot

As with the rotational ankle and metatarsal foot, the geometry of the rotational ankle, beam forefoot foot was selected to replicate the articulation of the physiological foot-ankle complex, with $h = 8\,\text{cm}$ and $d_{rigid} = 9.3\,\text{cm}$ [21]. The rigid structure length, d_{rigid}, was chosen such that during late stance, the effective rotational joint of the pseudo-rigid-body model of the cantilever beam forefoot would be approximately at the center of rotation of the metatarsal joint for the physiological data. The pseudo-rigid-body model approximates a cantilever beam with a vertical end load as a rigid link and a rotational joint with stiffness related to the beam bending stiffness [12].

A free body diagram for the rotational ankle, beam forefoot model is shown in Fig. 2-5e. When the instantaneous center of pressure is in the rigid portion of the foot ($x_{cp} < d_{rigid}$), the model behaves exactly as the rotational ankle and metatarsal model. The moment about the ankle, M_{ank}, and the orientation of the lower leg, θ_{LL}, can therefore be calculated with Eqs. (2.6) and (2.9).

When the ground reaction forces act on the cantilever beam, the analysis is more complex. The inputs used throughout this study are the horizontal and vertical ground reaction forces in the lab reference frame. In calculating the deformed shape of the cantilever beam forefoot, it is necessary to know the relative orientation between the ground and the beam (θ_{ff} in Fig. 2-5e), so that the ground reaction forces can be decomposed into loads acting transverse and axial to the beam. However, θ_{ff} cannot be found without knowing the transverse load on the beam. Thus the deformed shape of the beam was computed iteratively. Initially, it was assumed that $\theta_{ff} = 0$, so that the transverse load on the beam, F_{trans}, was equal to the vertical ground reaction force in the lab frame,

$$F_{trans} = GRF_y. \tag{2.12}$$

The resulting angle of the deformed beam at the point of action of the load was found with

$$\theta_{ff} = \tan^{-1}\left(\frac{F_{trans}(x_{cp} - d_{rigid})^2}{2EI}\right). \tag{2.13}$$

The transverse load on the beam was then calculated with the new θ_{ff},

$$F_{trans} = GRF_y \cdot \cos\theta_{ff} - GRF_x \cdot \sin\theta_{ff}. \tag{2.14}$$

The new F_{trans} was then used with Eq. (2.13) to obtain a new θ_{ff}, and so on until the difference between subsequent values of θ_{ff} was less than 0.5 degrees.

Once the orientation of the forefoot with respect to the ground, θ_{ff}, was obtained for the deformed foot, the moment about the ankle was calculated as

$$\begin{aligned} M_{ank} = GRF_y \cdot &\Big(x_{cp}\cos\theta_{ff} - (h-\delta)\sin\theta_{ff}\Big) \\ &+ GRF_x \cdot \Big(x_{cp}\sin\theta_{ff} + (h-\delta)\cos\theta_{ff}\Big), \end{aligned} \tag{2.15}$$

where δ is the transverse deflection of the beam at the point of application of the force, that is,

$$\delta = \frac{F_{trans}x_{cp}^3}{3EI}. \tag{2.16}$$

The angle at the ankle joint, θ_{ank}, was then found using Eq. (2.6). Similar to Eq. (2.5) for the rotational ankle and metatarsal foot, the orientation of the lower leg segment was given by

$$\theta_{LL} = \theta_{ank} + \theta_{ff}. \tag{2.17}$$

The x- and y-coordinates of the knee were found using the deformed geometry of the prosthesis model and by applying the no slip assumption between the floor and the foot. For each ankle and beam bending stiffness, x_{knee}, y_{knee}, and θ_{LL} were calculated for all times from foot flat to late stance. The LLTE value for that particular set of

design variables was then calculated using Eq. (2.1). This was repeated for each combination of design variable values in the range 3.0 N·m/deg $\leq$ k_{ank} $\leq$ 8.0 N·m/deg and 1.0 N·m^2 $\leq$ EI $\leq$ 20.0 N·m^2. These ranges were selected following the same method described for the preceding foot architectures.

2.4.3 Roll-Over Geometry Calculation and Optimization

The roll-over geometries for each foot architecture were calculated using a similar analysis as described in the previous sections. The deformed shape of each foot was found just as for the LLTE calculation, but rather than using this to obtain the position and orientation of the lower leg, it was used to find the position of the center of pressure on the deformed foot in the ankle-knee reference frame, which provided a single point on the roll-over curve for that foot. Repeating this for all times from foot flat to late stance gave the roll-over geometry for that portion of stance. The least squares error between the resulting roll-over geometry and the target roll-over geometry from the physiological data was then calculated. Each of the foot architectures was optimized to minimize this error by again grid sampling over the range of feasible design variable values.

2.4.4 LLTE Optimization Results

The Lower Leg Trajectory Errors for each of the model foot architectures over the range of design variables considered are shown in Fig. 2-6. The optimal designs are those with the lowest LLTE values. For the rigid foot model, the optimal design had a radius of 0.32 m and horizontal position of the center of the circle of 0.02 m, with an LLTE value of 0.292. For the rotational ankle and metatarsal foot, the optimal design had ankle stiffness of 4.4 N·m/deg and metatarsal stiffness of 4.8 N·m/deg, with LLTE value 0.229. For the rotational ankle, beam forefoot foot, the optimal design had ankle stiffness of 3.7 N·m/deg and beam bending stiffness of 16.0 N·m^2, with an LLTE value of 0.222. These LLTE values indicate that the optimal designs for both articulated feet offer a 30% improvement in how well the simulated lower leg

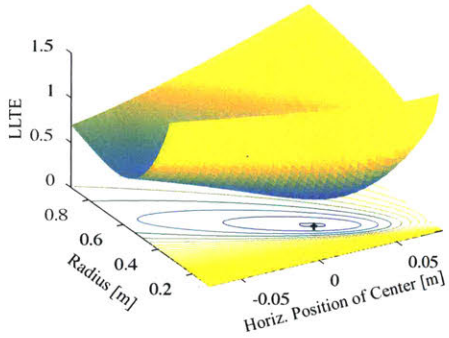

(a) Rigid Foot

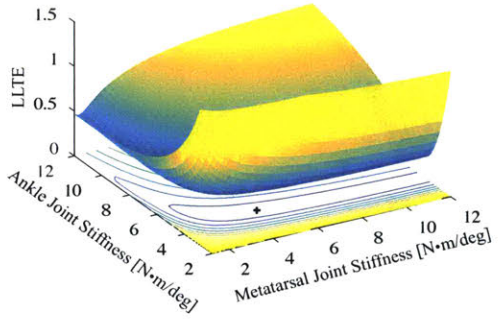

(b) Rotational Ankle and Metatarsal Foot

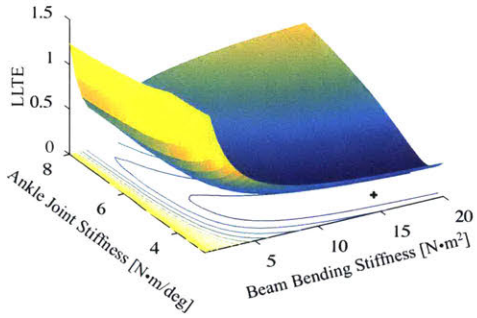

(c) Rotational Ankle, Beam Forefoot Foot

Figure 2-6: LLTE values calculated for each conceptual model foot over the prescribed ranges of the design variables: (a) rigid foot, (b) rotational ankle and metatarsal foot, and (c) rotational ankle, beam forefoot foot. The optimal designs are those which produce the minimum LLTE, indicated here by the cross.

Conceptual Model	Design Variables		LLTE
Rigid Foot	$R^* = 0.32$ m	$x_c^* = 0.02$ m	0.292
Rotational Ankle and Metatarsal Foot	$k_{ank}^* = 4.4$ N·m/deg	$k_{mct}^* = 4.8$ N·m/deg	0.229
Rotational Ankle, Beam Forefoot	$k_{ank}^* = 3.7$ N·m/deg	$EI^* = 16.0$ N·m^2	0.222

Table 2.1: Optimal design variables and LLTE values for the LLTE-optimal designs for all three prosthetic foot architectures

Conceptual Model	Design Variables		LLTE
Rigid Foot	$R^* = 0.37$ m	$x_c^* = 0.00$ m	0.334
Rotational Ankle and Metatarsal Foot	$k_{ank}^* = 7.0$ N·m/deg	$k_{mct}^* \to \infty$	0.808
Rotational Ankle, Beam Forefoot	$k_{ank}^* = 6.3$ N·m/deg	$EI^* = 25.0$ N·m^2	0.692

Table 2.2: Optimal design variables and LLTE values for the roll-over-optimal designs for all three prosthetic foot architectures

kinematics fit the target physiological data over the optimal rigid foot.

To further understand the LLTE value for each of these conceptual architectures,

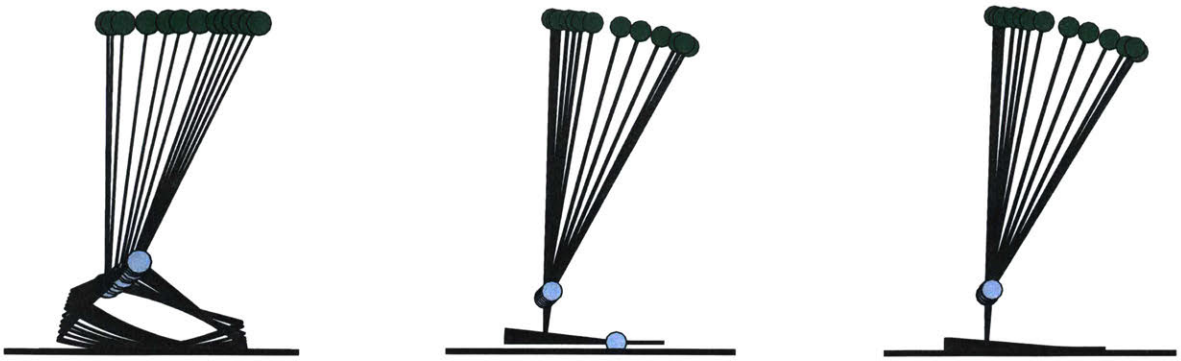

(a) Rigid Model

(b) Rotational Ankle and Metatarsal Model

(c) Rotational Ankle, Beam Forefoot Model

Figure 2-7: Lower leg trajectories for LLTE-optimal foot designs from foot flat to late stance.

the resulting lower leg trajectories are shown both by depicting the knee-ankle-foot system at equally spaced time intervals during stance phase (Fig. 2-7), and by examining each of the three spatial coordinates (x_{knee}, y_{knee}, and θ_{LL}) relative to physiological data (Fig. 2-8).

These results show that while the rigid foot allows the y-coordinate of the knee to replicate the physiological trajectory very closely, the x-coordinate and the orientation of the lower leg differ from the desired physiological trajectory. Consequently, the overall LLTE value is higher than for the other two foot architectures. The lower leg trajectories for both the rotational ankle and metatarsal foot and for the rotational ankle, beam forefoot foot are very similar due to similarities in the articulation of the feet. Consequently, the LLTE values of the optimal designs for each foot are also very close.

Tables 2.1 and 2.2 summarize the LLTE- and roll-over-optimal designs and their LLTE values. The LLTE values for the roll-over-optimal rigid foot, rotational ankle and metatarsal foot, and rotational ankle, beam forefoot foot were 0.334, 0.808, and 0.692, respectively, which are much higher than the minimum LLTE values found. Thus the feet optimized for roll-over geometry do not best replicate the physiological lower leg trajectory. The roll-over geometries of both the LLTE- and roll-over optimal designs are shown in Fig. 2-9. Particularly for the articulated feet, the roll-over opti-

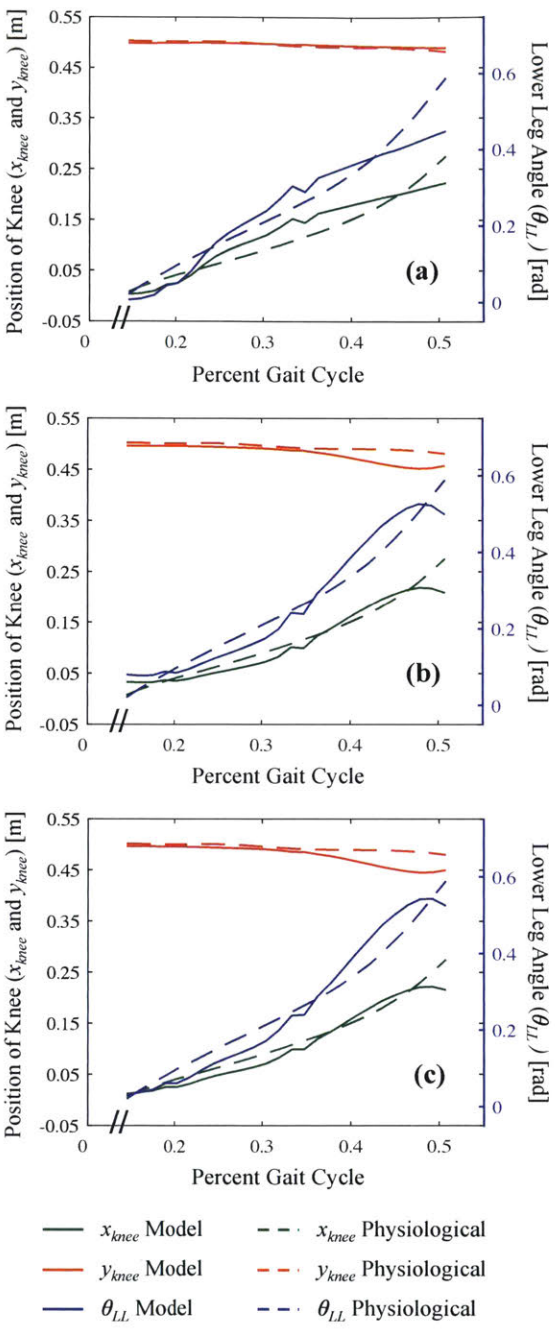

Figure 2-8: Individual parameters that make up the LLTE for LLTE-optimal designs: (a) rigid foot, (b) rotational ankle and metatarsal foot, and (c) rotational ankle, beam forefoot foot.

mal designs fit the physiological roll-over shape much better than the LLTE-optimal designs, further illustrating that the design with the best kinematics as measured by the LLTE is not necessarily the design with the best roll-over geometry.

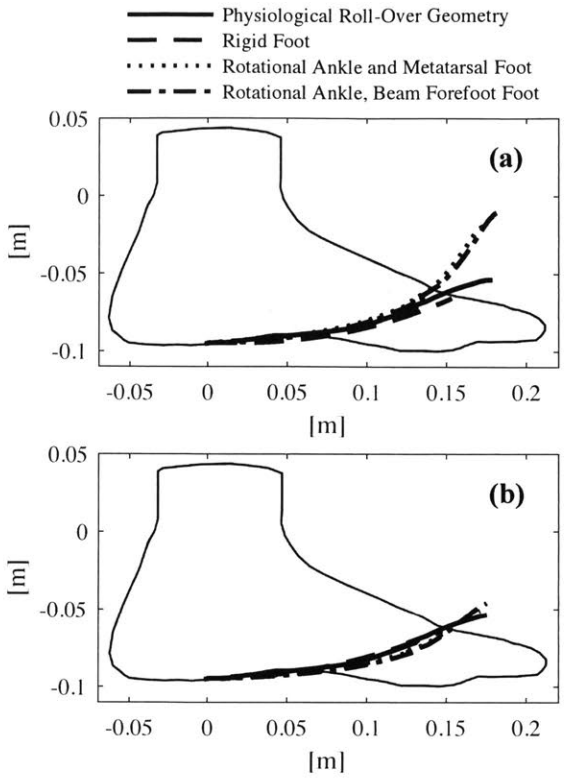

Figure 2-9: Roll-over geometries of the LLTE-optimal and the RO-optimal foot designs: (a) LLTE-optimal designs, and (b) roll-over-optimal designs.

2.5 Discussion

The presented framework can be used to evaluate feet, optimize design variables for a particular foot architecture, or compare different foot architectures. The LLTE optimization done in the previous section shows that the articulated architectures presented here outperform the rigid circular foot.

It is important to note that the lower leg trajectory error only captures the kinematic and kinetic performance of prosthetic feet. There are many other factors, such as manufacturability, weight, and cost, that must also be considered in early stage foot design. In this case, the rotational ankle, beam forefoot foot would likely be easier to build and lighter weight than the rotational ankle and metatarsal foot, as the cantilever beam requires fewer parts and less structural material than the additional rigid link and springs used in the rotational metatarsal joint. The presented framework should be used together with these other factors in early stage prosthetic

foot design.

Including the rigid circular foot model in the optimization allows for comparison with Adamczyk's clinical work, in which subjects walked on circular wooden rocker feet with various radii and center located 0.076 m anterior to the ankle-knee segment [1]. He found that the subjects were able to walk most efficiently on feet with radius equal to 30% of their leg length. At $x_c = 0.076$ m, the minimum LLTE occurs for a foot with radius 0.22 m, which is 27% of the leg length of the subject of the gait analysis used in this study. Thus the foot with the optimal LLTE subject to the constraint $x_c = 0.076$ m corresponds closely to the metabolically optimal design as found empirically in Adamczyk's clinical study.

Because the LLTE compares modeled values to physical values at each time interval during a step, it includes a temporal optimization element not present in the roll-over geometry. Most roll-over geometry investigations focus only on the shape itself or certain attributes of the shape, such as radius [1, 13, 14] or arc length [2, 10]. While it is possible to include temporal effects in roll-over geometry by evaluating the rate of progression of the center of pressure, the temporal aspect is not typically considered.

This analysis was performed using inputs from published able-bodied gait data. As previously mentioned, there are differences between the gait of persons with lower limb amputations and able-bodied persons. Additionally, the design of a particular prosthetic foot affects how a user walks. When a prosthetic foot is optimized for able-bodied gait data and then built and tested, there will be differences between the loads actually applied to the prosthesis and the able-bodied loads for which the foot was designed. Consequently, the response of the foot will be different from that predicted in the model.

As defined here, the error in each of the three variables comprising the lower leg trajectory, x_{knee}, y_{knee} and θ_{LL}, as well as all times throughout the step are weighted as equally as possible in the definition of the optimization parameter LLTE (detailed in Appendix A). As this analysis is purely theoretical, there is no reason to suspect that any one of these is more important than the others. In future work, testing

should be done to determine whether this is truly the case when a human user is involved, as well as to evaluate alternative cost function definitions, such as using different normalization factors or target data sets.

The proposed optimization parameter, LLTE, only addresses mid-stance kinematics, from foot flat to late stance. The heel strike to foot flat phase of stance can be investigated using the same method, but additional design variables should be added to the models to decouple the early stance and mid to late stance behavior of the foot. Many commercially available prosthetic feet already differentiate the response of the foot during these two separate phases by using, for example, one cantilever beam extending forward from the ankle and a second cantilever beam extending backward, or a rigid keel forefoot and a foam cushion heel, as in a SACH foot. The heel portion of these prosthetic feet have an additional purpose of providing shock absorption at heel strike.

The model foot architectures investigated in this study are intended only to demonstrate the usefulness of the presented framework of replicating target lower leg trajectories under a set of input loads in prosthetic foot design, and to provide conceptual architectures that could be easily prototyped for clinical validation of this work. The architectures presented are neither exhaustive nor representative of commercially available prosthetic feet.

The framework presented here is intended to be used only as a tool for early stage prosthetic foot design and analysis. In clinically evaluating existing feet, all of the resulting data, both kinematic and kinetic, must be measured. In the course of this work, kinetic data has been used as an input and kinematic data as an output, but in a clinical context it may be found that a person walks with near perfect gait kinematics with a foot with a very high LLTE value, but in order to do so the kinetics must deviate significantly from normative data. For a foot with a very low LLTE value, kinematic data close to the target kinematics will only be possible with kinetics close to those used as inputs, and vice versa. For such a foot with a low LLTE value, it is expected that both the kinematics and kinetics measured clinically will be close to those values used in the optimization process, as has been demonstrated in

Chapter 3 [17].

2.6 Conclusions

This chapter presents a novel framework that quantitatively connects the mechanical design of a prosthetic foot to its anticipated biomechanical performance. The framework uses kinetic inputs to predict kinematic outputs of the lower leg by knowing the geometry and stiffness of the foot. The error between the output kinematics and the target kinematics is evaluated using a root-mean-square error function that we call the Lower Leg Trajectory Error (LLTE). The LLTE can be used as an optimization parameter to tune the stiffness of a foot to produce accurate lower leg kinematics. The framework is agnostic to a specific foot design, as long as the constitutive behavior of the foot can be characterized. In this study, physiological kinetics were used as the input to the framework, with physiological kinematics as the targets; the framework is flexible and could accept alternate inputs and targets, depending on what performance and clinical objectives are desired.

Three model foot architectures were optimized using the LLTE-based framework. The results were compared to the same models optimized for roll-over geometries. It was shown that the feet with roll-over geometries closest to physiological do not necessarily result in the best lower leg kinematics. Roll-over geometry omits the kinematic constraint between a specific foot design and the ground, the orientation of the lower leg, and the temporal progression of the step – important parameters for both gait kinematics and joint reaction forces and moments. Consequently, it is possible for a prosthetic foot to exactly mimic the physiological roll-over shape, but greatly differ from physiological lower leg orientation. While further testing, such as that presented in Chapter 3, is required to validate the full clinical effectiveness of the Lower Leg Trajectory Error, incorporating more information than the roll-over geometry alone into the design of passive prostheses will facilitate improved replication of physiological gait.

THIS PAGE INTENTIONALLY LEFT BLANK

Bibliography

[1] Peter G Adamczyk, Steven H Collins, and Arthur D Kuo. The advantages of a rolling foot in human walking. *J. Exp. Biol.*, 209(Pt 20):3953–63, October 2006.

[2] Peter G Adamczyk and Arthur D Kuo. Mechanical and energetic consequences of rolling foot shape in human walking. *J. Exp. Biol.*, 216(Pt 14):2722–31, July 2013.

[3] Peter Gabriel Adamczyk and Arthur D Kuo. Mechanisms of gait asymmetry due to push-off deficiency in unilateral amputees. *IEEE Trans. Neural Syst. Rehabil. Eng.*, 2014.

[4] Nicholas P Fey, Glenn K Klute, and Richard R Neptune. Optimization of prosthetic foot stiffness to reduce metabolic cost and intact knee loading during below-knee amputee walking: a theoretical study. *J. Biomech. Eng.*, 134(11):111005, 2012.

[5] Nicholas P Fey, Glenn K Klute, and Richard R Neptune. Altering prosthetic foot stiffness influences foot and muscle function during below-knee amputee walking: a modeling and simulation analysis. *J. Biomech. Eng.*, 46(4):637–644, 2013.

[6] Robert Gailey, Kerry Allen, Julie Castles, Jennifer Kucharik, and Mariah Roeder. Review of secondary physical conditions associated with lower-limb amputation and long-term prosthesis use. *J. Rehabil. Res. Develop.*, 45(1):15, 2008.

[7] Brian J. Hafner. Clinical Prescription and Use of Prosthetic Foot and Ankle Mechanisms: A Review of the Literature. *Journal of Prosthetics and Orthotics*, 17(4):S5–S11, 2005.

[8] Matthew L Handford and Manoj Srinivasan. Robotic lower limb prosthesis design through simultaneous computer optimizations of human and prosthesis costs. *Scientific Reports*, 6, 2016.

[9] A. H. Hansen, D. S. Childress, and E. H. Knox. Prosthetic foot roll-over shapes with implications for alignment of trans-tibial prostheses. *Prosthet. Orthot. Int.*, 24(3):205–215, January 2000.

[10] Andrew H Hansen, Margrit R Meier, Pinata H Sessoms, and Dudley S Childress. The effects of prosthetic foot roll-over shape arc length on the gait of trans-tibial prosthesis users. *Prosthet. Orthot. Int.*, 30(3):286–99, December 2006.

[11] CJ Hofstad, H Van Der Linde, J Van Limbeek, and K Postema. Prescription of prosthetic ankle-foot mechanisms after lower limb amputation (Review). *The Cochrane Library*, (1), 2009.

[12] Larry L. Howell. *Compliant Mechanisms*. John Wiley & Sons, Inc, 2001.

[13] Elizabeth Klodd, Andrew Hansen, Stefania Fatone, and Mark Edwards. Effects of prosthetic foot forefoot flexibility on gait of unilateral transtibial prosthesis users. *J. Rehabil. Res. Develop.*, 47(9):899–910, 2010.

[14] Elizabeth Klodd, Andrew Hansen, Stefania Fatone, and Mark Edwards. Effects of prosthetic foot forefoot flexibility on oxygen cost and subjective preference rankings of unilateral transtibial prosthesis users. *J. Rehabil. Res. Develop.*, 47(6):543–552, 2010.

[15] M J Major, L P Kenney, M Twiste, and D Howard. Stance phase mechanical characterization of transtibial prostheses distal to the socket: a review. *Journal of Rehabilitation Research and Development*, 49(6):815–829, 2012.

[16] Matthew J Major, Martin Twiste, Laurence PJ Kenney, and David Howard. The effects of prosthetic ankle stiffness on ankle and knee kinematics, prosthetic limb loading, and net metabolic cost of trans-tibial amputee gait. *Clin. Biomech.*, 29(1):98–104, 2014.

[17] Kathryn M. Olesnavage and Amos G. Winter V. Clinical validation of predicting lower leg trajectory for passive prosthetic feet using physiological data as inputs. In review.

[18] K Postema, HJ Hermens, J De Vries, HFJM Koopman, and WH Eisma. Energy storage and release of prosthetic feet part 1: Biomechanical analysis related to user benefits. *Prosthet. Orthot. Int.*, 21(1):17–27, 1997.

[19] Harmen van der Linde, Cheriel J Hofstad, Alexander CH Geurts, Klaas Postema, Jan HB Geertzen, Jacques van Limbeek, et al. A systematic literature review of the effect of different prosthetic components on human functioning with a lower-limb prosthesis. *J. Rehabil. Res. Develop.*, 41(4):555–570, 2004.

[20] H W van Jaarsveld, H J Grootenboer, J de Vries, and H F Koopman. Stiffness and hysteresis properties of some prosthetic feet. *Prosthetics and orthotics international*, 14(3):117–24, dec 1990.

[21] David A. Winter. *Biomechanics and Motor Control of Human Movement*. John Wiley & Sons, Inc, 4th edition, 2009.

[22] Karl E Zelik, Steven H Collins, Peter G Adamczyk, Ava D Segal, Glenn K Klute, David C Morgenroth, Michael E Hahn, Michael S Orendurff, Joseph M Czerniecki, and Arthur D Kuo. Systematic variation of prosthetic foot spring affects center-of-mass mechanics and metabolic cost during walking. *IEEE Trans. Neural Syst. Rehabil. Eng.*, 19(4):411–419, 2011.

Chapter 3

Clinical Validation of Predicting Lower Leg Trajectory for Passive Prosthetic Feet Using Physiological Data as Inputs

3.1 Introduction

In Chapter 2, a novel approach to prosthetic foot design that uses a constitutive model of a foot to predict the lower leg trajectory under an assumed set of loading was introduced. A cost function, called the Lower Leg Trajectory Error (LLTE), is calculated to evaluate how close the predicted lower leg trajectory is to a set of target lower leg kinematic data. This method provides a means to connect the mechanical design of a prosthetic foot to its biomechanical functionality, and to optimize the design to achieve a particular functional requirement, that is, replicating physiological lower leg motion under typical loading. This method was demonstrated conceptually in Chapter 2 by optimizing the design of three different simple prosthetic foot models, each with two degrees of freedom [4]. The goal of this chapter is to show the clinical validity of this approach to modeling and designing prosthetic feet. The aims of this

work are:

1. to demonstrate that the constitutive model of foot deformation in response to loading accurately predicts lower leg position for known ground reaction forces and center of pressure positions, and

2. to test the assumption that physiological data are appropriate model inputs and target outputs, and a reasonable approximation for the actual kinetic and kinematic data measured for a subject with lower limb amputation using a prosthetic foot optimized with the LLTE.

3.1.1 Lower Leg Trajectory Error

As a brief summary of the work presented in Chapter 2, the Lower Leg Trajectory Error (LLTE) for a given prosthetic foot with known mechanical behavior is evaluated by applying an assumed set of horizontal and vertical ground reaction forces (GRF_x and GRF_y, respectively) to a constitutive model of the foot at locations defined by corresponding center of pressure position data, x_{cp}. Throughout this work, the assumed kinetic data were obtained from a set of published gait data for a typical, unimpaired subject [10]. Each of these variables, GRF_x, GRF_y and x_{cp}, are functions of time spanning stance phase. The deformed shape of the foot in response to the assumed loading at each time step is calculated quasi-statically using fundamental physics for simple prosthetic foot designs or finite element analysis for more complicated designs. By assuming no slipping occurs between the foot and the ground, the position of the lower leg segment in the saggital plane, which is defined here by the horizontal and vertical position of the knee, x_{knee} and y_{knee}, and the angular orientation of the lower leg segment with respect to vertical, θ_{LL}, is found at each time. The LLTE is a root-mean-square error comparing the trajectory of the modeled lower leg segment to a set of target lower leg trajectory data. The equation is provided in Chapter 2, Eqn. (2.1), but repeated here for the reader's convenience:

$$LLTE \equiv \left[\frac{1}{N} \sum_{n=1}^{N} \left\{ \left(\frac{x_{knee,n}^{model} - x_{knee,n}^{phys}}{\bar{x}_{knee}^{phys}} \right)^2 + \left(\frac{y_{knee,n}^{model} - y_{knee,n}^{phys}}{\bar{y}_{knee}^{phys}} \right)^2 + \left(\frac{\theta_{LL,n}^{model} - \theta_{LL,n}^{phys}}{\bar{\theta}_{LL}^{phys}} \right)^2 \right\} \right]^{\frac{1}{2}},$$

where the superscripts *model* and *phys* refer to values either predicted by the model or from the target physiological data set, which were taken from the same set of published able-bodied data used for the assumed loading data. The variable N is the total number of time intervals for which data were included in the calculation, with subscript n indicating each individual time step. Each term is normalized by the mean of the physiological variable across the portion of the step considered, notated as $\bar{x}_{knee}^{phys}$, etc. The decisions to use physiological data as input loading data and as target output kinematic data, as well as to use the means of the physiological variables as the normalization factors, are explained in detail in previous work [4]. These decisions are based on the assumptions that the loading a person with an amputation would apply to the foot will be similar to physiological loading for a person of the same body mass, and that symmetric gait is desirable for the user due to the superior aesthetics and the reduced risk of long term compensatory injury. The LLTE framework of predicting lower leg trajectory and comparing it to a target kinematic data set is easily adaptable to other objectives, but these will not be addressed here.

3.2 Methods

3.2.1 Experimental Prosthetic Foot Design

A prosthetic foot was designed specifically for this study based on previous work in which simple conceptual prosthetic feet were optimized to minimize $LLTE$ [4]. The basic architecture of the foot consists of a rotational pin joint at the ankle with constant rotational stiffness, k_{ank}, and a flexible cantilever beam forefoot with beam bending stiffness EI, where E is the modulus of elasticity and I is the area moment of inertia (Fig. 3-1). The ankle stiffness is provided by a pair of U-shaped flexures that

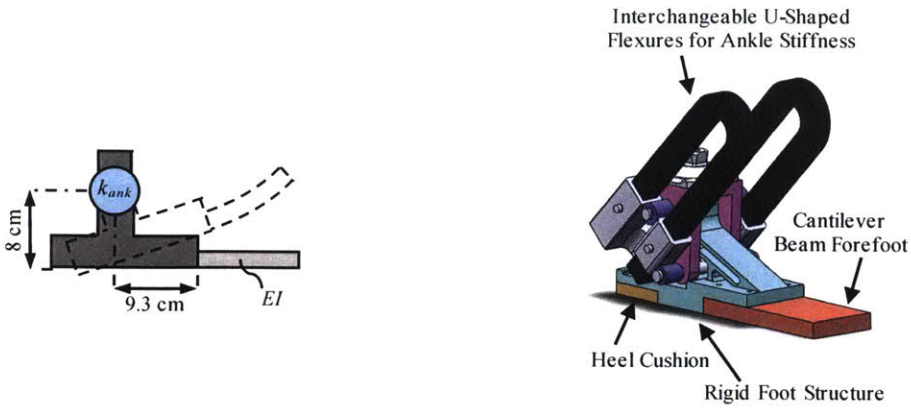

(a) (b)

Figure 3-1: (a) The conceptual architecture of the foot optimized for Lower Leg Trajectory Error (LLTE) in the author's previous work [4]. The foot consists of a purely rotational pin joint with constant rotational stiffness at the ankle and a flexible cantilever beam forefoot. The geometry of the foot was selected to replicate the articulation of the biological foot/ankle complex and was not included as a design variable to be optimized. (b) Solid model of the experimental foot built to function like the simple foot model in (a). The geometry of the U-shaped flexures dictate the stiffness of the ankle and can be substituted for other flexures to quickly change the ankle stiffness.

are interchangeable to alter the ankle stiffness value. The geometry of the forefoot was selected to give the desired bending stiffness. The remainder of the foot structure was designed to be rigid relative to these flexible components. A full description of the mechanical design of the foot can be found in [6].

The LLTE-optimal design for this conceptual foot architecture was previously found to be $k_{ank} = 3.7$ N·m/deg and $EI = 16.0$ N·m^2. Because the LLTE value is much more sensitive to ankle stiffness than it is to forefoot bending stiffness in the vicinity of this optimal design (Fig. 3-2), five different ankle stiffnesses were tested while the forefoot bending stiffness was held constant at the optimal value of 16.0 N·m^2 for all conditions. The ankle stiffness values tested were 1.5 N·m/deg, 2.9 N·m/deg, 3.6 N·m/deg, 4.9 N·m/deg, and 24.4 N·m/deg, labeled conditions A through E in order of increasing stiffness, with condition C being as close as possible to the previously found optimal value of 3.7 N·m/deg within manufacturing tolerances. In addition to spanning a wide range of LLTE values, these ankle stiffness values approximately correspond to biological ankle quasi-stiffness values as measured during

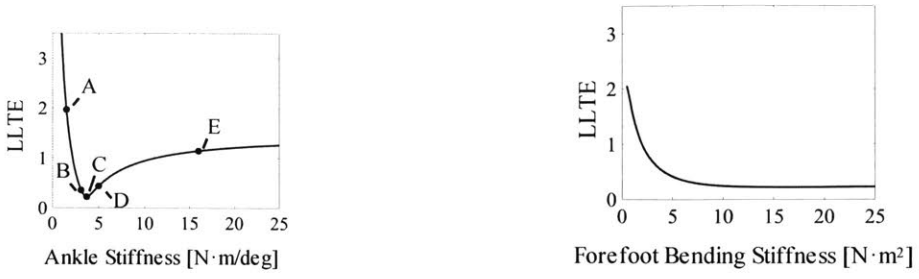

(a) (b)

Figure 3-2: LLTE values calculated for the foot architecture shown in Fig. 3-1 for (a) ankle stiffnesses ranging from 1 N·m/deg to 25 N·m/deg with the bending stiffness of the forefoot held constant at the optimal value, EI = 16 N·m/deg, and (b) for forefoot bending stiffness ranging from 1 N·m^2 to 25 N·m^2 with the ankle stiffness held constant at the optimal value, k_{ank} = 3.7 N·m/deg. Because the LLTE value is more sensitive to ankle stiffness than beam bending stiffness, the five experimental feet used in this study had five different ankle stiffnesses, labeled A through E in (a), but all had constant forefoot beam bending stiffness EI = 16 N·m/deg.

different phases of gait [7–9].

The experimental foot was tested on an Instron material testing machine with each of these sets of flexures to ensure the ankle stiffness matched the specified value (Fig. 3-3). Conditions A through C could safely reach a dorsiflexion angle of 26° without the material yielding and before hitting a hard stop. This angle is larger than expected during typical walking, with a maximum dorsiflexion angle of approximately 20° [2]. Condition D had a maximum dorsiflexion angle before yielding of 25°. Condition E used a hard stop only rather than a U-shaped spring to achieve a high enough stiffness, and had a maximum dorsiflexion angle before yielding of 6°. For D and E, the maximum deflection would only occur under an ankle moment much larger than expected during typical walking.

The rigid structure of the foot was machined from acetal resin. Nylon 6/6 was chosen for the U-shaped flexures and the cantilever beam forefoot, as nylon has a very high ratio of yield strength to elastic modulus, which allows the material to undergo very large deformations before yielding. The ankle joint was designed such that it could not plantarflex beyond the neutral position to limit the scope of this study to the controlled dorsiflexion portion of stance phase. The experimental foot was intended

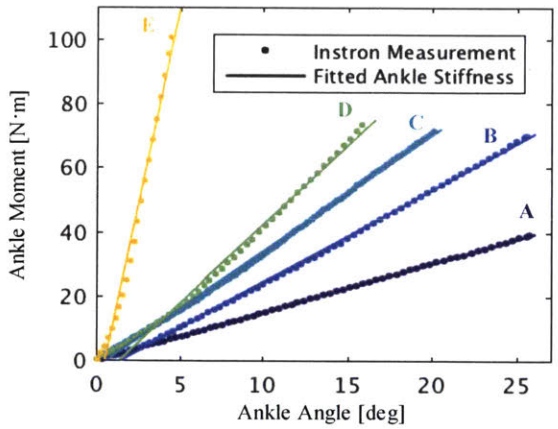

Figure 3-3: Instron-measured (dots) and linear fits (lines) rotational stiffness of the experimental prosthetic ankle with each of the five different sets of U-shaped flexures.

to be tested barefoot so that the presence of a shoe would not influence the mechanical behavior. An ethylene-vinyl acetate heel cushion with Shore A Durometer 35-40 was incorporated to minimize shock at heel strike. Rubber soling material intended for athletic shoes was epoxied to the bottom of the foot to provide traction. As tested, the mass of the foot ranged from 930 g to 1330 g, depending on the specific set of U-shaped flexures.

3.2.2 Data Collection

A single subject with unilateral transtibial amputation was used for this study. This particular subject was selected because her body mass (55.6 kg on average across multiple testing sessions) and her leg length (0.87 m) are similar to those of the subject in Winter's published gait data (56.7 kg and 0.83 m), which were used in optimizing the ankle rotational stiffness and forefoot beam bending stiffness of the foot. Due to timing constraints and to avoid fatiguing the subject, data were collected over two visits. In the first visit, conditions B, C, and D were tested. In the subsequent visit, conditions A and E were tested for the first time and condition C was tested a second time to ensure repeatability.

At the start of each visit, a qualified prosthetist fit the experimental foot to the subject's usual socket. A new pylon was used in place of the subject's own pylon so

that the overall height of the prosthesis was appropriate when the subject wore her own shoe on her sound limb, with no shoe on the prosthetic foot. After the prosthetist performed static and dynamic alignment, the subject was given as much time as she needed to acclimate to the foot. Reflective markers were then placed on the subject according to a Helen Hayes marker set [3], with additional markers on the prosthetic foot such that each component of the foot had a minimum of two markers defining its position. A digital motion capture system (Motion Analysis Corporation (MAC), Santa Rosa, CA) was used to collect kinematic data at 120 Hz. Six force plates (AMTI, Watertown, MA) embedded in the floor collected kinetic data at 960 Hz. After a static trial, the subject was instructed to walk back and forth along a 10 m walkway at a self-selected comfortable speed. The subject continued walking until five clean steps were collected on both the prosthetic and the sound side. Steps were only used if the subject's entire foot landed on a single force plate, and her opposite foot did not contact that same force plate. After five steps were collected on each side, the prosthesis was doffed and the U-shaped flexures were substituted for the next set without removing the foot from the rest of the prosthesis. With the new flexures in place, the subject once again donned the prosthesis. The prosthetist adjusted the alignment to best accomodate the new ankle stiffness if necessary. The trial procedure was then repeated starting with the acclimation period.

After data collection was completed, it was observed that there was both a spatial and a temporal misalignment between the motion capture data and the force plate data. This misalignment was confirmed with the equipment manufacturer, who provided a software patch to correct the spatial misalignment in post-processing. The temporal misalignment was measured experimentally to be four frames, or 0.03 seconds. The data collected with the motion capture system was shifted by four frames relative to the force plate data, as advised by the manufacturer.

3.2.3 Data Analysis

Constitutive Model Validation

If the constitutive behavior of a prosthetic foot is deterministic, the output motion of a lower leg prosthesis of known mechanical behavior can be accurately calculated from a set of input ground reaction force and center of pressure position data. This idea is analog to the stiffness of a spring relating force to displacement. To validate our constitutive model, the position of the knee (x_{knee} and y_{knee}) and orientation of the lower leg segment (θ_{LL}) were predicted using measured ground reaction force and center of pressure data applied to an analytical mechanical model of our experimental prosthetic foot. These calculations were similar to those performed in the initial design optimization explained above, but instead of using published able-bodied data, the kinetic data measured during *in vivo* testing were used. The expected position of the lower leg segment was calculated using

$$\begin{aligned}\theta_{LL} &= \theta_{ank} + \theta_{ff} \\ &= \frac{M_{ank}}{k_{ank}} + \theta_{ff} \\ &= \frac{1}{k_{ank}}(GRF_y \cdot x_{cp} + GRF_x \cdot h) + \theta_{ff}\end{aligned} \tag{3.1}$$

$$\begin{aligned}x_{knee} &= x_{ank} + L_{LL} \cdot \sin(\theta_{LL}) \\ &= x_{cp} \cdot (1 - \cos(\theta_{ff})) + L_{LL} \cdot \sin(\theta_{LL})\end{aligned} \tag{3.2}$$

$$\begin{aligned}y_{knee} &= y_{ank} + L_{LL} \cdot \cos(\theta_{LL}) \\ &= x_{cp} \cdot \sin(\theta_{ff}) + h \cdot \cos(\theta_{ff}) + L_{LL} \cdot \cos(\theta_{LL}),\end{aligned} \tag{3.3}$$

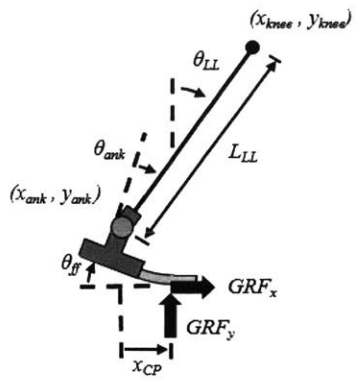

Figure 3-4: Graphical definition of variables used in Eqns. (3.1)-(3.3) to calculate the position of the lower leg segment under a particular set of ground reaction forces and center of pressure position.

where θ_{ff} is the angle of the foot relative to the ground due to deformation in the forefoot, θ_{ank} is the ankle angle, x_{ank} and y_{ank} are the horizontal and vertical position of the ankle, M_{ank} is the moment about the ankle, and h is the height of the center of the ankle pin joint off the ground when the foot is flat on the ground, which is defined by the geometry of the prototype (Fig. 3-4). In this case $h = 0.08$ m. θ_{ff} was calculated iteratively using Euler-Bernoulli beam bending, as the component of the GRF transverse to the beam could not be found without knowing this angle, and vice versa. Details of this calculation are published in [5].

The above calculations rely on the position of the lower leg segment being fully defined by the position of the center of pressure along the ground, the physical interaction between the ground and the foot, and the no slip assumption between the ground and the foot. This is not the case for the portion of stance phase immediately following heel strike and preceding toe-off, during which time the foot is in point-contact with the ground. At heel strike, the entire lower leg system rotates about the stationary center of pressure at the heel. At toe off, the same happens about the toe. During these times, the angle of the prosthesis relative to the ground cannot be determined from the center of pressure position and ground reaction force data without making additional assumptions about the subject's motion. The experimental feet used in this study were incapable of plantarflexion beyond the neutral position, so there was no motion within the foot until the applied moment (causing dorsiflexion)

became greater than zero. Therefore, only the portion of stance for which both (1) the moment about the ankle, M_{ank}, was greater than zero, and (2) the center of pressure was progressing forward, was considered in predicting the output motion of the lower leg.

The variables x_{knee}, y_{knee} and θ_{LL} were all defined based on the position of a single "knee" point that, under the assumptions of this analysis, lay on an imaginary vertical line drawn through the ankle joint when the foot was flat on the ground and unloaded. It was not expected that the knee joint motion tracking marker used during data collection would lie exactly on this vertical line, as the subject's socket covered her biological knee making anatomical features difficult to locate. To account for this discrepancy, a virtual knee marker was defined in post-processing that was the same distance from the ankle as the physical knee marker, but was directly vertically above the ankle when the foot was on the ground and unloaded. This virtual knee marker was assumed to be part of the same rigid body segment as the physical ankle and knee markers, so the offset angle between the virtual knee marker, the ankle marker, and the physical knee marker was kept constant.

Comparison of Physiological Inputs and Measured Data

In optimizing the design of the foot to minimize LLTE, six variables were used from able-bodied gait data. The horizontal and vertical ground reaction forces and center of pressure position data were used as assumed loading. The horizontal and vertical position of the knee and the orientation of the ankle-knee segment were used as target output kinematics, against which the predicted lower leg trajectory for a given prosthetic foot design was compared using the LLTE. The six variables from able-bodied gait data were then compared to the same variables measured during *in vivo* testing of the prototype feet to evaluate whether physiological data are appropriate model inputs and target outputs for designing a prosthetic foot. To account for anatomical differences between the test subject and the source of the physiological data, ground reaction forces were normalized by body weight. All variables expressing positions or distances (x_{knee}, y_{knee}, and x_{cp}) were scaled by the ratio of the vertical

distance from the knee marker to the floor during standing, such as

$$x_{knee}^{phys} = x_{knee}^{W} \frac{L^{meas}}{L^{W}}, \tag{3.4}$$

where x_{knee}^{phys} is the value to which the data collected in this study were compared, x_{knee}^{W} is the horizontal position of the knee as published by Winter, L^{meas} is the distance from the knee to the ground measured for the subject in this study during standing, and L^{W} is the distance from the knee marker to the ground for the subject in Winter's data. The timing of each variable was normalized over stance phase, such that heel strike occured at 0% and toe-off at 100%.

Evaluating Symmetry of Joint Angles, Moments and Powers

While the method employed here does not attempt to predict any motion above the knee joint, the underlying concept is that if the lower leg moves in a desirable way under loading that is comfortable for the user, the rest of his or her body will be able to move in a close-to-typical manner. Or, at the very least, if the lower leg does not move in a desireable way, the user will necessarily have to change other aspects of his or her gait to compensate. Thus the ankle, knee, and hip joint angles, moments, and powers were obtained directly from the OrthoTrak software. Each of these values were averaged over the five steps on each side with each ankle stiffness condition and compared to typical, able-bodied values.

To evaluate and compare gait symmetry for each of the five ankle stiffness conditions, local maxima and minima were identified in the joint angle, moment and power data. For a particular extremum, such as maximum ankle dorsiflexion angle, for example, the difference between the sound side and prosthetic side values were calculated for each of the five ankle stiffness conditions. The condition with the smallest difference between the two sides was considered the most symmetric in that particular regard (e.g. with regards to maximum ankle dorsiflexion angle). Similarly, the condition with the largest difference was the least symmetric. The most and least symmetric conditions were identified for every local extrema for the ankle, knee,

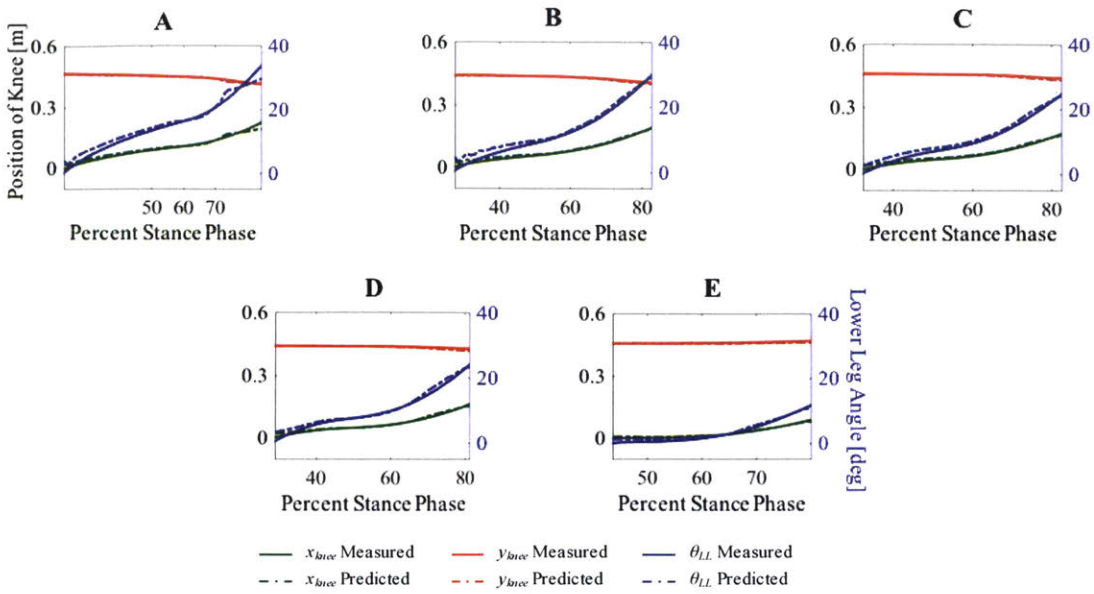

Figure 3-5: Lower leg trajectory, defined by x_{knee}, y_{knee}, and θ_{LL}, predicted by the constitutive model using *in vivo* measured GRF_x, GRF_y and x_{cp} values as inputs, compared to the corresponding kinematic data measured *in vivo*. A single representative step is shown here for each of the five ankle stiffness conditions. The x-axis spans the range of times covered by the model, beginning when the ankle dorsiflexion angle is first greater than zero, and ending when the center of pressure ceases to progress forward.

and hip joint angles, moments, and powers. Since the design optimization used here does not address swing phase, only local extrema that occurred during stance phase were included. Extrema that were not distinguishable on both the prosthetic side and sound side for all five ankle conditions were omitted. For each ankle stiffness condition, the total number of extrema for which that condition was the most symmetric and the least symmetric was tallied and compared to the other ankle stiffness conditions to evaluate symmetry across joint angles, moments, and powers combined rather than focusing on any one particular attribute.

3.3 Results

Five steps were collected for both the sound and the prosthetic side for each of the five ankle stiffness conditions. The x_{knee}, y_{knee}, and θ_{LL} values were predicted for

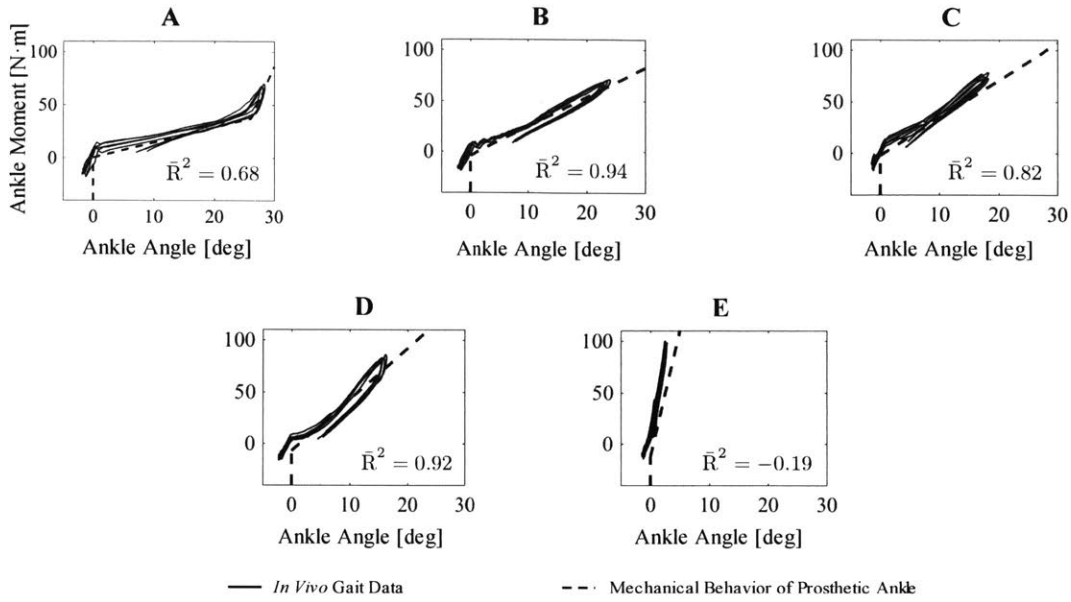

Figure 3-6: Prosthetic-side ankle moment versus ankle angle measured during *in vivo* testing for each of the five ankle conditions. Each solid black line represents one captured step; the dashed lines show the ankle stiffness measured on an Instron machine. Note in condition A the ankle hit the hard stop at 26°, at which point the stiffness increased beyond predicted.

each individual prosthetic side step, for 25 steps total, and compared to the values measured *in vivo* of these variables (Fig. 3-5). Across all data points collected, the average of the absolute value of the difference between the predicted and measured values for each of these variables were 1.0 cm for x_{knee}, 0.3 cm for y_{knee}, and 1.5° for θ_{LL}.

The ankle angle-moment curves as measured during *in vivo* testing were also compared against the mechanical behavior of the experimental foot ankle joint as measured on an Instron machine (Fig. 3-6). During the controlled dorsiflexion phase of stance, the *in situ* ankle angle-moment curves fit the Instron measured experimental foot behavior with R^2 values of 0.68, 0.94, 0.82, 0.92, and -0.19 for conditions A through E in that order, demonstrating that the analytical model of a purely rotational pin joint with the specified constant rotational stiffness adequately represented the ankle of the experimental foot for conditions A through D. For condition A, Fig. 3-6 shows an increase in stiffness at 26°, corresponding to the ankle hitting the hard

stop; the reported R^2 value reported is only for the linear elastic region of the curve. For condition E, the negative R^2 value indicates that the ankle behavior as measured on the Instron machine does not describe its mechanical behavior as measured during *in vivo* testing. This is due to the fact that, because the range of motion of the ankle is so small, the fit of the *in vivo* and Instron data is extremely sensitive to the neutral, unloaded position of the ankle, which was calculated from swing phase data. If the neutral ankle angle is decreased by 1° from the angle found from swing phase, the average R^2 value for condition E increases to 0.88.

The measured kinematic and kinetic data that directly contributes to calculating lower leg trajectory (x_{knee}, y_{knee}, θ_{LL}, GRF_y, GRF_x, and x_{cp}) for both the sound and prosthetic sides, are shown in Fig. 3-7 with the physiological data used initially in designing and optimizing the experimental feet. Because the feet used in this study are passive, they could not replicate the power-generation reflected in the physiological data at the end of stance. The instant at which the biological joint becomes a net power generator is demarcated in Fig. 3-7 with a vertical dotted line.

The average ankle, knee, and hip joint angles, moments, and powers are compared to typical, able-bodied values in Figs. 3-8, 3-9, and 3-10, respectively. Following the method described above, 21 local extrema were identified: two each in the ankle, knee, and hip angle data, two in the ankle and hip moment data, three in the knee moment data, four in ankle power data, one in the knee power data, and three in the hip power data. Of these 21 local extrema, ankle condition D was the most symmetric more frequently than any other condition, with seven instances in which the difference between the sound side and prosthetic side data was the smallest, compared to four instances for conditions A and E, and three instances each for conditions B and C (Table 3.1). Ankle stiffness conditon A was the least symmetric most frequently, with eight instances in which the difference in data between sides was the greatest, followed closely by condition E, with seven instances, then condition C with four instances, and finally conditions B and C with one instance each.

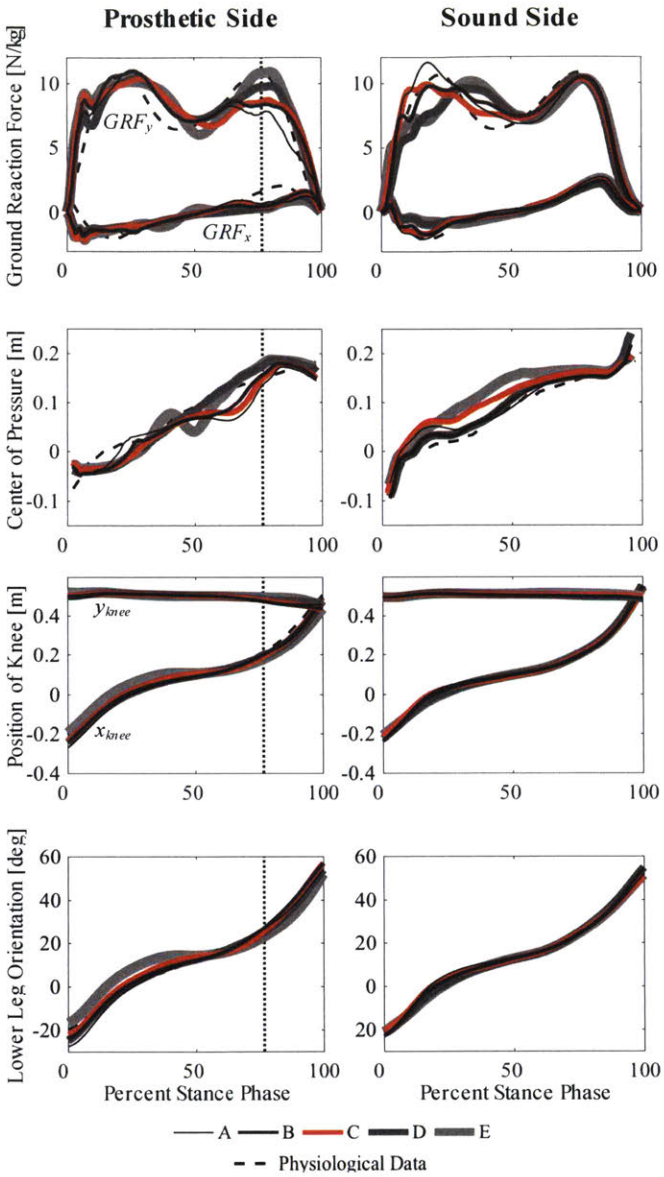

Figure 3-7: Average kinetic and kinematic variables over stance phase measured during *in vivo* testing for each of the five ankle stiffness conditions compared to the corresponding physiological data used in the initial optimization. The vertical dotted line on the prosthetic-side plots marks the moment in stance when the net work done by the biological ankle joint becomes positive. Because the experimental foot could not generate power, the *in vivo* data were not expected to match the physiological data to the right of this line.

3.4 Discussion

3.4.1 Accuracy of Constitutive Model

As evidenced by both the ankle angle versus moment curves in Fig. 3-6, and the measured x_{knee} and θ_{LL} values in Fig. 3-5, the stiffness of the ankle clearly affected

	Number of Extrema for which Condition is:	
Ankle Stiffness Condition	**Most Symmetric**	**Least Symmetric**
A	4	8
B	3	1
C	3	4
D	7	1
E	4	7
Total Num. Extrema:	**21**	**21**

Table 3.1: Number of instances each ankle stiffness condition was found to be the most and least symmetric, as calculated by the difference between the sound side and prosthetic side data values at each of 21 local maxima and minima identified in the ankle, knee, and hip joint angle, moment and power data.

the subject's gait mechanics. Across these different ankle stiffness conditions, the model predicted lower leg kinematics very well and to a high level of geometric accuracy. This indicates that the assumptions of the model – that there is no slipping between the foot and the ground, that the deformation of the foot can be calculated quasistatically, and that the prosthetic socket and pylon are rigid – are reasonably accurate during the controlled dorsiflexion portion of stance phase. These results also demonstrate the LLTE is able to quantitatively relate the mechanical design of a foot to its biomechanical performance.

The hard stop angle was only reached for the most compliant ankle, condition A, but the stiffness of all of the ankles were subject to some error due to limitations in measuring the exact moment arm and angle of the ankle during Instron loading. The ankle stiffnesses were measured on different days, which showed that the Instron-measured rotational ankle stiffnesses were repeatable to within ± 0.1 N·m/deg. With more accurate stiffness measurements, the model-predicted lower leg trajectory would likely be even closer to the measured trajectory.

As previously discussed, the model can only be used to predict the lower leg trajectory during foot-flat; prior to this, the foot is pivoting about a single point

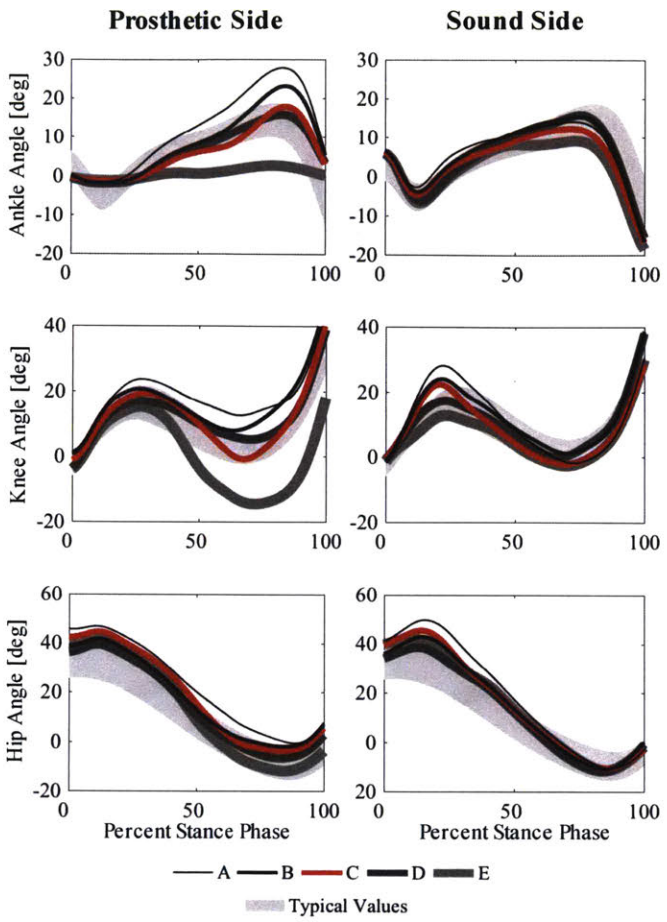

Figure 3-8: Average ankle, knee, and hip angles over stance phase for each ankle stiffness condition

at the heel, so the orientation of the prosthesis is indeterminate. Once the moment about the ankle becomes positive, the model can be used to predict the lower leg trajectory until the heel and most of the forefoot lift off the ground, at which point the foot is pivoting about the tip of the toe. This time was identified in the gait data as the instant the center of pressure ceased to progress forward. Consequently, the portion of stance for which the lower leg trajectory could be predicted varied for each foot. The lower leg trajectory for ankle stiffness condition A could be calculated for the largest percentage of stance, 59%, followed by conditions B, C, D, and E with 53%, 50%, 49% and 42%, respectively. This does not mean that the subject spent less time in stance on the foot with ankle stiffness condition E than with condition A, but rather that, of the time she was in stance on the prosthetic side for condition E,

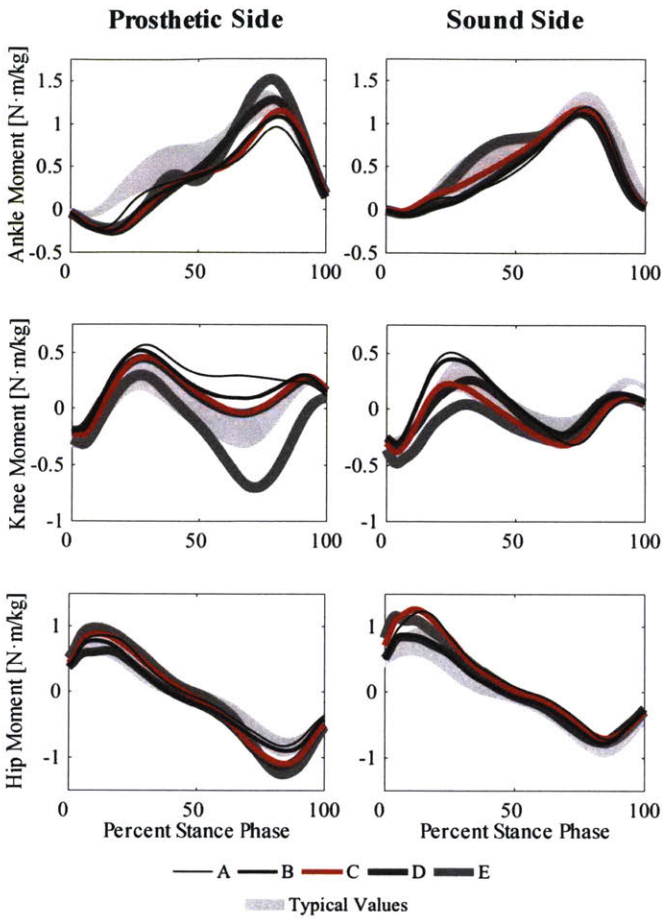

Figure 3-9: Average ankle, knee, and hip moments over stance phase for each ankle stiffness condition

she spent less of that time with her foot flat on the ground in controlled dorsiflexion and more time pivoting about the heel or toe.

3.4.2 Physiological Data as Model Inputs and Target Outputs

In general, the data measured during *in vivo* testing were similar in trends and magnitudes to the physiological data used in optimizing the foot design. Because the passive experimental feet in this study could not generate power, the prosthetic side *in vivo* data diverge from the physiological data during late stance when the net work from the biological ankle over the course of the step becomes positive, indicated by the vertical dotted line in Fig. 3-7. Prior to this point in stance, the negative ankle work exactly balances the positive ankle work, so it is theoretically possible for a per-

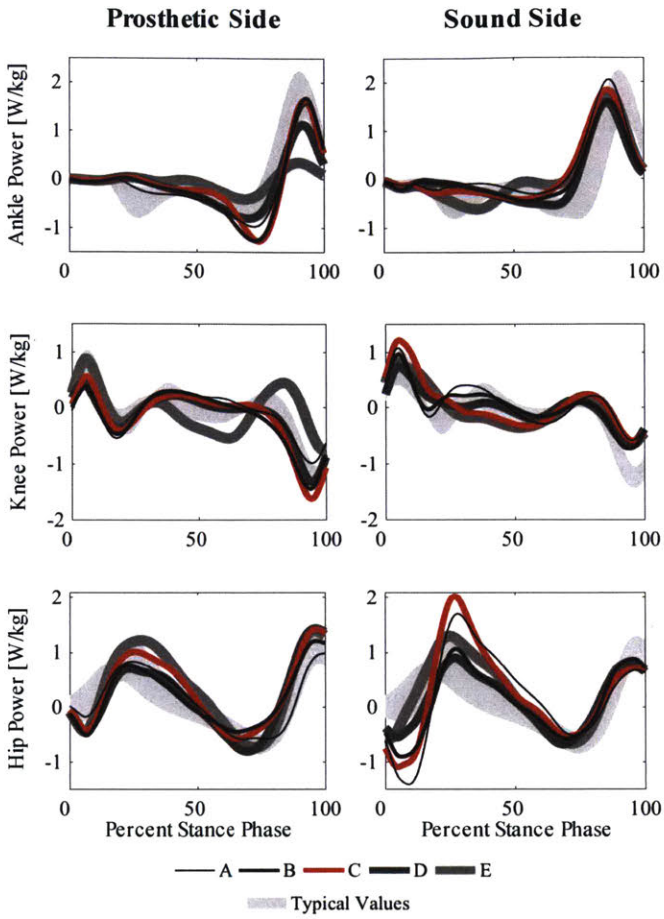

Figure 3-10: Average ankle, knee and hip powers over stance phase for each ankle stiffness condition

fectly efficient energy storage and return foot to exactly replicate physiological kinetic and kinematic data up until this point. In practice, however, energy losses (due to friction and viscoelasticity) mean that only some of the work done on the prosthetic foot will be recovered and used to do positive work later in stance. Consequently, the prosthetic side ground reaction forces and center of pressure position diverge from physiological values slightly before this zero net work line. When the prosthetic side is not able to replicate physiological values, the corresponding contralateral data also diverges to compensate, as seen in the increased sound side ground reaction forces in early stance, suggesting that targeting physiological loading and motion could reduce this compensatory motion.

While the different ankle stiffness conditions affected the lower leg kinematic vari-

ables during the foot flat portion of stance (Fig. 3-5), over the entirety of stance phase, there was very little variation in lower leg kinematics. The differences in tibial progression during controlled dorsiflexion were compensated by changes in motion before or after foot-flat. Despite these differences, the *in vivo* kinematic variables, x_{knee}, y_{knee} and θ_{LL}, over stance phase closely matched the physiological target data without much variation between conditions. This could indicate that this particular subject walked in such a way as to maintain close-to-typical motion regardless of the foot she was given. In order to do this while using feet with higher LLTE values, the loading patterns on the feet must necessarily have deviated from typical physiological values, as evidenced by the divergence in ground reaction forces, center of pressure progression, or compensation in the knee and/or hip joint. With the single subject tested here, this cannot be generalized to the entire population of persons with unilateral transtibial amputations. However, if it were found that this trend to maintain typical kinematics is generally applicable, the method of optimization employed here, in which typical kinetic data are assumed as inputs and used to calculate output kinematics, is still valid, as the prosthetic foot structure defines a reciprocal relationship between loading and motion. That is, in the same way the motion of a prosthetic foot can be calculated in response to a given loading scenario, the loads necessary to produce that motion can also be calculated. The purpose of minimizing lower leg trajectory error as a design objective is to create a foot that, under typical loading, replicates physiological lower leg motion as closely as possible. Reciprocally, that same foot undergoing typical motion can only do so if the loading on the foot is close to physiological. In the purely hypothetical case of a theoretical foot with LLTE = 0, from a fundamental physics perspective, the only way this foot could exactly replicate physiological motion is if the loading on the foot were identical to physiological loading, and vice versa.

Stating that physiological data is a reasonable choice for target values in designing a prosthetic foot for someone with an amputation is not to say that able-bodied gait data is the *only* reasonable choice for model inputs, nor that symmetric gait is the *only* possible objective. The methods described here could be repeated with the objective

of obtaining a specific asymmetric gait, which, according to some simulation studies, may decrease the metabolic cost of walking [1]. However, frequent interaction with lower limb prosthesis users has lead the author to firmly believe that, in practice, symmetric gait is desirable, as it is perceived as more aesthetically pleasing and reduces the risk of long-term injuries due to asymmetries.

Furthermore, stating that it is appropriate to use physiological data as model inputs and target outputs in designing a prosthetic foot does not intend to imply that the predicted model outputs (x_{knee}, y_{knee}, and θ_{LL} here), which are calculated from the assumed physiological inputs (GRF_x, GRF_y, and x_{CP}), will always be representative of the actual data measured when a human subject uses the prosthetic foot. If the predicted output variables differ significantly from typical data (that is, the prosthetic foot has a high LLTE value), it is expected that the human user will compensate by altering any and/or all aspects of their gait mechanics in an unpredictable manner to make walking with that foot as comfortable as possible. With such a foot, the loading will differ from the physiological data assumed in initially calculating the LLTE value; the predicted output motion is then meaningless. However, predicting a high LLTE value for a foot is still meaningful, as it indicates that it is not possible for someone to walk on that foot with close-to-typical loading and close-to-typical motion simultaneously. Some aspects of the gait mechanics will necessarily have to deviate from typical, able-bodied values with such a foot.

For the same reason that the predicted outputs are not always expected to be meaningful, it is not expected that an LLTE value calculated comparing the x_{knee}^{meas}, y_{knee}^{meas}, and θ_{LL}^{meas} values measured *in vivo* with each of the five experimental prosthetic feet to the physiological x_{knee}^{phys}, y_{knee}^{phys}, and θ_{LL}^{phys} values using Eqn. (2.1) would follow the same trend predicted during the initial LLTE calculation using the assumed physiological loading data. It is expected though that across all aspects of gait, including both kinematics and kinetics, that prosthetic feet with smaller LLTE values will lead to gait mechanics that are more symmetric and closer-to-physiological data than feet with larger LLTE values. Qualitatively, this can be seen by inspecting Figs. 3-7 through 3-10. Ankles C, D, and E, which had predicted LLTE values near the min-

ima, more consistently fell within the range of typical physiological values. Ankles A and E, on the other hand, demonstrated more drastic deviations from typical in many of the gait metrics, as can be seen in the center of pressure data in Fig. 3-7, the prosthetic side ankle and knee angles in Fig. 3-8, the prosthetic side knee moment in Fig. 3-9, and the prosthetic side ankle and knee power in Fig. 3-10. Given the difficulty comparing each and every gait parameter (which have differing units) to identify a "best" foot, measuring symmetry between the prosthetic and sound side was chosen as a metric to contrast the performance of the five prototype feet.

3.4.3 Effect of LLTE values on gait symmetry

A single subject, as was used in this study, is insufficient to draw definitive conclusions about how persons with unilateral transtibial amputations will generally respond to the five feet with varying LLTE values used in this study. However, since the ultimate goal of LLTE optimization is to deterministically design prosthetic feet that offer some benefit to the user, the differences in gait mechanics observed in this single subject study merit discussion. Ankle stiffness condition D appeared to yield the most symmetric gait, with the difference between sound and prosthetic side data values smaller than for any of the other ankle stiffnesses for 7 of the 21 identified extrema. Unexpectedly, D was more symmetric than the optimal ankle stiffness C, which was the most symmetric condition for three of the extrema and the least symmetric for four. This could be due to differences between the weight and/or leg length of the test subject and the subject in Winter's gait data that was used to calculate the optimal ankle stiffness value. Some prosthesis users also have personal preferences toward stiffer or more compliant prosthetic feet, so if the subject preferred or was more accustomed to stiffer prosthetic feet, she may have been more comfortable with a stiffer-than-theoretically-optimal ankle, especially given the short time available for her to acclimate to each ankle stiffness.

While evaluating symmetry in this way provides a wholistic view of various aspects of gait, it does not give any insight into how much symmetry differed between the five ankle conditions for each local maxima or minima in the data. Only the conditions

that were the most or least symmetric for each extrema were included in the final results, but often the difference between sound and prosthetic side values for other conditions were very close. Additionally, the LLTE value for ankle stiffness condition D was 0.42, only slightly greater than condition C at 0.22, and approximately equal to that of condition B at 0.46; all three ankles were close to the LLTE minima shown in Fig. 3-2 and yielded relatively similar performance. For the local extrema where conditions B, C, and D were the least symmetric, the differences between sound and prosthetic side data values were usually only slightly less symmetric than other conditions, whereas conditions A and E were often outliers, such as for the knee moment minimum for condition E (Fig. 3-9), and ankle angle data for condition A (Fig. 3-8).

As previously stated, this study was designed to demonstrate the validity of the method of predicting lower leg trajectories for prosthetic feet using physiological data as inputs and target outputs. Future work should include testing a similar range of feet on a larger sample size over a longer period of time. This future study should utilize not only an analysis of gait symmetry, but also spatiotemporal factors, such as walking speed and step length, metabolic costs of transport, and subjective user preferences.

3.5 Conclusions

The primary objectives of this study were to demonstrate that

1. the physics of the constitutive model introduced in Chapter 2 and used to predict lower leg trajectories are clinically valid, and

2. physiological data are appropriate model inputs and target outputs, and a reasonable approximation for the actual kinetic and kinematic data measured for a subject with lower limb amputation using a prosthetic foot optimized with the LLTE.

A single subject with unilateral transtibial amputation tested an experimental foot consisting of a rotational pin joint at the ankle with adjustable rotational stiffness and a flexible cantilever beam forefoot under five different ankle stiffness conditions, ranging from 1.5 N·m/deg to 24.4 N·m/deg. When the measured ground reaction forces and center of pressure data were used as inputs for the constitutive model, the position of the knee joint was predicted to within an average error of 1.0 cm in the horizontal direction and 0.3 cm in the vertical direction. The angular orientation of the lower leg segment was predicted to within an average of 1.5°. Therefore the constitutive model accurately predicts the lower leg trajectory under a known set of ground reaction force and center of pressure data, provided that enough information is known about the mechanical behavior (stiffness, geometry, and kinematics) of the foot.

In general, the *in vivo* measured data – that is, the ground reaction forces, center of pressure, horizontal and vertical positions of the knee, and angular orientation of the lower leg segment – were similar in trends and magnitudes to the physiological data used in calculating the LLTE and optimizing the foot designs. There were some deviations between these measured data and the physiological data due to the physical limitations of the experimental feet, such as the inability to generate power or to plantarflex beyond the neutral position. When the measured gait kinematics or kinetics departed from the physiological inputs, the contralateral side compensated in the opposite direction, particularly with the ground reaction forces.

The similarity in trends and magnitudes between the measured and physiological data, as well as contralateral compensation when the measured data did depart from physiological values, suggest that physiological data are reasonable model inputs and target outputs for a patient with unilateral transtibial amputation using a prosthetic foot optimized with the LLTE, even if limitations of the prosthetic foot do not allow these data to be replicated exactly. While conclusions about general trends cannot be made using a single subject, for the particular subject used in this study, it was observed that the feet with predicted LLTE values near the minima were generally more symmetric in terms of joint angles, moments, and powers than the feet with

larger LLTE values. We do not claim that feet with low LLTE values will be superior to existing commercial feet; only proof-of-concept prototypes were tested in this study, and users may value attributes of feet not captured by the LLTE (such as weight and standing stability). Future work will include a larger study with many subjects and longer acclimation periods to determine whether feet with smaller LLTE values offer benefits in gait symmetry, metabolic cost of walking, and subjective user preference.

THIS PAGE INTENTIONALLY LEFT BLANK

Bibliography

[1] Matthew L Handford and Manoj Srinivasan. Robotic lower limb prosthesis design through simultaneous computer optimizations of human and prosthesis costs. *Scientific Reports*, 6, 2016.

[2] International Organization for Standardization. Prosthetics - structural testing of lower-limb prostheses - requirements and test methods. ISO Standard No. 10328, 2006.

[3] Mrn P Kadaba, HK Ramakrishnan, and ME Wootten. Measurement of lower extremity kinematics during level walking. *Journal of orthopaedic research*, 8(3):383–392, 1990.

[4] Kathryn M. Olesnavage and A. G. Winter V. A novel framework for quantitatively connecting the mechanical design of passive prosthetic feet to lower leg trajectory. In Review.

[5] Kathryn M. Olesnavage and Amos G. Winter V. Design and preliminary testing of a prototype for evaluating lower leg trajectory error as an optimization metric for prosthetic feet. In *ASME International Design Engineering Technical Conferences and Computers and Information in Engineering Conference (IDETC/CIE)*, 2016.

[6] V. Prost, K. M. Olesnavage, W. B. Johnson, M. J. Major, and A. G. Winter V. Design and testing of a prosthetic foot with interchangable custom rotational springs for evaluating lower leg trajectory error, an optimization framework for prosthetic feet. *In Review.*

[7] Elliott J. Rouse, Levi J. Hargrove, Eric J. Perreault, and Todd A. Kuiken. Estimation of human ankle impedance during the stance phase of walking. *IEEE Transactions on Neural Systems and Rehabilitation Engineering*, 22(4):870–878, 2014.

[8] Kamran Shamaei, Gregory S. Sawicki, and Aaron M. Dollar. Estimation of quasi-stiffness of the human hip in the stance phase of walking. *PLoS ONE*, 8(12), 2013.

[9] Elhanan Singer, Gideon Ishai, and Eitan Kimmel. Parameter estimation for a prosthetic ankle. *Annals of biomedical engineering*, 23(5):691–696, 1995.

[10] David A. Winter. *Biomechanics and Motor Control of Human Movement.* John Wiley & Sons, Inc, 4th edition, 2009.

Chapter 4

Passive Single-Part Prosthetic Foot Shape and Size Optimization Using Lower Leg Trajectory Error

4.1 Introduction

The aim of this chapter was to develop a framework to optimize the design of a single-part compliant prosthetic foot to best replicate physiological lower leg trajectory when typical loads are applied, then use this framework to design and build a low-cost, mass-manufacturable prosthetic foot. As discussed in Chapter 1, this work was motivated by Bhagwan Mahaveer Viklang Sahayata Samiti (BMVSS), an organization based in Jaipur, India, that distributes approximately 26,000 units of its prosthetic foot, the Jaipur Foot, each year [1]. The Jaipur Foot was designed to meet the needs of persons with amputations living in India. It can withstand harsh environmental conditions (such as barefoot use and submersion in water), it looks like a biological foot to help users avoid social stigmas against mobility aids, and it permits culturally-specific activities (such as squatting). The Jaipur Foot costs approximately $10 USD to make, but is given to users for free through donations and government subsidies that fund BMVSS. It is generally regarded as a high-performing prosthetic foot, not

only in the context of emerging markets, but also compared to feet many times more expensive [3]. However, the Jaipur Foot is handmade, which leads to quality variation. It is also much heavier (at approximately 1,000 g for a 27 cm foot) than other low-cost passive prosthetic feet, such as the SACH foot (at 625 g [32]). The goal of this work is ultimately to design a prosthetic foot that facilitates near-able-bodied walking kinematics to avoid stigmas associated with disability, is lighter than the Jaipur Foot, costs no more than $10 USD to produce, and can be mass-manufactured to maintain product uniformity. This chapter focuses on the foundation of this endeavor: the creation of low-cost, single-part, energy-storing, plastic keel that can fit within a cosmetic covering.

Connecting the geometry and stiffness of the keel to the anticipated kinematics and kinetics of the user is critical for designing a prosthetic foot with a desired biomechanical performance. The novel design objective developed in this dissertation, the Lower Leg Trajectory Error (LLTE), quantifies how closely the position of the lower leg segment for a given prosthetic foot is able to replicate target physiological lower leg position, in both space and time, throughout the course of a step [29, 31]. LLTE was presented in Eqn. (2.1), but because it is central to this work is repeated here once more:

$$LLTE \equiv \left[\frac{1}{N} \sum_{n=1}^{N} \left\{ \left(\frac{x_{knee,n}^{model} - x_{knee,n}^{phys}}{\bar{x}_{knee}^{phys}} \right)^2 + \left(\frac{y_{knee,n}^{model} - y_{knee,n}^{phys}}{\bar{y}_{knee}^{phys}} \right)^2 + \left(\frac{\theta_{LL,n}^{model} - \theta_{LL,n}^{phys}}{\bar{\theta}_{LL}^{phys}} \right)^2 \right\} \right]^{\frac{1}{2}},$$

with variables as defined in Chapter 2. Each of these variables refers to the global, or lab-based, reference frame, as shown in Fig. 4-1. Once again, throughout the course of this dissertation, all physiological gait data came from Winter's published data, which were obtained from a subject of body mass 56.7 kg and leg length 0.83 m [35].

The focus of this chapter is not the definition of LLTE as a cost function for designing prosthetic feet, but rather developing a framework that can be used to design a prosthetic foot to meet specific needs while minimizing the value of a cost function. A detailed discussion of why the author believes that this particular cost

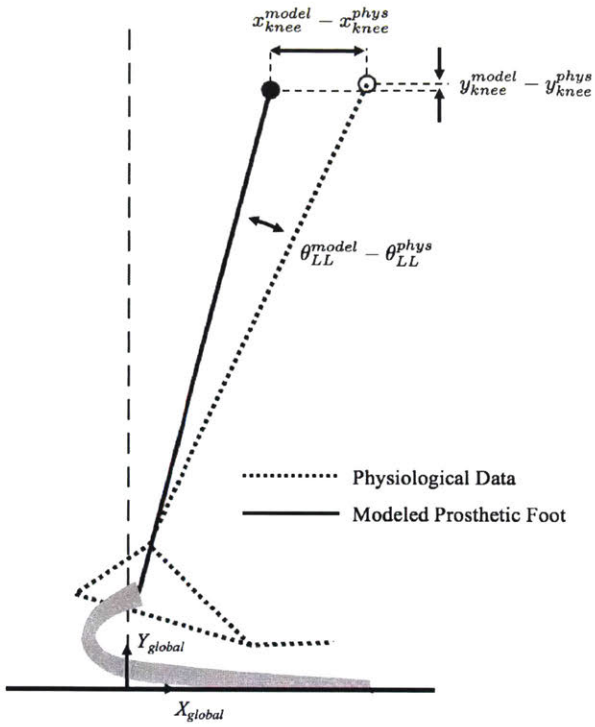

Figure 4-1: Lower leg position for modeled prosthetic foot (solid line) and target physiological gait data (dotted line) at one particular time interval during a step, with variables used in Eqn. (2.1) shown. Note that physiological data comes from markers placed at anatomically relevant positions on a human subject, resulting in a gap between the marker positions and the ground.

function, including the selection of the specific variables and normalization factors in Eqn. (2.1), produces a foot that best replicates physiological gait kinematic and kinetic data can be found in Chapter 3. However, the methodology presented in this chapter could similarly be employed with a different cost function to optimize the foot for other goals.

Three simple prosthetic foot architectures, each with two degrees of freedom, were optimized using LLTE to demonstrate its usefulness as a design tool in Chapter 2. The first model was a rigid circular foot, with the radius of the circle, R, and the horizontal position of the center of the circle, x_c, as design variables (Fig. 2-4a). The second consisted of rotational pin joints at the ankle and metatarsal joints, with the rotational stiffness of each joint, k_{ank} and k_{met}, as the design variables (Fig. 2-4b). The third and final model considered also consisted of a rotational ankle joint, but replaced the metarsal joint with a compliant cantilever beam forefoot, with the

ankle stiffness, k_{ank}, and the forefoot beam bending stiffness, EI (where E is the modulus of elasticity and I is the area moment of inertia), as design variables (Fig. 2-4c). Multiple prototypes based on these simple architectures have been built and used in clinical testing to validate the LLTE optimization method (see Chapter 3, Appendices B and C) [28,30]. We showed in Chapter 3 that prosthetic foot prototypes with LLTE values near optimal are able to promote gait symmetry and accurately replicate both physiological kinematics and kinetics, and that feet with larger LLTE values induce compensatory behaviors that cause gait asymmetries [27]. While the simple, two degree-of-freedom architectures have been useful tools to rapidly iterate through experimental prototypes and effectively prove the concept of prosthetic foot optimization based on LLTE, the resulting prototypes are too large to fit within a shoe, heavy (between 980 g and 2 kg), and consist of relatively complex mechanisms, with part counts on the order of 10 and moving components that would require frequent maintenance (Figures 3-1b, B-9, B-10, C-7, and C-8). In order to translate these experimental prototypes to commercial products, a lighter, more robust, and easier to manufacture design is required.

In this chapter, compliant mechanism optimization techniques were used to design a single-part foot that minimizes the LLTE to best replicate physiological lower leg kinematics. The design space parametrization, based on a wide Bézier curve, is discussed, together with constraints that were applied to ensure only physically-meaningful shapes were considered. The evaluation of the LLTE value for a given design using MATLAB (The MathWorks, Inc., Natick, MA) and ADINA (ADINA R & D, Inc., Watertown, MA) finite element analysis software is described. The optimal design is presented and compared to the simple analytical models previously optimized. A prosthetic foot (which will form the keel in our eventual commercial product foot with a cosmetic covering) was built based on the optimal design and tested on an Instron material testing machine (Illinois Tool Works Inc., Norwood, MA) to show that the finite element results used in the optimization accurately represented the foot. The foot was then tested with six subjects with unilateral transtibial amputations at BMVSS' facility in Jaipur, India. Feedback indicated that, once

a cosmetic and protective cover is designed for the foot, the prototype is ready for extended field trials without significant changes to the structure of the keel.

4.2 Method

4.2.1 Size and Shape Parameterization

The goal of this work was to develop a framework to design and optimize a prosthetic foot structure consisting of a single part that, when acted upon by typical ground reaction forces, deforms in such a way as to best replicate typical lower leg kinematics, as quantified by minimizing the Lower Leg Trajectory Error. By responding to a specific loading scenario and deforming elastically to achieve a desired output motion, the foot meets the definition of a compliant mechanism [18]. Because the primary goal of this work was to develop a framework to produce an optimal prosthetic foot with minimal LLTE value, the design of the foot was kept as simple as possible for rapid implementation and iteration through the methodology. Therefore only the design of the forefoot was optimized, as many prosthetic feet de-couple early stance from the rest of stance phase by using a separate mechanism, such as a cushion or a secondary compliant mechanism, for the heel portion of the foot. Several ways in which complexity could be added back in to the design, including adding a heel in the optimization process, are discussed in Section 4.4.

There is a plethora of literature on topology synthesis and optimization for compliant mechanisms [5,6,9,23,24,33,34], including continuum element density approaches, frame element-based structures, and pseudo-rigid body models. However, the outputs of these topology optimizations have several practical limitations; for example, some consist only of uniform elements or uniform cross-sections, have unclear boundaries or checkerboard patterns, or result in localized flexural hinges with high stress concentrations [7]. Furthermore, the topology of a prosthetic foot does not need to be complicated. All that is required is material at the ankle that can be attached to the rest of the prosthesis, and a flat bottom surface of the foot upon which the center

of pressure can progress smoothly from heel-strike to toe-off. What remains to be optimized is only the size and shape of the mechanism connecting the ankle to the bottom of the foot.

Several methods for compliant mechanism size and shape optimization were considered [15, 21, 36], but ultimately our foot was realized using a wide Bézier curve, as presented by Zhou and Ting [38]. A wide Bézier curve is a parametric curve with a shape dictated by a series of control points. With a Bézier curve, a cubic curve can be defined by the position of four control points, reducing a potentially complex shape to a limited number of design variables. The width of the curve is added as a variable by using control circles rather than control points and defining the width of the wide Bézier curve as a function of the diameters of these control circles. Unlike typical outputs of most topology synthesis and optimization methods, the output of the optimization method employed here is a 2D extruded shape that is easily manufacturable with minimal post-processing, which means the theoretical optimization result can be built as a physical prototype quickly and easily.

The shape and width of the Bézier curve (and resulting forefoot) was defined by four control points (C_1, C_2, C_3 and C_4 in Fig. 4-2), each of which had an x-position, y-position, and a diameter, denoted by subscripts x, y, and d, respectively. The first node, C_1, was the point of attachment between the foot and the rest of the prosthesis, and was fixed at $(C_{1x}, C_{1y}) = (0, 0)$. Throughout the course of this work, all measurements and coordinates are in units of meters, unless otherwise stated. The height of the foot from the attachment point to the bottom of the foot was h, such that $C_{4y} \equiv -h + \frac{1}{2}C_{4d}$, where C_{4d} was the width of the foot at C_4. To prevent any kinks in the structure, the tangent to the Bézier curve at point C_4 was made horizontal by enforcing $C_{3y} \equiv C_{4y}$. The coordinate C_{4x} was defined by the horizontal position of the center of pressure at the first instant in Winter's published gait data for which the center of pressure was anterior to the ankle in the ankle-knee reference frame, that is, $C_{4x} = 0.02$ m. The foot extended forward from C_4 to the tip of the foot, C_5, with $C_{5x} = 0.15$ m. Together, C_{4x} and C_{5x} determined the length of the forefoot and were selected to cover the distance the center of pressure progresses

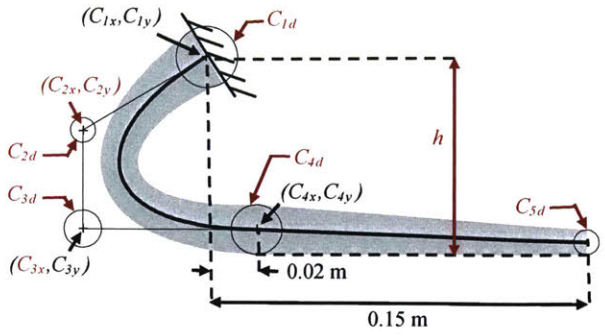

Figure 4-2: Parameterization of the keel of the foot. The shape and size of the keel are defined with nine independent design variables shown in red.

in Winter's gait data from foot flat to toe-off. The width of the forefoot decreased linearly from C_4 to the tip of the foot, with the design variable ff_{frac} defining the ratio of the width of the tip of the forefoot to the width of the foot at C_4. That is, $ff_{frac} \equiv C_{5d}/C_{4d}$. In order to keep the foot flat and stable on the ground when it was unloaded, $C_{5y} \equiv -h + \frac{1}{2} ff_{frac} \cdot C_{4d}$. Thus there were nine independent design variables to be optimized:

$$X = [h, C_{1d}, C_{2x}, C_{2y}, C_{2d}, C_{3x}, C_{3d}, C_{4d}, ff_{frac}] \tag{4.1}$$

Upper and lower bounds were imposed on each of the variables to constrain the shape and size of the structure to approximately fit within the envelope of a biological foot. The initial bounds were

$$lb = [0.06, 0.005, -0.15, -0.10, 0.005, -0.15, 0.005, 0.005, 0.1] \tag{4.2}$$

and

$$ub = [0.15, 0.04, 0.07, 0.10, 0.04, 0.01, 0.04, 0.04, 1] \tag{4.3}$$

These preliminary bounds were very loose on the variables h, C_{2x}, C_{2y}, and C_{3x} to avoid constraining the design space more than necessary. After an optimal design was found, these bounds were modified to enforce the requirement that the optimal design could not be larger than a biological foot. The thickness of the foot into the plane of the page was fixed at 0.06 m such that the foot can easily fit into a shoe or cosmesis.

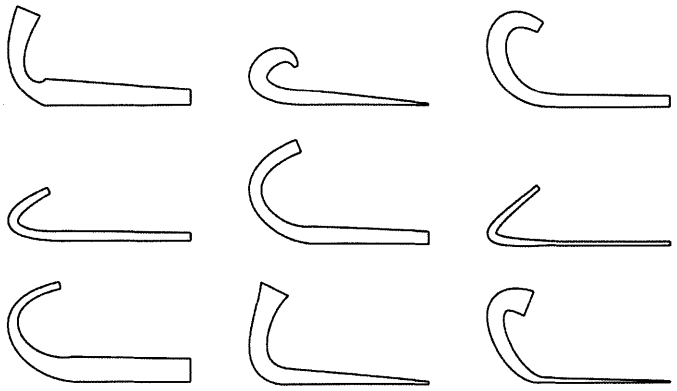

Figure 4-3: Various possible keel designs that fall within the defined design space

Examples of possible foot shapes explored through this particular parametrization are shown in Fig. 4-3.

4.2.2 Materials

The optimization was performed using nylon 6/6, with elastic modulus $E = 2.41$ GPa and yield strength $\sigma_y = 82.7$ MPa. Nylon was selected as a reasonable material choice for a low-cost prosthetic foot because the high ratio of yield strength to elastic modulus allows it to achieve a high strain energy density, and thus high deformations before yielding.

4.2.3 Constraints

Particular sets of design variables could yield wide Bézier curves that intersect themselves, resulting in a shape with no physical meaning. Self-intersection occurs either when the radius of curvature of the center Bézier curve is less than half the width of the outer shape (Fig. 4-4a), or the center curve creates a loop (Fig. 4-4b). These self-intersections can be prevented with the following constraints:

$$\max\left(0.5w_c - \rho\right) \leq 0 \tag{4.4}$$

and

(a) Self-Intersection Constraint Violation

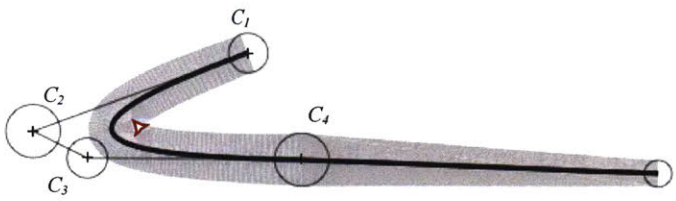

(b) Loop Constraint Violation

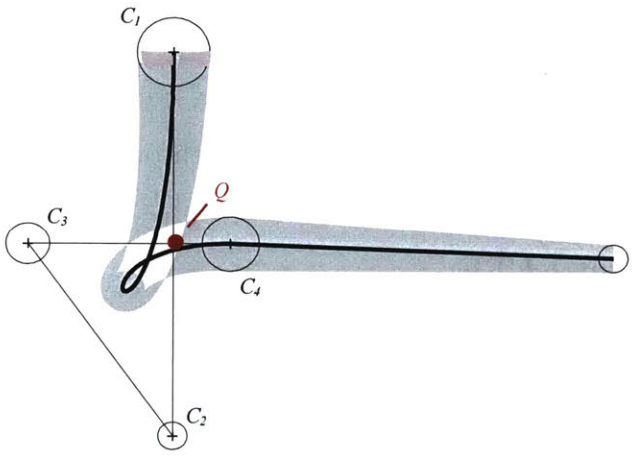

Figure 4-4: Certain combinations of design variables result in the keel shape intersecting itself, creating a design that is not physically meaningful. Constraints were imposed to prevent cases like those shown here from being included in the optimization.

$$(\frac{l\overline{C_1C_2}}{l\overline{QC_1}} - \frac{4}{3})(\frac{l\overline{C_2C_3}}{l\overline{QC_2}} - \frac{4}{3}) - \frac{4}{9} \leq 0, \tag{4.5}$$

where ρ is the radius of curvature of the center Bézier Curve, Q the point of intersection of line segments $\overline{C_1C_2}$ and $\overline{C_3C_4}$, as shown in Fig. 4-4b, and $l\overline{C_1C_2}$ is the length of the line segment between control points C_1 and C_2 and so on.

Since the size and shape parameterization defined $C_{3y} \equiv C_{4y}$ and the shape has been defined such that the bottom of the control circle C_4 is the bottom of the foot, if C_3d were greater than C_{4d} then the foot could protrude below the intended bottom surface. Therefore the linear inequality constraint

$$C_{3d} - C_{4d} \leq 0 \tag{4.6}$$

was included.

Finally, a constraint was imposed to limit the maximum stress in the foot structure:

$$\sigma_{max} - \sigma_{allow} \leq 0, \tag{4.7}$$

where $\sigma_{allow} \equiv \frac{\sigma_y}{F.S.}$ with $F.S.$, the factor of safety, equal to two in this case. The maximum stress in the structure, σ_{max}, was found through finite element analysis.

4.2.4 Evaluating LLTE

For the simple foot architectures optimized for LLTE in Chapter 2, shown in Fig. 2-4, the deformation of the foot under a given load could be calculated analytically. Thus each $x_{knee,n}^{model}$, $y_{knee,n}^{model}$, and $\theta_{knee,n}^{model}$ calculation in Eqn. (2.1) was computationally inexpensive, so it was possible to find these values for every time interval during a step for which data were available. Using Winter's published data set and only considering the portion of stance for which the ankle angle is less than 90°, there are data for a total of $N = 26$ time intervals, all of which were used in calculating the LLTE during optimization of the simple architectures in Chapter 2.

For the shapes of prosthetic feet considered in this work, there is no analytical solution to find the deformation of the foot structure in response to a given load. Rather, finite element analysis is required. To evaluate the LLTE for a single design, FEA must be performed N times to calculate the deformation at each of the N time intervals. Since FEA is computationally expensive, it is advantageous to minimize the number of time intervals required. To determine how many time intervals were necessary and which instances during the step best represented the step as a whole, the LLTE optimization was performed for the simple analytical prosthetic foot models from Chapter 2 using each possible subset of the 26 total data points. It was found that with $N = 5$, the optimal design variable values were each within 5% of those

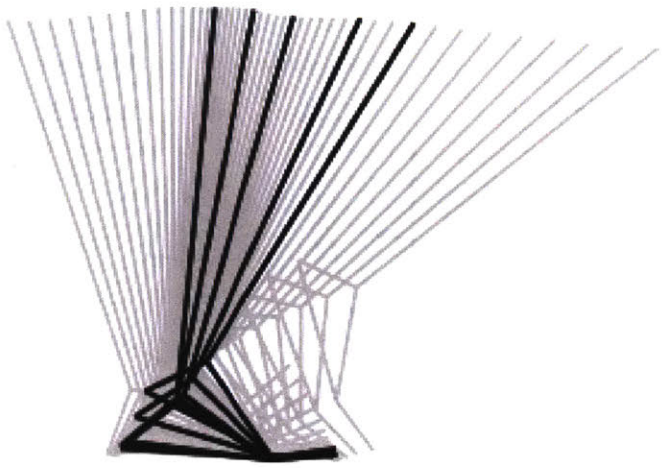

Figure 4-5: Of the 43 time intervals during stance included in Winter's published gait data [35] shown in grey, the foot is flat on the ground and the ankle is in dorsiflexion for 26. Of those 26, the five shown in black were found to best represent the entire step. When these five data points were used, the optimal design variable values for each of the two degree-of-freedom analytical models from Chapter 2 were each within a maximum difference of 5% of the optimal design variable values as found when all 26 available data points were used.

values found using all 26 data points if the five data points used were at 33%, 48%, 60%, 74%, and 81% of stance, where 0% is heel strike, 24% is the instant at which the ankle begins to dorsiflex past a neutral position, and 100% is toe-off (Fig. 4-5). As an example of the data used as model inputs and target outputs, the ground reaction forces and the positions of the lower leg segment for three of these five time intervals from Winter's data are shown in Fig. 4-6. For a given foot design, FEA was performed on the foot five times, once for each of the five time intervals.

The x, y, and θ coordinates of the knee and lower leg segment can be found from just the position of the node at which the GRFs were applied, given by (x_{load}, y_{load}) and the position of a node at the tip of the foot, (x_{end}, y_{end}), where each of those positions refer to the deformed foot under loading. For the purposes of this calculation, the end node to which (x_{end}, y_{end}) refers was a virtual point added to the FEA model at a position of 20 cm anterior to the ankle. This was 5 cm beyond the end of the physical foot, but provided a useful point that could be used to calculate the angle of the ground relative to the foot in the ankle-knee reference frame, particularly when the

(a) Global Reference Frame

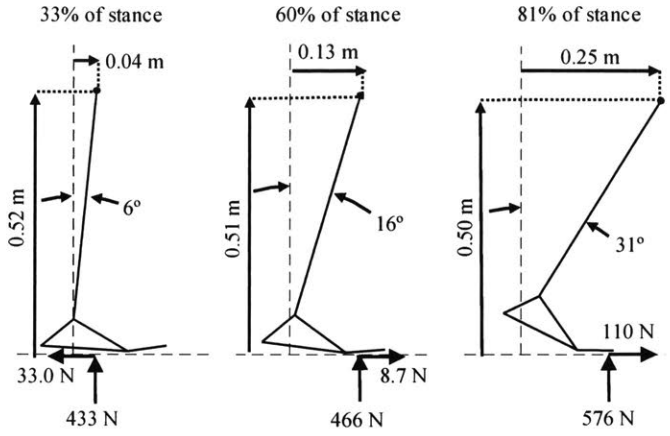

(b) Ankle-Knee Reference Frame

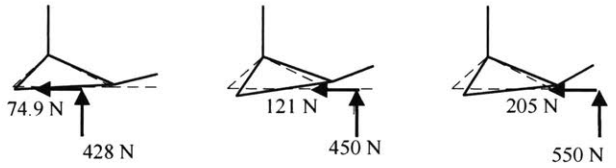

Figure 4-6: Free body diagrams of the ground reaction forces on the feet and the lower leg position during three of the five time intervals used in the finite element LLTE evaluation

center of pressure was very close to the tip of the physical foot. Because the toe of the foot was unconstrained and the only external loads were the ground reaction forces, there were no internal bending moments within the foot structure between the point at which the GRFs are applied and the tip of the finite element model of the foot. Consequently, this portion of the foot is undeformed, and the bottom of the foot distal to the loading point remains straight. For the center of pressure between the foot and the ground to indeed be at the node at which the loads have been applied, this entire segment of the foot, between the load point and the end of the foot, must be flat on the ground. The virtual end point on the finite element model does not affect these results; it only makes the length of the segment in contact with the ground longer, making the calculation of the angle of that segment more accurate. This is true as long as the center of pressure is proximal to the very end of the physical foot. When the center of pressure is at the end of the foot, the foot is only in point contact with the ground and can rotate rigidly about that point, so the position of the prosthesis

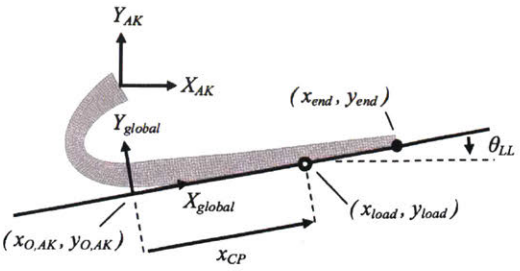

Figure 4-7: Example of a deformed foot result from the FE model in the ankle-knee reference frame with the variables used in Eqn. (4.8) - (4.10) labeled. The variables X_{AK}, Y_{AK}, X_{global}, and Y_{global} denote the x- and y-axes of the ankle-knee reference frame and the global reference frame, respectively.

is underconstrained by just the ground reaction forces and center of pressure and cannot be calculated from the ground reaction forces and center of pressure position without additional assumptions. Thus only the portion of stance right up until the center of pressure reaches this point is included in the optimization.

The angle between the ground and the horizontal in the ankle-knee reference frame in which the FEA was performed, and, equivalently, the angle of the lower leg segment with respect to vertical in the global reference frame, was calculated from the FEA results as

$$\theta_{LL} = \tan^{-1}\left(\frac{y_{end} - y_{load}}{x_{end} - x_{load}}\right), \tag{4.8}$$

as shown in Figure 4-7.

In the global reference frame, the origin was defined as the point of intersection between the ankle-knee axis and the ground when the ankle-knee axis is perpendicular to the ground during stance. Because the center of pressure data used as an input to the model is measured in the global reference frame, the x-coordinate of the center of pressure in the global reference frame is the distance between the center of pressure and the origin of the global reference frame along the ground. Then the coordinates of the global origin in the ankle-knee reference frame, $x_{O,AK}$ and $y_{O,AK}$ are given by

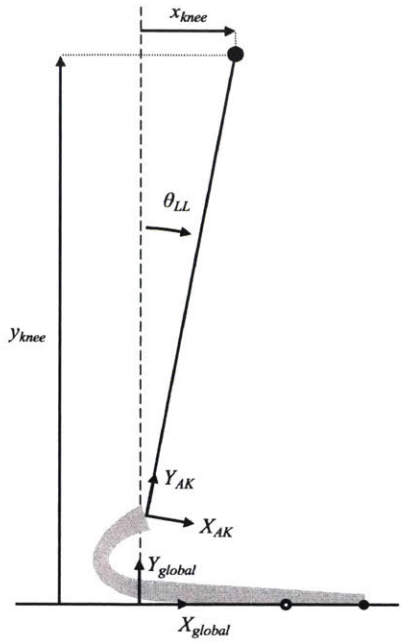

Figure 4-8: Deformed foot finite element results from Fig. 4-7 rotated into the global reference frame. The variables x_{knee}, y_{knee} and θ_{LL} shown here for the modeled foot are input into Eqn. (2.1) to compare these resulting kinematics to the target physiological data.

$$\begin{bmatrix} x_{O,AK} \\ y_{O,AK} \end{bmatrix} = \begin{bmatrix} x_{load} - x_{cp}\cos\theta_{LL} \\ y_{load} - x_{cp}\sin\theta_{LL} \end{bmatrix}. \tag{4.9}$$

Finally, the position of the knee in the global reference frame was found by taking the vector from the global reference frame origin to the knee in the global reference frame, then rotating the vector by θ_{LL} (Fig. 4-8). That is,

$$\begin{bmatrix} x_{knee} \\ y_{knee} \end{bmatrix} = \begin{bmatrix} \cos\theta_{LL} & \sin\theta_{LL} \\ -\sin\theta_{LL} & \cos\theta_{LL} \end{bmatrix} \cdot \begin{bmatrix} x_{AK} - x_{O,AK} \\ y_{AK} - y_{O,AK} \end{bmatrix}, \tag{4.10}$$

where x_{AK} and y_{AK} are the coordinates of the knee in the ankle-knee reference frame, so $x_{AK} = 0$ and $y_{AK} = L_{AK}$, with L_{AK} the length of the shank between the ankle and the knee, which is the distance from the knee to the ground in the input physiological data set minus the height of the prosthetic foot, h, for the particular design in consideration.

To automate the LLTE calculation for a particular design to allow for optimization, a custom MATLAB script was used to write and save text files containing input batch commands for ADINA, the commercially available FEA software used in this optimization. The commands within the text files defined the foot geometry as a 2D plane stress solid, meshed the surfaces using nine-node elements with edge length 2 mm, defined the material properties, and applied the appropriate loads. The displacement and strain options for the solver were left to their default value, which allows the solver to determine whether large or small displacement and strain formulations are more appropriate. A boundary condition was applied at the ankle to fix all degrees of freedom, as the analysis was performed in the ankle-knee reference frame, so any external loads would be opposed by reaction forces and moments at the ankle point, where the prosthetic foot would connect to the rest of the prosthesis. The finite element analysis was run via command line prompts executed through MATLAB. The results, namely the deformed position of the load node and the end node, were saved in another text file, which was read and processed via another custom MATLAB script, which calculated the $x_{knee,n}^{model}$, $y_{knee,n}^{model}$, and $\theta_{LL,n}^{model}$ corresponding to that load case using Eqns. (4.8) - (4.10). This was repeated for the other four load cases. Finally, the $x_{knee,n}^{model}$, $y_{knee,n}^{model}$, and $\theta_{LL,n}^{model}$ and the target physiological $x_{knee,n}^{phys}$, $y_{knee,n}^{phys}$, and $\theta_{LL,n}^{phys}$ values for all five cases were used with Eqn. (2.1) to calculate the LLTE value for that set of design variables.

4.2.5 Optimization Problem Formulation

The following optimization problem was solved to design the foot.

$$\left.\begin{aligned} \min_X: \quad & \mathrm{LLTE}(X) \\ \\ \text{subject to:} \quad & \max(0.5w_c - \rho) \leq 0 \\ : \quad & \left(\frac{l\overline{C_1C_2}}{l\overline{QC_1}} - \frac{4}{3}\right)\left(\frac{l\overline{C_2C_3}}{l\overline{QC_2}} - \frac{4}{3}\right) - \frac{4}{9} \leq 0 \\ : \quad & C_{3d} - C_{4d} \leq 0 \\ : \quad & \sigma_{max} - \sigma_{allow} \leq 0 \end{aligned}\right\} \tag{4.11}$$

The optimization was performed using a hybrid of MATLAB's built-in genetic algorithm function and pattern search optimization function. The objective function was a custom script which returned the LLTE value of a particular design following the previously described method. A custom mutation function was used in the genetic algorithm to increase the likelihood of valid mutations within the design variable bounds. The default mutation function in MATLAB for a bounded problem attempts a single random mutation without regards to bounds, then only uses this mutation in the next generation if all bounds happen to be met. If any one of the design variables is outside of its bounds, the mutation is not used. The original design is passed on to the next generation unchanged. This results in premature convergence on local minima. The custom mutation function changed each variable individually by a random amount selected from a normal distribution, similar to the default MATLAB mutation function for unbounded optimization problems. To account for the bounds, the standard deviation for one side of the normal distribution was decreased when a design variable was very close to one of its bounds such that it was unlikely that a mutated design variable would exceed the bound. If it did exceed the bound, that design variable was set equal to the bound it exceeded in the following generation.

This mutation function increased the diversity of designs explored through the genetic algorithm, increasing the likelihood that the optimal design found by the

algorithm was indeed the global minimum. To further ensure this was the case, the optimization was repeated five times to check that each of the optimal designs returned were nearly identical.

4.2.6 Prototype Fabrication and Finite Element Model Validation

Once the optimal keel design was found, a heel and a surface to attach the ankle of the foot to the rest of the prosthesis were incorporated. The heel was designed to be as thin as possible while maintaining a minimum factor of safety of two on the structure so that the bending of the heel beam would mimic early stance plantarflexion. The thickness of the heel beam was approximated by analytically calculating the thickness that would result in a factor of safety of two at the base of the heel beam. A heel beam of the calculated thickness was then added to the finite element model of the foot. The maximum heel strike ground reaction force from Winter's gait data was applied to the finite element model, and the resulting stress calculated. The width of the heel beam was adjusted until the minimum factor of safety in the structure was approximately equal to two.

The ankle of the finite element model foot used in the optimization was rigidly fixed to the rest of the prosthetic leg. To best replicate this condition without increasing the height of the foot more than necessary, material was added to the ankle portion of the foot, creating a horizontal surface to which a male pyramid adapter, the standard attachment method for prosthetic components, could be afixed.

Finally, the toe and heel of the foot were rounded in response to feedback obtained during previous testing of the simple prototypes discussed throughout this dissertation. According to subjects, the rounded heel and toe allow for smoother transitioning to and from the prosthetic foot, as well as improved maneuverability. The vertical thickness of the foot was adjusted to maintain the same bending stiffness in the toe despite the change in width into the plane of the page.

The prototype was machined from nylon 6/6 and a male pyramid adapter was

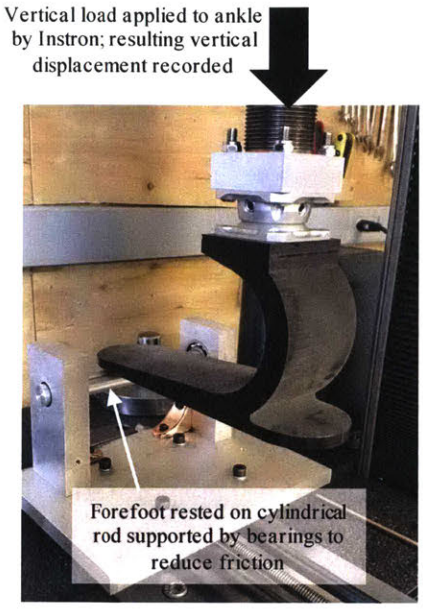

Figure 4-9: Experimental set up used to measure vertical displacement of the forefoot in response to applied vertical loading up to 658 N to validate finite element model of foot

attached to the ankle. An Instron material testing machine was used to measure the displacement of the prosthetic foot in response to loading and verify that the finite element analysis accurately modeled the prosthetic foot. To constrain the position of the load acting on the foot, the forefoot was placed on a cylindrical rod mounted on rotational bearings in a jig rigidly affixed to the lab bench (Fig. 4-9). This setup ensured the contact load on the forefoot would be normal to the face of the rod. The vertical load applied by the Instron was increased from 0 N to 658 N. At regular intervals during loading, the vertical displacement and the angle of the forefoot relative to the fixed circular rod were measured and recorded. The forefoot angle was used to calculate the horizontal load acting on the foot, as the Instron controls and records only vertical loads.

The measured vertical loads and calculated horizontal loads at seven different instances throughout loading were applied to the finite element model of the foot, including the heel and ankle attachment surface. A fully fixed boundary condition was applied to the surface of the ankle to which the male pyramid adapter was attached. The vertical displacement of the load point in response to these loads was

computed and compared to the equivalent value measured during Instron testing.

4.2.7 Preliminary Testing in India

Prototype feet were brought to India for qualitative testing at BMVSS to determine whether there were any obvious shortcomings of the methodology or this particular foot that needed to be addressed before an extensive study could be performed to quantitatively evaluate the foot. A total of six subjects with unilateral transtibial amputation, all of whom had at least one year of experience using the Jaipur Foot, were fit with the prototype. The subjects walked around a room with a smooth, tiled floor until they were comfortable with the foot. They were then asked to go up and down stairs and ramps, then finally outside to walk on uneven surfaces. This testing lasted no more than one hour. After completing these activities, the subjects provided qualitative assessments of the prototype. Quantitative metrics, such as Lichert scales, were not used, as experience has shown that subjects at BMVSS, most of whom are illiterate and have little to no formal education, are unfamiliar with the concept of numerical ratings, even if the numbers are replaced by textual descriptions (e.g. very bad, bad, ok, good, very good, etc.). Consequently, results from such studies are unreliable and can be misleading. However, if asked to qualitatively compare a prototype foot to his or her own prosthetic foot, the subjects are able to provide insightful responses that are informative for future design iterations.

4.3 Results

With the initial bounds given in Eqn. (4.2) and (4.3), the optimal design resulting from the optimization was

$$X = [0.0791, 0.0307, -0.1499, 0.0725, 0.0357, -0.1488, 0.0135, 0.0169, 0.1010],$$

with an LLTE value of 0.145. However, this design extended 12.2 cm posterior to the

ankle, far too much to fit in a standard shoe (Fig. 4-10). The lower bounds on C_{2x} and C_{3x} were then increased from -0.15 m to -0.07 m to limit the length of the foot in the posterior direction. Additionally, the upper bound on C_{2y} was decreased from 0.10 m to 0.00 m to force the foot to not extend above the ankle, which would make attaching the foot to the rest of the prosthesis difficult. With these new bounds, the optimization was run again, yielding an optimal design of

$$X = [0.1461, 0.0142, -0.0698, -0.0455, 0.0202, -0.0690, 0.0156, 0.0170, 0.1031],$$

with an LLTE value of 0.153. The optimal design no longer extended too far posterior to the ankle, but was very tall, with the vertical distance from the bottom of the foot to the ankle, h, nearly 15 cm. This would preclude users with long residual limbs from using the foot. To obtain the final optimal result, the upper bound for h was decreased from 0.15 m to 0.10 m, producing an optimal design of

$$X = [0.996, 0.0142, -0.0556, -0.0139, 0.0178, -0.0389, 0.0160, 0.0162, 0.1034],$$

which had an LLTE value of 0.186 and fit completely within the envelope of a biological foot. The maximum stress in this final optimal design was 41.3 MPa, for a minimum factor of safety of 2.00. The position of the modeled lower leg segment for this final optimal design, as calculated using finite element analysis, is compared to the target physiological lower leg trajectory in Fig. 4-11.

A heel and ankle attachment surface were designed following the method described above (Fig. 4-12). The foot was machined from nylon 6/6 and weighed 368 g. Using the supplier-provided elastic modulus defined in Section 4.2.2 of $E = 2.41$ GPa, the FEA solution gave a vertical displacement of 4.0 cm under a vertical load of 658 N applied at a horizontal distance of 13 cm from the ankle, 0.5 cm more than the Instron-measured displacement of 3.5 cm (Fig. 4-13). The elastic modulus of the material was later measured to be $E = 2.54$ GPa. With this measured modulus, the

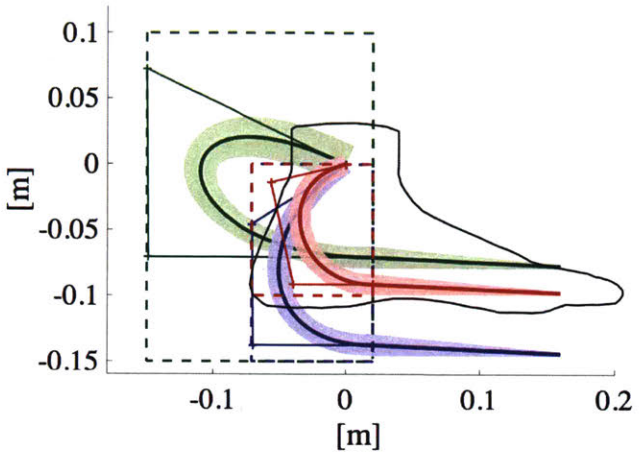

Figure 4-10: Optimal keel designs found through the wide Bézier curve optimization method. The inital bounds resulted in a foot with an LLTE value of 0.145 (shown in green), but too large to fit within the envelope of a biological foot (shown in black). The subsequent designs, shown in blue, and finally in red, have higher LLTE values, at 0.153 and 0.186, respectively, but only the final optimal design (red) meets the size and shape requirements of a prosthetic foot that can be used in daily life. Note that in this figure, the three designs and the outline of the foot are aligned by the ankle position as defined in Section 4.2.1. The length of the pylon connecting the user's socket to the ankle of the foot would be adjusted to ensure the length of the prosthetic-side leg was equal to that of the biological leg.

FEA solution gave a vertical displacement of 3.8 cm under the same vertical load, reducing the difference between the FEA and measured results to 0.3 cm.

Subjects who tested the foot provided mixed feedback. Younger subjects who prioritized mobility over stability liked the foot's energy storage and return compared to the Jaipur foot, which returns very little energy to the user. One subject commented that he could not run with the Jaipur Foot, but could with the prototype. Older subjects and some particularly cautious younger subjects felt unstable on the prototype. Most subjects liked the reduced weight of the prototype relative to the Jaipur Foot, which weighs between 800 g and 1 kg, however one subject commented that because of the lighter weight, he was afraid the foot would break. All subjects commented that they would need a cosmetic cover for the prototype to make it look like a biological foot before they could use it daily. The doctors who run BMVSS and the author agreed that the negative comments were all either related to the particular subject

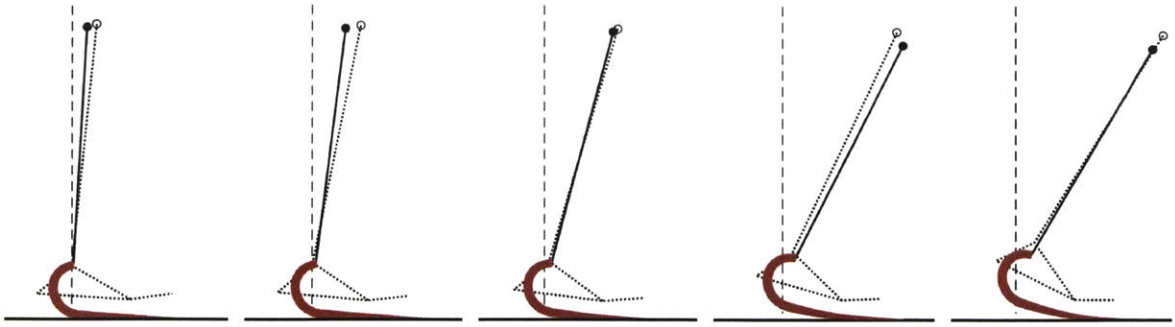

Figure 4-11: Lower leg trajectory for the final optimal compliant foot (red foot design in Fig. 4-10, solid line showing lower leg trajectory here) compared to the target physiological lower leg trajectory (dotted line) for each of the five loading scenarios considered. The phyisological data shows the position of the markers at the knee, ankle, heel, metatarsal, and toe as collected during typical, unimpared walking. Because these markers were placed at physical locations on the subject's foot, there is space between the markers and the ground in the physiological data.

Figure 4-12: Solid model of foot based on optimal design, with added heel and male pyramid adapter to attach the foot to the rest of the prosthesis

not being a candidate for an energy storage and return-type foot, which are typically only prescribed to more active subjects, or to the prototype being very different from the Jaipur Foot, which the subjects had been using for a minimum of 10 years and a maximum of 47 years. None of the feedback necessitated significant changes to the design. The BMVSS doctors and the author agreed that the foot will be ready for an extended field trial over the course of several weeks as soon as a cosmetic cover is incorporated. This cosmetic cover must both look like a biological foot and be able to withstand harsh environments, such as barefoot use on rough terrain and submersion in water.

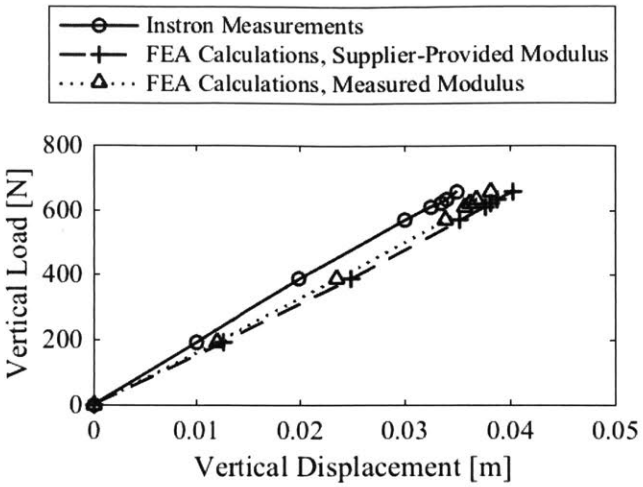

Figure 4-13: Comparison of Instron-measured and FEA-calculated vertical displacements under loads applied at a horizontal distance of 13 cm from the ankle for both the supplier-provided elastic modulus, $E = 2.41$ GPa, and the measured elastic modulus, $E = 2.54$ GPa

4.4 Discussion

To contextualize the optimal design from this wide Bézier curve optimization, the LLTE-optimal designs for the simple foot architectures from Chapter 2 had LLTE values of 0.269 for the rigid circular foot, 0.172 for the foot with the rotational ankle and metatarsal joints, and 0.187 for the foot with a rotational ankle joint and a cantilever beam forefoot when evaluated using the same fives loading scenarios as were used for the single part prototype. Note that these values are different than those found in Table 2.1 as these values were calculated using only the five loading scenarios used in the single part foot optimization employed here, rather than using all 26 loading scenarios as was done in Chapter 2. The first two optimal designs of the single part keel (green and blue curves in Fig. 4-10) had smaller LLTE values than any of the simple foot architectures, so they would better replicate the target physiological lower leg trajectory under the five loading scenarios used. When the size of the single part keel was constrained to fit within the envelope of a biological foot, the LLTE value increased to 0.186, approximately equivalent to the simple foot with the rotational ankle and cantilever beam forefoot, and slightly larger than that for the foot with roational ankle and metatarsal joints. However, the single part keel was

the only foot that met the critical requirement of being smaller than a biological foot, which would allow it to fit within a cosmetic and protective cover and be used in shoes. Therefore, this slight decrease in performance is necessary to produce a prosthetic foot for daily use. Additionally, because the wide Bézier curve design does not require multiple parts, such as a spring, axis of rotation, or rigid structural elements, it can be made significantly lighter than either of the articulated simple architectures presented. Multiple experimental prototypes have been made to replicate the optimal designs of the simple architectures while minimizing the mass of the foot, such as those shown in Fig. 3-1b and C-7, but the minimum mass achieved was 980 g, approximately 2.7 times the mass of the wide Bézier curve foot. Furthermore, the method presented here yields a design that is much easier to manufacture than the prototypes with articulated ankle joints, as the wide Bézier curve foot consists of a single nylon part that could easily be injection molded or extruded.

The genetic algorithm optimization took an average of 15 hours, 1 min and 44 seconds to run. The subsequent pattern search optimization took an additional 1 hour, 38 min and 51 seconds on average. Evaluating the LLTE value for a single design took an average of 6.06 seconds. The primary purpose of this work was to develop a framework to use wide Bézier curve parameterization and a combination of MATLAB scripts and ADINA FEA software to produce a single-part prosthetic foot with a minimal LLTE value.

The following limitations to this work affected the general applicability of the resulting optimal foot, but were not addressed here because they would increase the optimization run time. Further analyses will be performed in the future to determine which of these limitations impact the results significantly enough to merit the additional optimization time that would be required to resolve them. The complexity of the final design was limited by the definition of the design space, as was shown in Fig. 4-2. In future work, a more comprehensive design space will be explored by adding complexity with additional design variables, such as using higher-order Bézier curves to define the shape of the foot. The heel could also be incorporated into the optimization rather than optimizing the keel and forefoot and then designing a heel

around that structure. Loading scenarios from early stance plantarflexion, when the center of pressure is posterior to the ankle, could then be included in the LLTE evaluation. Similarly, the surface to which the male pyramid adapter was attached could be included to improve the accuracy of the boundary conditions on the finite element model.

The shape of the foot has been optimized based on only five loading scenarios that are assumed to be adequately representative of the entire step. The lower leg trajectory of the prosthetic foot designed through the optimization may better replicate physiological gait kinematics throughout the whole step if more loading scenarios are included. The optimization runtime should scale linearly with the number of loading scenarios included, as each LLTE evaluation would perform an additional FEA simulation for each additional loading scenario, and the LLTE evaluation time is dominated by the FEA simulations. The number of function evaluations would not change significantly so long as the rate of convergence was not affected by the number of loading scenarios. Future work may include using more than five loading scenarios to determine if and how much the optimal design is affected.

Another potential source of error that could limit how accurately the FEA represents the kinematics of the foot during actual use is the direction of the GRF applied on the FE model. The input GRFs were measured in the global reference frame, then translated into the ankle-knee reference frame based on the orientation of the lower leg in the physiological data set to be applied to the ankle-knee reference frame-based FE model. The orientation of the ankle-knee reference frame of the wide Bézier curve foot during a particular load scenario depends on the deformed shape of the foot, which is dependent on the direction of the applied load. Thus, if and only if the foot deforms in such a way as to exactly replicate the orientation of the ankle-knee reference frame in the physiological data set, that is, $\theta_{LL,n}^{model} - \theta_{LL,n}^{phys} = 0$ in Eqn (2.1), the loading in the FEA is exactly equivalent to that in the input physiological gait data when both are rotated back into the global reference frame. Otherwise, the GRF magnitude is equivalent, but it is rotated by an amount equal to $\theta_{LL,n}^{model} - \theta_{LL,n}^{phys}$ relative to the GRF as measured in the global reference frame. For the optimal wide Bézier

curve foot design presented here, the loading was rotated by a maximum of 4.18° relative to the direction of the GRF measured in the global reference frame. This source of error could be eliminated through iteratively solving for the orientation of the ankle-knee reference frame for the wide Bézier curve foot. This iterative process would have to be repeated for each loading scenario, with each iteration requiring an additional FEA simulation until the orientation of the ankle-knee reference frame used to calculate the loads applied to the FE model converged with the ankle-knee reference frame found from the deformed shape of the foot. This would consequently significantly increase the runtime of the LLTE evaluation for a single design, but would most likely not affect the number of evaluations required for the optimization.

Because a set of published gait data for a single person was used both for the input kinetic data and for the target kinematic data, the optimal design is valid only for people of similar body mass and leg lengths as the subject with whom the data was recorded. After preliminary testing on subjects of similar size to clinically validate the method presented here, the method can be applied using sets of gait data for various body masses and leg lengths to produce a range of prosthetic feet to accommodate all potential users. Further, the input data can easily be adjusted proportionally to different users' body weight and size. The flexibility of the design and optimization presented here may enable the creation of customized, 3D printed prosthetic feet for specific individuals.

4.5 Conclusions

The shape and size of a prosthetic foot was optimized as a compliant mechanism with the objective of minimizing the Lower Leg Trajectory Error (LLTE) compared to able-bodied values. The forefoot was parameterized as a wide Bézier curve with constraints imposed such that only physically meaningful shapes were considered. The deformed shape of each foot design was calculated for five different loading scenarios representative of different phases of stance using ADINA finite element analysis software, run through a custom MATLAB script. From the deformed shape of the

foot, the position of the knee and the orientation of the lower leg segment were found and used to evaluate the LLTE for that particular design. A hybrid of the genetic algorithm and pattern search optimization functions built into the MATLAB optimization toolbox was used to perform the optimization. The final optimal design had an LLTE value similar to previously analyzed articulated prototypes, but unlike these prototypes, the compliant foot fit within the envelope of a biological foot, a critical requirement for a daily-use prosthetic foot. Furthermore, at 368 g, the optimal foot was less than half the weight of the articulated prototypes. The single-part design compliant foot is also far easier to manufacture.

The resulting design was built and tested on an Instron material testing machine to demonstrate that the finite element analysis used to optimize the foot indeed matched the physical foot. Under a load of 682 N applied at a horizontal distance of 13 cm from the ankle, the maximum difference between the Instron-measured vertical displacement and finite element results was 0.3 cm, or 9% of the FEA predicted displacement, which is within the expected error of the measurement apparatus. The foot was tested qualitatively with our partner organization in India, which revealed no major design flaws. In the near future, a cosmetic and protective cover will be built for the foot so that an extended field trial can be conducted for more feedback in how the foot performs in daily activities.

THIS PAGE INTENTIONALLY LEFT BLANK

Bibliography

[1] Jaipurfoot.org. Accessed 9/9/2017.

[2] Peter Gabriel Adamczyk and Arthur D Kuo. Mechanisms of gait asymmetry due to push-off deficiency in unilateral amputees. *IEEE Transactions on Neural Systems and Rehabilitation Engineering*, 23(5):776–785, 2015.

[3] A. P. Arya, A. Lees, H. C. Nirula, and L. Klenerman. A biomechanical comparison of the SACH, Seattle and Jaipur feet using ground reaction forces. *Prosthetics and Orthotics International*, 19:37–45, 1995.

[4] Xavier Bonnet, Coralie Villa, Pascale Fode, Francois Lavaste, and Helene Pillet. Mechanical work performed by individual limbs of transfemoral amputees during step-to-step transitions: effect of walking velocity. *Proceedings of the Institution of Mechanical Engineers. Part H, Journal of engineering in medicine*, 228(1):60–66, 2014.

[5] Tyler E Bruns and Daniel A Tortorelli. Topology optimization of non-linear elastic structures and compliant mechanisms. *Computer Methods in Applied Mechanics and Engineering*, 190(26):3443–3459, 2001.

[6] Lin Cao, Allan T Dolovich, and Wenjun Chris Zhang. Hybrid compliant mechanism design using a mixed mesh of flexure hinge elements and beam elements through topology optimization. *Journal of Mechanical Design*, 137(9):092303, 2015.

[7] Sangamesh R Deepak, M Dinesh, Deepak K Sahu, and GK Ananthasuresh. A comparative study of the formulations and benchmark problems for the topology optimization of compliant mechanisms. *Journal of Mechanisms and Robotics*, 1(1):011003, 2009.

[8] Nicholas P. Fey, Glenn K. Klute, and Richard R. Neptune. The influence of energy storage and return foot stiffness on walking mechanics and muscle activity in below-knee amputees. *Clinical Biomechanics*, 26:1025–1032, 2011.

[9] M I Frecker, G K Ananthasuresh, S Nishiwaki, N Kikuchi, and S Kota. Topological Synthesis of Compliant Mechanisms Using Multi-Criteria Optimization. *Journal of Mechanical Design*, 119(2):238–245, jun 1997.

[10] Brian J. Hafner. Clinical Prescription and Use of Prosthetic Foot and Ankle Mechanisms: A Review of the Literature. *Journal of Prosthetics and Orthotics*, 17(4):S5–S11, 2005.

[11] A. H. Hansen, D. S. Childress, and E. H. Knox. Prosthetic foot rollâĂŘover shapes with implications for alignment of transâĂŘtibial prostheses. *Prosthetics and Orthotics International*, 24(3):205–215, 2000.

[12] Andrew H Hansen and Dudley S Childress. Effects of shoe heel height on biologic rollover characteristics during walking. *Journal of Rehabilitation Research & Development*, 41(4):547–554, 2004.

[13] Andrew H. Hansen and Dudley S. Childress. Effects of adding weight to the torso on roll-over characteristics of walking. *The Journal of Rehabilitation Research and Development*, 42(3):381, 2005.

[14] Andrew H. Hansen, Dudley S. Childress, and Erick H. Knox. Roll-over shapes of human locomotor systems: effects of walking speed. *Clinical Biomechanics*, 19:407–414, 2004.

[15] J A Hetrick and S Kota. An Energy Formulation for Parametric Size and Shape Optimization of Compliant Mechanisms. *Journal of Mechanical Design*, 121(2):229–234, jun 1999.

[16] CJ Hofstad, H Van Der Linde, J Van Limbeek, and K Postema. Prescription of prosthetic ankle-foot mechanisms after lower limb amputation (Review). *The Cochrane Library*, (1), 2009.

[17] Han Houdijk, Eveline Pollmann, Marlies Groenewold, Han Wiggerts, and Wojtek Polomski. The energy cost for the step-to-step transition in amputee walking. *Gait & Posture*, 30(1):35–40, 2009.

[18] Larry L Howell. *Compliant mechanisms*. John Wiley & Sons, 2001.

[19] Elizabeth Klodd, Andrew Hansen, Stefania Fatone, and Mark Edwards. Effects of prosthetic foot forefoot flexibility on oxygen cost and subjective preference rankings of unilateral transtibial prosthesis users. *Journal of Rehabilitation Research & Development*, 47(6):543–552, 2010.

[20] Elizabeth Klodd, Andrew Hansen, Stefania Fatone, B P O Hons, and Mark Edwards. Effects of prosthetic foot forefoot flexibility on gait of unilateral transtibial prosthesis users. *Journal of Rehabilitation Research & Development*, 47(9):899–910, 2010.

[21] Chao-Chieh Lan and Yung-Jen Cheng. Distributed shape optimization of compliant mechanisms using intrinsic functions. *Journal of Mechanical Design*, 130(7):072304, 2008.

[22] Van Der Linde, J Cheriel, and C H Alexander. A systematic literature review of the effect of different prosthetic components on human functioning with a lower-limb prosthesis. *Journal of Rehabilitation Research & Development*, 41(4):555–570, 2004.

[23] Kerr-Jia Lu and Sridhar Kota. Topology and dimensional synthesis of compliant mechanisms using discrete optimization. *Journal of Mechanical Design*, 128(5):1080–1091, 2006.

[24] Naesung Lyu and Kazuhiro Saitou. Topology optimization of multi-component structures via decomposition-based assembly synthesis. In *ASME International Design Engineering Technical Conferences and Computers and Information in Engineering Conference*, pages 269–281. American Society of Mechanical Engineers, 2003.

[25] M J Major, L P Kenney, M Twiste, and D Howard. Stance phase mechanical characterization of transtibial prostheses distal to the socket: a review. *Journal of Rehabilitation Research and Development*, 49(6):815–829, 2012.

[26] Marc J. Nederhand, Edwin HF Van Asseldonk, Herman van der Kooij, and Hans S. Rietman. Dynamic Balance Control (DBC) in lower leg amputee subjects; contribution of the regulatory activity of the prosthesis side. *Clinical Biomechanics*, 27(1):40–45, 2012.

[27] Kathryn M. Olesnavage and Amos G. Winter V. "Clinical validation of predicting lower leg trajectory for passive prosthetic feet using physiological data as inputs". In review.

[28] Kathryn M. Olesnavage and Amos G. Winter V. Design and qualitative testing of a prosthetic foot with rotational ankle and metatarsal joints to mimic physiological roll-over shape. In *ASME International Design Engineering Technical Conferences and Computers and Information in Engineering Conference (IDETC/CIE)*, 2015.

[29] Kathryn M. Olesnavage and Amos G. Winter V. Lower Leg Trajectory Error: A novel optimization parameter for designing passive prosthetic feet. In *IEEE International Conference on Rehabilitation Robotics (ICORR)*, pages 271–276, 2015.

[30] Kathryn M. Olesnavage and Amos G. Winter V. Design and preliminary testing of a prototype for evaluating lower leg trajectory error as an optimization metric for prosthetic feet. In *ASME International Design Engineering Technical Conferences and Computers and Information in Engineering Conference (IDETC/CIE)*, 2016.

[31] Kathryn Michelle Olesnavage and Amos G. Winter V. "A novel framework for quantitatively connecting the mechanical design of passive prosthetic feet to lower leg trajectory". In revision.

[32] Ottobock US. professionals.ottobockus.com, Accessed 9/26/2017.

[33] M Santer and S Pellegrino. Topological optimization of compliant adaptive wing structure. *American Institute of Aeronautics and Astronautics Journal*, 47(3):523–534, 2009.

[34] A Saxena and G K Ananthasuresh. Topology Synthesis of Compliant Mechanisms for Nonlinear Force-Deflection and Curved Path Specifications. *Journal of Mechanical Design*, 123(1):33–42, sep 1999.

[35] David A. Winter. *Biomechanics and Motor Control of Human Movement.* John Wiley & Sons, Inc., Hoboken, New Jersey, 4th edition, 2009.

[36] Dong Xu and G K Ananthasuresh. Freeform Skeletal Shape Optimization of Compliant Mechanisms. *Journal of Mechanical Design*, 125(2):253–261, jun 2003.

[37] Karl E. Zelik, Steven H. Collins, Peter G. Adamczyk, Ava D. Segal, Glenn K. Klute, David C. Morgenroth, Michael E. Hahn, Michael S. Orendurff, Joseph M. Czerniecki, and Arthur D. Kuo. Systematic variation of prosthetic foot spring affects center-of-mass mechanics and metabolic cost during walking. *IEEE Transactions on Neural Systems and Rehabilitation Engineering*, 19(4):411–419, 2011.

[38] Hong Zhou and Kwun-Lon Ting. Shape and size synthesis of compliant mechanisms using wide curve theory. *Journal of Mechanical Design*, 128(3):551–558, 2006.

Chapter 5

Conclusion

This thesis has presented a novel method to connect the mechanical design of a prosthetic foot to its biomechanical functionality using fundamental physics, as well as a framework to use this method in optimizing the design of a prosthetic foot. This approach was used to optimize the designs of three different simple conceptual foot models to demonstrate the its functionality. One of these simple foot models was built as an experimental prototype with variable ankle stiffness and tested by a subject with a unilateral transtibial amputation under five different ankle stiffness conditions. Across five ddifferent prosthetic-side steps on the experimental foot with each of the five ankle stiffness conditions, the constitutive model used in the optimization method accurately predicted the position of the knee to within an average of 1.0 cm in the horizontal direction and 0.3 cm in the vertical direction. The angular orientation of the lower leg was predicted to within an average of 1.5°, demonstrating that the theoretical method is valid in a clinical context. Finally, a framework was developed to optimize the shape and size of a single-part compliant prosthetic foot to best replicate the target physiological lower leg trajectory. The resulting optimal foot design was built out of nylon and tested qualitatively with BMVSS, a partner organization in India.

Future work will involve further evaluating the framework presented here both to better understand prosthetic foot performance as well as expand the potential applications, while simultaneously continuing to develop the single-part foot designed

in Chapter 4 to provide BMVSS with a new product that meets their needs while also being mass-manufacturable. For the foot designed for BMVSS, a cosmetic and protective cover will be designed to ensure test subjects are comfortable wearing the foot in their daily lives. Subjects from BMVSS will then be fit with the prototype feet and asked to use them for several weeks while providing feedback as part of an extended field trial. This will provide insight into the functionality of the foot in daily activities not explicitly incorporated in the optimization process as well as the durability of the foot during typical use in India. Feedback from the extended field trial will be used to further refine the design. Once the foot design is deemed satisfactory, it will be transitioned to a commercial product with the help of our partnership with BMVSS and local manufacturers.

The framework presented here will be further explored in parallel to better understand the factors that drive prosthetic foot performance. Clinical gait studies will continue to be conducted to evaluate Lower Leg Trajectory Error (LLTE) as a design objective for prosthetic feet. In addition to studies in which experimental feet are designed using the LLTE framework, such as that described in Chapter 3, the LLTE value can be measured for commercially available prosthetic feet to investigate whether correlations exist between LLTE values and clinical performance metrics, such as metabolic cost of walking, gait symmetry, and subjective user preference. The methodology can also be expanded to incorporate activities other than flat ground walking. The quantitative LLTE function provides the means to understand tradeoffs in prosthetic foot performance, which gives designers the tools to tune feet for different applications or users. Different sets of target physiological gait data can be used to customize prosthetic feet for particular users, such as women, children, or a person of a particular height, weight, and activity level.

While the novel framework presented here may or may not lead to an overall improvement in prosthetic foot performance, it will certainly lead to an improved understanding of how the mechanical design of a prosthetic foot affects its functionality.

Appendix A

Considerations in Selecting Particular Variables and Normalization Factors in LLTE Definition

The focus of this work is the novel framework of predicting the lower leg trajectory for a modeled prosthetic foot and comparing that trajectory to a target lower leg trajectory, thereby creating a prosthesis that seamlessly integrates into the body's natural motion and loading. In order to use this approach to optimize prosthetic feet, it was necessary to define a particular cost function, that given in Eq. (2.1). As is often the case in formulating optimization problems, there are an infinite number of potential cost functions that could be used to quantify the difference between a modeled and physiological lower leg trajectory. Clinical studies, such as that performed by the authors in conjunction with this work [1], are required to better inform the definition of this cost function. In the absence of clinical evidence at the time of writing, the authors have defined the cost function to provide what they believe is the most logical comparison between modeled and targeted data. The rationale for the definition of the cost function as defined in this work is described here.

Exactly three independent variables define the position of a line segment in two-dimensional space. There are an infinite number of variables that could be chosen to define the position of the lower leg segment at each time, but if more than three are

used, any variables beyond the initial three can always be defined in terms of these three variables and constants inherent to the problem. For example, if the x- and y-positions of both the ankle and the knee were selected (four variables total), the y-position of the knee could be written as

$$y_{knee} = y_{ank} + \sqrt{L_{shank}^2 - (x_{knee} - x_{ank})^2}, \tag{A.1}$$

where L_{shank} is the length of the lower leg segment, which remains constant. Writing y_{knee} in terms of x_{ank}, y_{ank}, and x_{knee} shows that y_{knee} is a dependent variable rather than a fourth independent variable.

Of the infinite number of possibilities, two sets of three independent variables were identified by the authors as the most intuitive: (1) the x- and y- position of the ankle joint and the angular orientation of the lower leg segment with respect to vertical, and (2) the x- and y- position of the knee joint and the angular orientation of the lower leg segment with respect to vertical. These sets of variables were selected because markers are typically placed on the ankle and knee during gait analysis studies, so data for the position of these two anatomical positions are readily available without additional post-processing. The angle of the lower leg segment with respect to vertical was included as the third variable because it was more logical to the authors to use the angle rather than one or the other of the x and y positions of either the ankle or knee joint as the third variable. In the ICORR paper that first presented this framework, the lower leg trajectory was defined using the position of the ankle and the orientation of the lower leg segment [2]. In the time since that work was published, the authors reached the conclusion that the knee was a preferrable reference point, as the motion at the knee is much larger than the motion at the ankle during stance phase, so any differences in position are magnified at the knee relative to the ankle. Additionally, a person with a transtibial amputation receives direct feedback from his or her biological knee joint and consequently may be more sensitive to kinematic differences at the knee than at the ankle.

Regardless of the variables chosen, a normalization factor must be used to evaluate

the cumulative distance between two data sets containing three different variables. Even if the variables have the same units, such as the x- and y-positions of the knee joint, a normalization factor is necessary to provide context for the difference between modeled and measured data, as a difference of 5 cm may not be much for the x-position of the knee, which moves a total of 26 cm during controlled dorsiflexion, but may be substantial for the y-position of the knee, which moves 2 cm in the same time period. Therefore, regardless of the choice of variables used to define the position of the lower leg segment, it will always be necessary to select a normalization factor.

The most common normalization factors in comparing model-predicted values to a measured data set (the physiological gait data in this context) are the mean of the measured data set, the range of the measured data set, or the individual data point values. In Eq. (2.1), the physiological mean is used as the normalization factor. If the range or individual data point values were used instead, the cost function equation would become

$$LLTE \equiv \left[\frac{1}{N}\sum_{n=1}^{N}\left\{\left(\frac{x_{knee,n}^{model}-x_{knee,n}^{phys}}{\max\left(x_{knee}^{phys}\right)-\min\left(x_{knee}^{phys}\right)}\right)^2 + \left(\frac{y_{knee,n}^{model}-y_{knee,n}^{phys}}{\max\left(y_{knee}^{phys}\right)-\min\left(y_{knee}^{phys}\right)}\right)^2 + \left(\frac{\theta_{LL,n}^{model}-\theta_{LL,n}^{phys}}{\max\left(\theta_{knee}^{phys}\right)-\min\left(\theta_{knee}^{phys}\right)}\right)^2\right\}\right]^{\frac{1}{2}} \tag{A.2}$$

or

$$LLTE \equiv \left[\frac{1}{N} \sum_{n=1}^{N} \left\{ \left(\frac{x_{knee,n}^{model} - x_{knee,n}^{phys}}{x_{knee,n}^{phys}} \right)^2 + \left(\frac{y_{knee,n}^{model} - y_{knee,n}^{phys}}{y_{knee,n}^{phys}} \right)^2 + \left(\frac{\theta_{LL,n}^{model} - \theta_{LL,n}^{phys}}{\theta_{LL,n}^{phys}} \right)^2 \right\} \right]^{\frac{1}{2}}. \tag{A.3}$$

Ideally, the normalization factors serve the purpose of weighting each term in the above equations as equally as possible, both in time over the course of the step, and in each of the three variables, x_{knee}, y_{knee}, and θ_{LL}. In the previous ICORR publication, the physiological range was used as the normalization factor. This was appropriate with the x- and y-position of the ankle defining the lower leg position, since the range for both variables was similarly small. However, the x-position of the knee and the angular orientation of the lower leg segment vary much more than the y-position of the knee during stance. Consequently, the normalization factor for the y-term in Eq. (A.2) was very small, causing the y-term to dominate the LLTE value for a given design, which resulted in an optimal design that replicated the y-position of the physiological knee very closely, but were far from the x-position of the knee and the angular orientation of the lower leg, as shown in Fig. A-1a for the rotational ankle and metatarsal foot architecture.

Ultimately, normalizing by physiological means was chosen in this work rather than by individual phsyiological data point values, as the optimal designs more closely replicated all three variables throughout the entire step, particularly toward the beginning of the controlled dorsiflexion phase, as shown in comparing Fig. A-1b to Fig. 2-8b.

As previously stated, it is necessary to define a cost function, such as that in Eq. (2.1), to design feet using this framework, which can then be used to evaluate and refine the framework, and, in particular, the cost function definition. Such work requires substantial time and effort, but cannot begin without an initial definition of

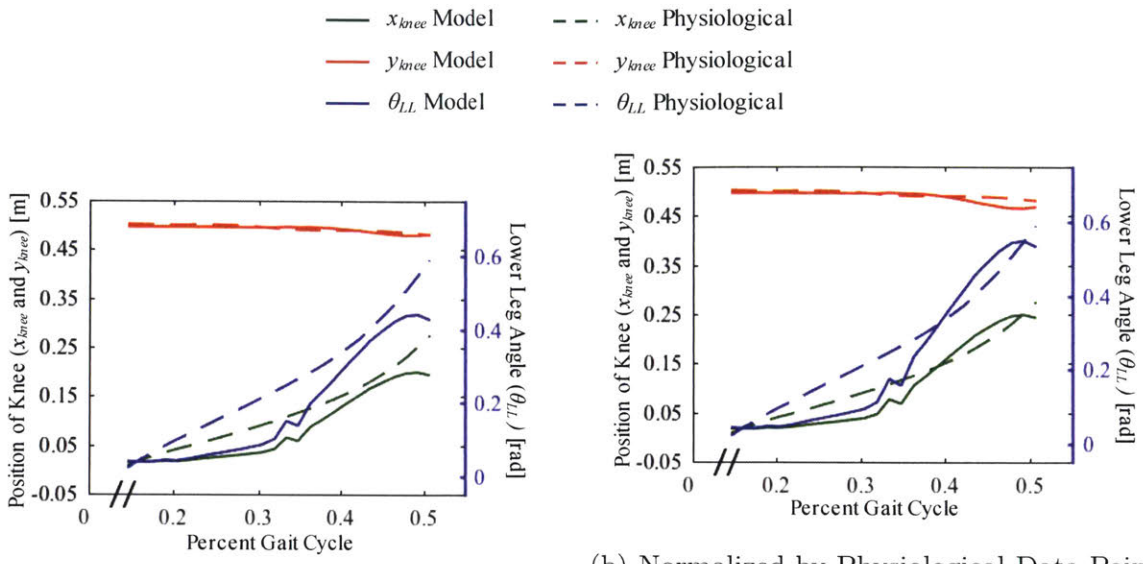

(a) Normalized by Physiological Range

(b) Normalized by Physiological Data Point Value

Figure A-1: x_{knee}, y_{knee}, and θ_{LL} for optimal designs for the rotational ankle and metatarsal foot architecture using cost functions with terms normalized by (a) physiological range (Eq. (A.2), $k^*_{ank} = 9.0$ N·m/deg, $k^*_{met} = 2.2$ N·m/deg) and (b) physiological data point values (Eq. (A.3), $k^*_{ank} = 8.2$ N·m/deg, $k^*_{met} = 1.6$ N·m/deg). The error was distributed better both in time across the step and between each of the three spatial variables when the physiological mean was used as the normalization factor as in Eq. (2.1) (Fig. 2-8b).

the cost function. The authors encourage other researchers to employ this framework with variations on the cost function. Regardless of the exact cost function definition, the framework presented here provides a means to connect the mechanical design of a prosthetic foot to its biomechanical functionality in terms of kinetics and kinematics, that will aid in understanding differences observed when multiple prosthetic feet of different mechanical designs are compared.

THIS PAGE INTENTIONALLY LEFT BLANK

Bibliography

[1] Kathryn M. Olesnavage and Amos G. Winter V. Clinical validation of predicting lower leg trajectory for passive prosthetic feet using physiological data as inputs. In review.

[2] Kathryn M. Olesnavage and Amos G. Winter V. Lower leg trajectory error: A novel optimization parameter for designing passive prosthetic feet. In *IEEE International Conference on Rehabilitation Robotics (ICORR)*, pages 271–276, August 2015.

THIS PAGE INTENTIONALLY LEFT BLANK

Appendix B

Design and Qualitative Testing of a Prosthetic Foot with Rotational Ankle and Metatarsal Joints to Mimic Physiological Roll-Over Shape

Appendices B and C were left out of the body of this dissertation as they each describe work that was done prior to settling on the definition of LLTE given in Eqn. (2.1). *However, they are included in the appendix as valuable lessons were learned through the work that informed both the LLTE framework and the functional requirements of a prosthetic foot to meet the needs of the intended users. Appendix B describes optimizing the design of the simple prosthetic foot architecture with rotational joints at the ankle and metatarsal, discussed in Chapter 2, to replicate physiological roll-over geometry. After performing this optimization, it was clear to the author that the roll-over optimal result would not produce close-to physiological kinematics when acted upon by physiological ground reaction forces, which lead her to further explore roll-over geometry and its limitations as a design objective, as discussed in Chapter 2. The design optimized here in Appendix B was also built and tested with subjects at BMVSS, which showed that this architecture was very difficult to keep lightweight in*

implementation, leading the author to consider the beam forefoot architecture, which was first built as described in Appendix C, then further improved upon to yield the design presented in Chapter 3. Thus while the exact methodologies presented in Appendices B and C are outdated, they are included here to provide the reader with a more complete rationale for the work in this dissertation.

B.1 Introduction

Bhagwan Mahaveer Viklang Sahayata Samiti (BMVSS), based in Jaipur, India, is one of the world's largest distributors of assitive devices [5]. In 2013, they distributed 24,000 of their prosthetic feet, the Jaipur Foot. The Jaipur Foot was designed in 1968 to meet the specific needs of persons with lower limb amputations living in India: it lasts 3-5 years in the field, can be used barefoot, allows users to squat, and costs approximately $10 USD [23]. A study comparing the Jaipur Foot to two different prosthetic feet available in the western market found that the Jaipur Foot allowed a the most natural gait [3]. However, the current foot is handmade, which is relatively costly in terms of both time and money, and causes quality to vary from foot to foot. The goal of this work is to create an upgraded replacement to the Jaipur Foot that meets the needs of the nearly one million persons with lower limb amputations living in India to replace the original Jaipur Foot [18]. Before manufacturability can be addressed, first the mechanism must be designed, tested, and iterated via proof of concept prototypes.

Most prosthetic feet used in developing countries are solid ankle cushioned heel, or SACH, feet [22]. The SACH foot consists of a rigid structure, or keel, and a cushioned heel to provide shock absorption at heel strike. While inexpensive and robust, the SACH foot does not meet the needs of persons with lower limb amputations, particularly in India. The original motivation behind the design of the Jaipur Foot was that the solid ankle of SACH-type feet does not allow squatting, a critical requirement for most people in India [23].

In the past two decades, energy storage and return, or ESAR, feet have become

a popular alternative to SACH feet in the western world. The human ankle is a net power generator over the course of a step. At the end of stance phase, the muscles around the ankle provide a power input to aid in push-off. Powered prosthetic ankle/feet have successfully lowered the metabolic cost of walking compared to passive prosthetic feet by replicating this power input with onboard actuators, sensors, and batteries [4]. However, these robotic prostheses are expensive and would not withstand the sand, mud and water in which prosthetic feet are commonly used in developing countries. ESAR feet may be able to capture some of the benefit of providing energy input during push-off while still meeting the cost and durability constraints of developing countries.

Most, if not all, commercially available ESAR feet consist of one or more compliant beams of varying geometry. As the foot is loaded, the beams deflect, which both mimics dorsiflexion in physiological walking, and stores strain energy, which is released in late stance to assist in push-off. These types of feet do not permit squatting, which requires purely rotational motion at the ankle joint (Fig. B-1). Numerous studies have compared various ESAR feet and other types of feet using mechanical testing, biomechanical gait analysis, and subjective feedback. Comprehensive reviews of this literature come to the conclusions that there is insufficient evidence to prove that any particular ESAR foot is superior to any other foot, including the SACH foot [14], and that the connection between mechanical properties of prosthetic feet on human function are not yet understood [24].

While the complete relationship between mechanical design and prosthetic functionality is unclear, one property stands out in prosthetic foot literature as a promising design objective: the roll-over shape. The roll-over shape is defined as the path of the center of pressure from heel strike to toe off in the ankle knee reference frame [9]. Roll-over shapes vary little for people of similar leg lengths. The roll-over shape has been found to be invariant to walking speed [12], added weight [11], and shoe heel height [10]. Studies suggest that prosthetic feet with roll-over shapes similar to physiological roll-over shapes result in higher symmetry in loading between prosthetic and non-prosthetic sides [9] and higher metabolic efficiency while walking [1, 2].

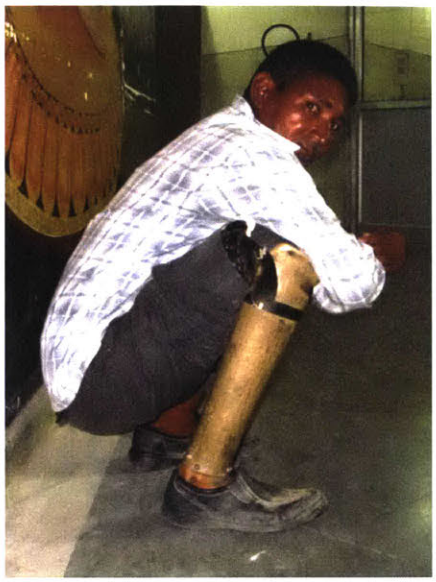

Figure B-1: Subject squats with the Jaipur Foot. Squatting requires pure rotational motion at the ankle joint that the compliant beam-type feet available on the western market do not permit.

This paper presents the design and preliminary testing of a proof of concept prototype which provides energy storage and return, replicates a physiological roll-over shape, and allows rotational motion at the ankle joint such that it can be adapted to allow squatting more easily than compliant beam-type prosthetic feet. The analytical optimization, mechanical implementation of the prototype, and preliminary qualitative feedback are reported.

B.1.1 Biomechanical Gait Data

Throughout this paper, the adjective "typical" is used to describe data measured from persons with no amputations or other physical impairments and under no special conditions. The set of gait data published in Winter's *Biomechanics and Motor Control of Human Movement* is used in this study as an example of typical gait kinematics and ground reaction forces. These data were collected over a single step for a subject of body mass 56.7 kg [25]. The ground reaction forces and the location of the center of pressure from the published data were considered typical loading the prosthetic foot might experience during walking. The center of pressure and joint

kinematic data were used to obtain a roll-over shape for Winter's subject, referred to as the physiological roll-over shape. This physiological roll-over shape served as a basis for comparison for the roll-over shapes found for the prototype, as described in the subsequent section.

Because Winter's subject had body mass 56.7 kg, the prototype was optimized for a subject of a similar body mass. As this prototype further progresses toward a commercial product, there is potential to optimize it for various body mass ranges, as is sometimes done with prosthetic feet in the U.S. However, in order to reduce cost, the collaborators at BMVSS would prefer feet available in different lengths, but all optimized for the body mass of the average Jaipur Foot user, which is approximately 60 kg.

While it is known that persons with lower limb amputations have slower self-selected walking speeds [8, 19, 20], increased nonprosthetic side leg loading [21], and decreased gait symmetry [6, 13, 15, 21, 26] compared to persons with no physical impairments, typical, unimpaired gait data were used in calculating the roll-over shape of the prototype in this study. Typical loading is often assumed in measuring the roll-over shape of prosthetic feet through mechanical testing [7, 9, 22]. Also, powered prostheses designed to reproduce the ankle angle versus moment curve as measured during typical walking have been shown to lower the metabolic cost of walking relative to passive prostheses [4]. For these reasons, the authors believe that using typical, unimpaired gait data in calculating the roll-over shapes of this prototype is the best option.

B.2 Prototype Concept and Optimization

The prototype consists of a rigid structure with pin joints at the ankle and metatarsal, with springs providing rotational stiffness at both joints. The dimensions of the prototype are based on the anatomy of the subject of Winter's published gait data, as shown in Fig. B-2. The rotational stiffnesses, k_{ank} and k_{met}, are defined as

$$k_{ank} = \frac{M_{ank}}{\theta_{ank}} \tag{B.1}$$

and

$$k_{met} = \frac{M_{met}}{\theta_{met}} \tag{B.2}$$

where M_{ank} and M_{met} are the moments about the ankle and metatarsal joints respectively, and θ_{ank} and θ_{met} are the angular rotations (i.e. dorsiflexions) at each of these joints.

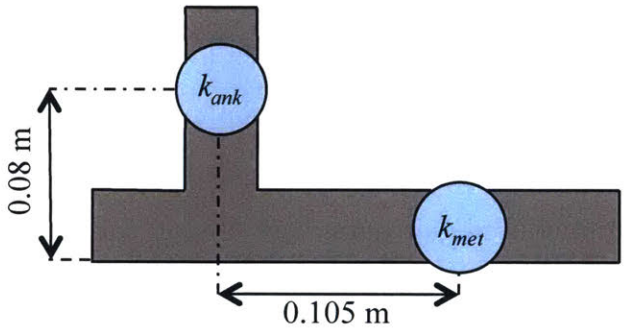

Figure B-2: Conceptual architecture of the prototype. Dimensions are based on the joint center of rotations for Winter's published gait data [25]

When unloaded, the prototype is in a neutral position. Both joints allow dorsiflexion when the foot is loaded, but the geometry does not permit plantarflexion in either joint. The springs that provide the rotational stiffnesses store energy when the foot is loaded during early stance. The stored energy is then released during late stance to aid in push-off.

For a given set of stiffness values, k_{ank} and k_{met}, the roll-over shape of the prototype can be found by assuming typical loading and calculating the resulting deformation of the prototype. These values were optimized for the best fit between the roll-over shape of the prototype and of a physiological foot using the following procedure.

B.2.1 Rotational Stiffness Optimization for Roll-Over Shape

At a given time during a step, the horizontal and vertical components of the ground reaction force (GRF_x and GRF_y) and the horizontal position of the center of pressure relative to the ankle (x_{cp}) can all be found for typical walking from published gait analysis data. This loading condition was applied to the prototype analytically (Fig. B-3). Using quasistatic moment and force balances, the resulting moment about the ankle joint is given by

$$M_{ank} = x_{cp} \cdot GRF_y + 0.08\,\mathrm{m} \cdot GRF_x \tag{B.3}$$

When the center of pressure is posterior to the metatarsal joint, the moment about the metatarsal joint is zero. When the center of pressure is anterior to the metatarsal joint, the moment about the metatarsal joint is given by

$$M_{met} = (x_{cp} - 0.105\,\mathrm{m}) \cdot GRF_y \tag{B.4}$$

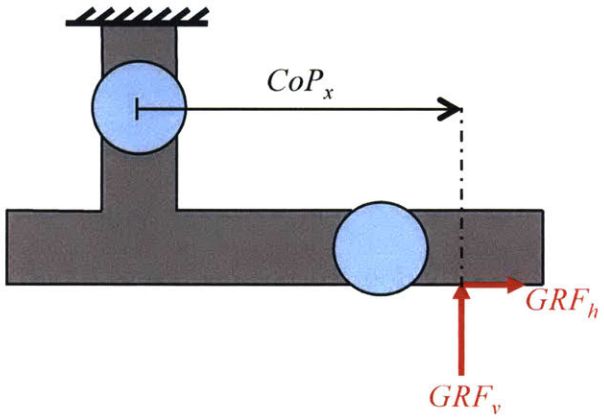

Figure B-3: Free body diagram of loading applied analytically to prototype corresponding to a particular instantaneous time during the step. The values of the vertical ground reaction force (GRF_y), the horizontal ground reaction force (GRF_x), and the horizontal position of the center of pressure (x_{cp}) were taken from Winter's published gait data [25].

Equations (B.3) and (B.4) are valid only under quasistatic loading. This assumption is often used in analyzing prosthetic feet as the loading frequency is one to two

orders of magnitude smaller than the fundamental frequency for typical prosthetic feet [16, 17, 22]. Physiological roll-over shapes measured quasistatically vary little from those measured during walking at typical speeds [9].

For specified joint stiffnesses k_{ank} and k_{met}, the deflection at both joints under the applied moments, θ_{ank} and θ_{met}, were found using Eq. (B.1) and Eq. (B.2). Together, θ_{ank} and θ_{met} define the deformed shape of the foot at time t, as shown in Fig. B-4. The position of the center of pressure on the deformed foot is a single point corresponding to time t on the roll-over shape for specified values of k_{ank} and k_{met}. This was then repeated for all times from foot flat through opposite heel strike to yield the complete roll-over shape. Because the prototype does not allow plantarflexion, no motion occurs in the prototype when the center of pressure is posterior to the ankle. Consequently the roll-over shape posterior to the ankle is a straight line.

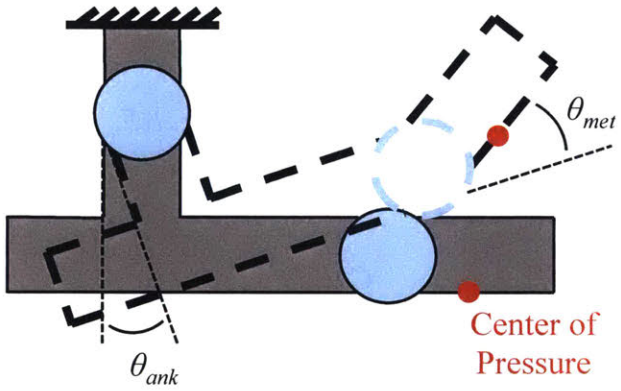

Figure B-4: Deformed shape of the foot corresponding to a particular instantaneous time during the step

Note that equations (B.3) and (B.4) provide the joint moments assuming the undeformed geometry. In the deformed state, the moment arm for the vertical ground reaction force increases while the moment arm for the horizontal ground reaction force decreases. The net resulting error on the moment calculated using undeformed geometry versus deformed geometry is very small for deformations of the size required to reproduce the physiological roll-over shape. For example, if the center of pressure in the deformed state of the model were to fall exactly on the physiological roll-over shape at the point of maximum deflection, the moment calculated using the deformed

geometry differs from that calculated using the undeformed geometry by less than 0.03%. Thus calculating the joint moments using the undeformed geometry is a reasonable simplification.

Once the roll-over shape for the foot model was obtained, an R^2 value was calculated to measure the goodness of fit between the roll-over shape of the model and points interpolated along the physiological roll-over shape from Winter's gait data. The joint stiffnesses, k_{ank} and k_{met}, were varied across a range of values to find the best roll-over shape fit between the analytical models and the physiological foot. These calculations were all performed using a MATLAB (The MathWorks, Inc.) script written by the researchers.

Preliminary Optimization Results

The best roll-over shape fit was found for $k_{ank} = 7.1$ N·m/deg with k_{met} approaching infinity. That is, the best fit for roll-over shape occured for a rigid foot with a single rotational degree-of-freedom at the ankle joint. The resulting roll-over shape, shown in Fig. B-5 had an R^2 value of 0.94 compared with the physiological roll-over shape.

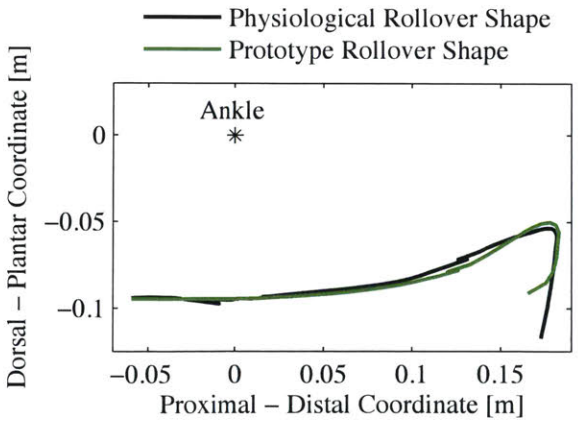

Figure B-5: The best roll-over shape fit ($R^2 = 0.94$) was found for a prototype with ankle stiffness 7.1 N·m/deg and metatarsal stiffness approaching infinity.

Adjustment for Metatarsal Motion

While the analysis showed that the best fit to the physiological roll-over shape came from a rigid foot with a single degree-of-freedom rotational ankle joint, such a foot would not allow the motion required for typical walking. When the heel lifts off the ground during late stance in typical walking, the foot pivots about the contact point between the ground and the metatarsal joint. When the heel lifts off the ground with a single degree-of-freedom foot as described above, the foot must pivot about the contact point between the toe and the ground (Fig. B-6a). The ankle must consequently lift much higher than if the prototype had an articulated metatarsal joint (Fig. B-6b).

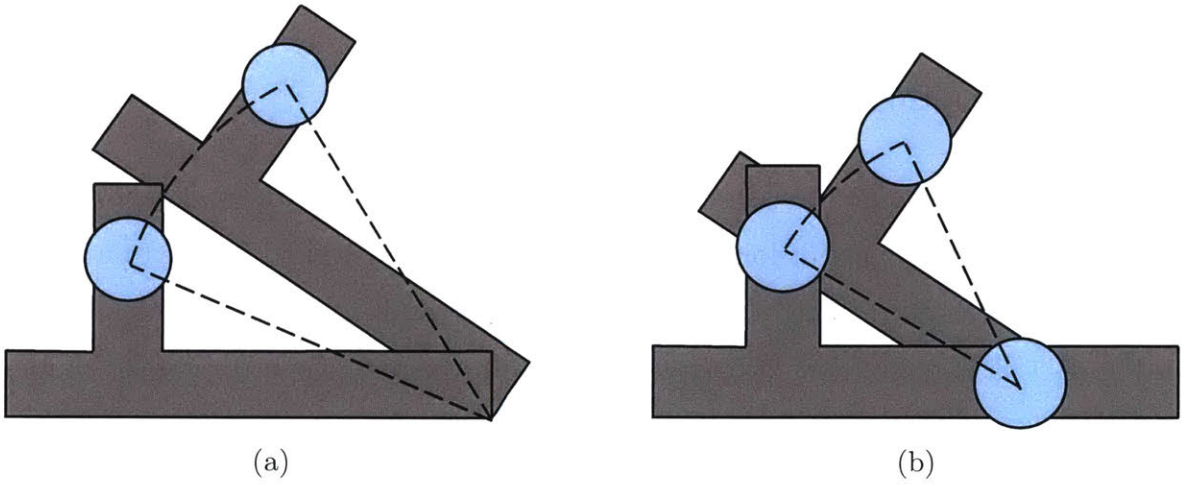

(a) (b)

Figure B-6: While the best roll-over geometry fit was found for a rigid prosthetic foot with a single degree-of-freedom ankle joint, such a foot does not permit natural motion (a). The ankle must lift much higher during late stance than for a similar foot with an articulated metatarsal joint (b).

The rigid foot with only an ankle joint forces an unnatural walking motion. Since the roll-over shape analysis assumed typical loading, the analytical results from the simplified model would most likely not be replicated in vivo.

To allow natural motion, which is more likely to result in ground reaction forces similar to those used in the analysis and consequently validate the analytically calculated roll-over shapes, a metatarsal joint was added. In the published gait data, the metatarsal joint flexes a maximum of 30° [25]. As k_{met} decreases from infinity, the

prototype permits more motion at the metatarsal, but the roll-over shape fit becomes worse. To balance between permitting natural motion and replicating the physiological roll-over shape, a metatarsal joint stiffness of $k_{met} = 2.0$ N·m/deg was selected such that the metatarsal joint in the analytical model reached a maximum angle of 15° under the applied loads.

With $k_{met} = 2.0$ N·m/deg, k_{ank} was varied to find the best fit between the roll-over shapes of the model and of the physiological foot using the method previously described. The resulting roll-over shape R^2 values for a range of ankle stiffnesses are shown in Fig. B-7. The best roll-over shape fit with the prescribed $k_{met} = 2.0$ N·m/deg occured at $k_{ank} = 9.3$ N·m/deg, with $R^2 = 0.81$ The roll-over shape calculated for these stiffnesses is shown in Fig. B-8.

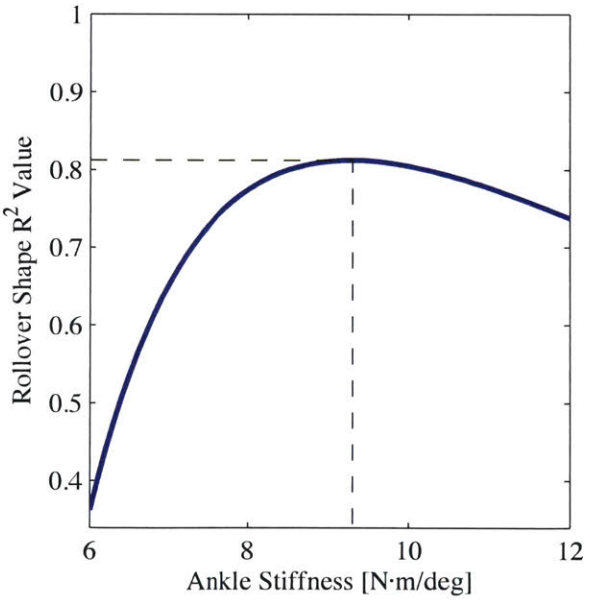

Figure B-7: R-squared values comparing roll-over geometries of physiological foot to prototype feet with metatarsal stiffness 2.0 N·m/deg for a range of ankle stiffness values. The maximum R^2 value is 0.81 for ankle stiffness 9.3 N·m/deg, shown by dotted lines.

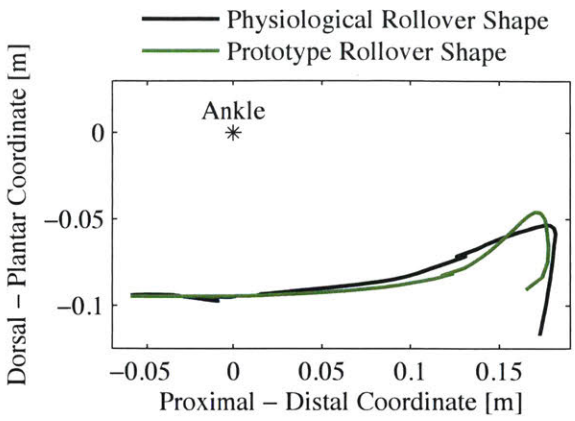

Figure B-8: Best roll-over shape fit ($R^2 = 0.81$) with adjustment for natural metatarsal motion occured for prototype with metatarsal stiffness 2 N·m/deg and ankle stiffness 9.3 N·m/deg.

B.3 Mechanical Design

Based on the analysis above, a mechanical prototype consisting of rotational ankle and metatarsal joints connected with rigid structural components was built. Because torsion springs of stiffnesses in the range of the optimal values require custom manufacturing and are prohibitively large, linear compression and extension springs were offset from the pin joints to provide the rotational joint stiffnesses. The geometry of the foot assures that the spring forces act at a constant radius from each joint, resulting in a constant rotational stiffness.

A solid model of the final design of the foot is shown in Fig. B-9. Off-the-shelf springs with appropriate linear stiffnesses in the smallest form factors were selected. The remaining foot geometry was determined by these springs. Two extension springs, each with a linear stiffness of 51.8 N/cm, provided the ankle stiffness. These were positioned such that the moment arm from the spring force about the ankle was 7 cm, resulting in a nominal torsional ankle stiffness of 4.4 N·m/deg per spring, or 8.8 N·m/deg total. This is slightly lower than the optimal ankle stiffness of 9.3 N·m/deg. Constraints due to the availability of off-the-shelf springs and the overall size and weight of the prototype precluded the exact replication of the optimal value.

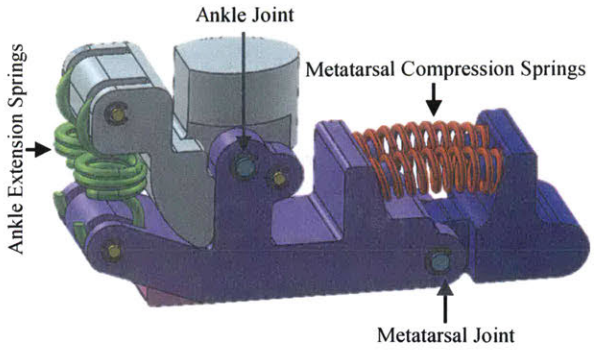

Figure B-9: Solid model of the foot prototype

Similarly, two compression springs of stiffness 210 N/cm provided the metatarsal joint stiffness. The springs were positioned such that the moment arm from the spring force about the metatarsal joint was 5 cm, resulting in a nominal metatarsal torsional stiffness of 0.92 N·m/deg per spring, or 1.8 N·m/deg for the joint as a whole. As with the ankle, the exact optimal metatarsal stiffness of 2.0 N·m/deg could not be achieved with off-the-shelf springs within the limits of reasonable prosthetic foot geometry.

The rigid components linking the joints were machined from delrin and sized such that deflection within these components was negligible compared to motion about the ankle and metatarsal joints, and the factor of safety for all foreseeable failure modes under expected loading was greater than two. A pin provided a mechanical stop to prevent any possible overloading at the ankle from occuring. A rubber heel wedge served to absorb some shock during heel strike. Rubber strips were epoxied along the bottom of the foot to increase traction.

The Jaipur Foot is typically attached to plastic sockets fitted at BMVSS by heating the bottom of the sockets, sliding them over the ankle block of the foot, and securing the foot in place with four radial wood screws. The ankle block of the prototype was dimensioned such that this same method could be used to attach the prototype to the sockets of the test subjects with no adaptations. The final prototype as tested is shown in Fig. B-10.

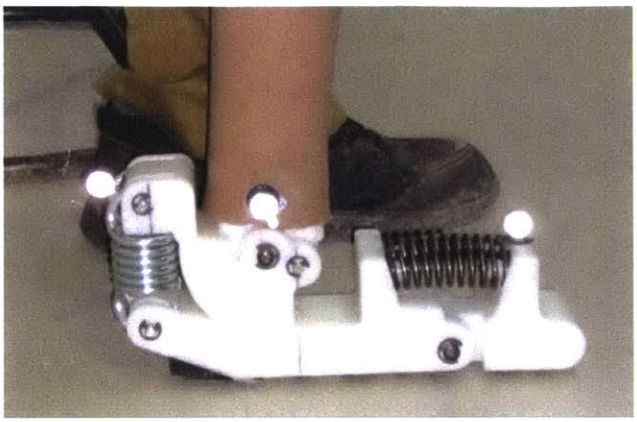

Figure B-10: Picture of the final prototype as tested

B.4 Preliminary Testing Results and Discussion

The prototype was tested in accordance with an MIT Committee on the Use of Humans as Experimental Subjects (COUHES)-approved protocol to get early feedback on the viability of the design concept. Six male subjects, all experienced Jaipur Foot users with unilateral transtibial amputations and no other physical impairments, were fitted with the prototype by prosthetists at BMVSS. The subjects had body masses ranging from 45 kg to 80 kg. The subjects wore the prototype for between 30 minutes and an hour while walking around the BMVSS facility. After this time, they were asked qualitative questions about the prototype with the help of a translator.

Despite the large mass of the finished prototype, at 2 kg as compared to the 0.8 kg Jaipur Foot, the prototype was positively received. Five of the subjects liked the energy storage and return aspect of the prototype, with several of them stating that they felt like they could run or jump with the prototype. Three of the subjects commented that although the foot was noticably heavier than the Jaipur Foot, it did not feel very heavy when they were wearing it. Two of the subjects said that the weight negatively affected their movement while wearing the foot, but they would be very happy with the foot if it weighed less.

Nearly all of the subjects commented that the springs felt too stiff, or that the prototype did not provide enough dorsiflexion, with subjects of lower body mass disliking

the stiffness more than the subjects of higher body mass. Based on observations, the subjects almost always favored their sound limb more with the prototype than they did with the Jaipur Foot, adopting a slight limp to keep the majority of their weight on their sound limb. This means that the loads on the prosthetic foot were less than the typical loading that was assumed in the analysis and stiffness optimization, which would result in less than the intended dorsiflexion. Two possible explanations for this are that 1) the subjects were not given adequate time to get comfortable wearing the prototype foot, and 2) the fact that the foot looks like an experimental prototype rather than a commercial product could have made the subjects wary of the durability of the prototype. One subject verbalized this latter sentiment. If subjects were given more time to acclimate to the prototype, they would likely become more comfortable loading the prototype with their full body weight. The loads would then approach typical loading, and the amount of dorsiflexion would increase. Further testing for longer durations is required to determine whether the spring stiffnesses are indeed too high.

The prototype as built did not allow squatting, which requires a lower ankle rotational stiffness than is optimal for walking. During squatting, the moment at the ankle produced by a 60 kg user can be up to a maximum value of approximately 53 N·m if the weight is distributed equally between his or her legs and the center of pressure is under the toes of the foot. With the prototype's nominal ankle stiffness of 8.8 N·m/deg, this load would result in 6° of dorsiflexion. Between 15° and 30° are required for squatting. However, because the ankle joint permits purely rotational motion, the prototype can be adapted to allow squatting more easily than compliant beam-type feet. For example, the ankle joint stiffness can be optimized for walking with a mechanism that disengages the spring to allow free motion during squatting, a mechanism can be designed that has a bi-modal stiffness, where after the ankle reaches a certain angle, the stiffness drops significantly, or the ankle stiffness can be reduced to find a compromise that may not be the optimal value for either squatting or walking, but permits both. Once the analysis is validated and the prototype is optimized for natural walking, the prototype will be adapted to permit squatting

while maintaining the best possible performance for walking.

While qualitative feedback from six subjects is insufficient to conclusively compare this prototype to the Jaipur Foot or any other prosthetic foot on the market, the positive responses suggest that this design concept merits further development and testing. As the design progresses, more rigorous testing, including longer duration, quantitative gait analysis, and activities beyond level-ground walking will be used to further refine the design of the foot.

B.5 Conclusion

The goal of this work is to design a prototype prosthetic foot that meets the needs of persons with lower limb amputations living in India. A prototype that consisted of a rigid structure with rotational joints at the ankle and metatarsal was designed. The rotational stiffnesses at each of these joints were optimized such that the prototype roll-over shape, calculated analytically using typical loading from published gait data, best fit the physiological roll-over shape from that same published gait data.

The best roll-over shape fit was found for a prototype with an ankle stiffness of 7.1 N·m/deg and metatarsal stiffness approaching infinity, with $R^2 = 0.94$. This corresponds to a rigid foot with a single degree-of-freedom rotational ankle joint. However, such a foot does not permit a natural walking motion, as the ankle must be lifted higher during late stance than for a similar foot with an articulated metatarsal joint. The ankle stiffness optimization process was repeated with the metatarsal stiffness set to 2.0 N·m/deg, such that the metatarsal joint reached a maximum angle of 15° under the maximum load. With this constraint, the best roll-over shape fit was found for ankle stiffness 9.3 N·m/deg, with $R^2 = 0.81$.

A prototype was built using pin joints to produce the ankle and metatarsal joint motion and off-the-shelf linear compression and extension springs to provide the joint stiffnesses. The final prototype as built had nominal ankle stiffness 8.8 N·m/deg and metatarsal stiffness 1.8 N·m/deg. The availability of off-the-shelf springs and geometric constraints limited how closely the prototype joint stiffnesses could match

the optimal values.

The prototype was tested in India on six male subjects with unilateral transtibial amputations. Despite weighing more than twice as much as the original Jaipur Foot, the prototype received mostly positive feedback. Several subjects commented that the springs were too stiff. Further testing for longer durations and with qualitative gait analysis is required to determine whether this comment is a consequence of the subjects having insufficient time using the prototype to become comfortable with it.

The generally positive response to the foot is sufficient to warrant further refinement of this prototype. Future work will focus on 1) obtaining quantitative biomechanical gait data with the current prototype to validate the analysis, 2) improving the optimization method, with a particular focus on developing a quantitative design objective that accounts for whether the prototype allows natural motion, and 3) designing a new mechanism that can achieve the same type of motion as this prototype, but fits in a smaller, lighter package and is mass-manufacturable. Once the mechanism is satisfactory, the final step will be to incorporate a foam cosmesis that makes the prosthetic foot look like a biological foot while simultaneously protecting the internal mechanism from the environment.

THIS PAGE INTENTIONALLY LEFT BLANK

Bibliography

[1] Peter G Adamczyk, Steven H Collins, and Arthur D Kuo. The advantages of a rolling foot in human walking. *The Journal of Experimental Biology*, 209(Pt 20):3953–63, October 2006.

[2] Peter G Adamczyk and Arthur D Kuo. Mechanical and energetic consequences of rolling foot shape in human walking. *The Journal of experimental biology*, 216(Pt 14):2722–31, July 2013.

[3] A. P. Arya, A. Lees, H.C. Nirula, and L. Klenerman. A biomechanical comparison of the SACH, Seattle and Jaipur feet using ground reaction forces. *Prosthetics and Orthotics International*, 19:37–45, 1995.

[4] Samuel K Au, Hugh Herr, Jeff Weber, and Ernesto C Martinez-Villalpando. Powered ankle-foot prosthesis for the improvement of amputee ambulation. *Conference proceedings : ... Annual International Conference of the IEEE Engineering in Medicine and Biology Society. IEEE Engineering in Medicine and Biology Society. Conference*, 2007:3020–6, January 2007.

[5] Bhagwan Mahaveer Viklang Sahayata Samiti. Jaipurfoot.org. `http://www.jaipurfoot.org`.

[6] James Breakey. Gait of unilateral below-knee amputees. *Orthotics and Prosthetics*, 30(3):17–24, 1976.

[7] Carolin Curtze, At L Hof, Helco G van Keeken, Jan P K Halbertsma, Klaas Postema, and Bert Otten. Comparative roll-over analysis of prosthetic feet. *Journal of Biomechanics*, 42:1746–1753, 2009.

[8] Joseph M Czerniecki and Andrew J Gitter. Gait analysis in the amputee: has it helped the amputee or contributed to the development of improved prosthetic components? *Gait & Posture*, 4(3):258–268, 1996.

[9] a. H. Hansen, D. S. Childress, and E. H. Knox. Prosthetic foot rollâĂŘover shapes with implications for alignment of transâĂŘtibial prostheses. *Prosthetics and Orthotics International*, 24(3):205–215, January 2000.

[10] Andrew H Hansen and Dudley S Childress. Effects of shoe heel height on biologic rollover characteristics during walking. *Journal of Rehabilitation Research & Development*, 41(4):547–554, 2004.

[11] Andrew H. Hansen and Dudley S. Childress. Effects of adding weight to the torso on roll-over characteristics of walking. *The Journal of Rehabilitation Research and Development*, 42(3):381, 2005.

[12] Andrew H. Hansen, Dudley S. Childress, and Erick H. Knox. Roll-over shapes of human locomotor systems: effects of walking speed. *Clinical Biomechanics*, 19:407–414, 2004.

[13] Y Hermodsson, C Ekdahl, BM Persson, and G Roxendal. Gait in male trans-tibial amputees: a comparative study with healthy subjects in relation to walking speed. *Prosthetics and orthotics international*, 18(2):68–77, 1994.

[14] C Hofstad, H Linde, J Limbeek, and Klaas Postema. Prescription of prosthetic ankle-foot mechanisms after lower limb amputation. *Cochrane Database Syst Rev*, 1, 2004.

[15] Glenn K Klute, Carol F Kallfelz, and Joseph M Czerniecki. Mechanical properties of prosthetic limbs: adapting to the patient. *Journal of rehabilitation research and development*, 38(3):299–307, 2000.

[16] J F Lehmann, R Price, S Boswell-Bessette, A Dralle, and K Questad. Comprehensive analysis of dynamic elastic response feet: Seattle Ankle/Lite Foot versus SACH foot. *Archives of physical medicine and rehabilitation*, 74(8):853–861, August 1993.

[17] J F Lehmann, R Price, S Boswell-Bessette, A Dralle, K Questad, and B J DeLateur. Comprehensive analysis of energy storing prosthetic feet: Flex Foot and Seattle Foot Versus Standard SACH foot. *Archives of physical medicine and rehabilitation*, 74(11):1225–1231, November 1993.

[18] National Sample Survey Organization. Disabled Persons in India. Technical Report 485, Ministry of Statistics and Programme Implementation, Government of India, New Delhi, India, 2003.

[19] Jacquelin Perry, Lara A Boyd, Sreesha S Rao, and Sara J Mulroy. Prosthetic weight acceptance mechanics in transtibial amputees wearing the single axis, seattle lite, and flex foot. *Rehabilitation Engineering, IEEE Transactions on*, 5(4):283–289, 1997.

[20] JL Robinson, GL Smidt, and JS Arora. Accelerographic, temporal, and distance gait factors in below-knee amputees. *Physical therapy*, 57(8):898âĂŤ904, August 1977.

[21] Todd D Royer and Carolyn A Wasilewski. Hip and knee frontal plane moments in persons with unilateral, trans-tibial amputation. *Gait & posture*, 23(3):303–306, 2006.

[22] M. Sam, A. H. Hansen, and D. S. Childress. Characterisation of prosthetic feet used in low-ĂŘincome countries. *Prosthetics and Orthotics International*, 28(2):132–140, January 2004.

[23] P. K. Sethi, M. P. Udawat, S. C. Kasliwal, and R. Chandra. Vulcanized rubber foot for lower limb amputees. *Prosthetics and Orthotics International*, 2:125–136, 1978.

[24] Harmen van der Linde, Cheriel J Hofstad, Alexander CH Geurts, Klaas Postema, Jan HB Geertzen, and Jacques van Limbeek. A systematic literature review of the effect of different prosthetic components on human functioning with a lower-limb prosthesis. *Journal of rehabilitation research and development*, 41(4):555–570, 2004.

[25] David A. Winter. *Biomechanics and Motor Control of Human Movement.* John Wiley & Sons, Inc, fourth edition edition, 2009.

[26] David A Winter and Susan E Sienko. Biomechanics of below-knee amputee gait. *Journal of biomechanics*, 21(5):361–367, 1988.

THIS PAGE INTENTIONALLY LEFT BLANK

Appendix C

Design and Preliminary Testing of a Prototype for Evaluating Lower Leg Trajectory Error as an Optimization Metric for Prosthetic Feet

As discussed at the beginning of Appendix B, both Appendices B and C describe foot prototypes which were designed prior to defining LLTE as in Eqn. (2.1). *Because the work lead to valuable contributions fundamental to the body of this dissertation, they are included here in the appendix for the reader's reference. In Appendix C, a foot with rotational ankle joint and cantilever beam forefoot is optimized using an early definition of LLTE, which used the x and y position of the ankle joint rather than the knee joint to define the lower leg trajectory, and normalized each term in the equation by the range of the physiological variables rather than the mean. To avoid confusion, the alternative definition of LLTE used here in Appendix C is referred to as LLTE† to denote that it is not identical to the LLTE value defined in Eqn.* (2.1). *The prototype designed here in Appendix C was instrumental in developing the prototype used in the clinical validation study in Chapter 3.*

C.1 Introduction

Bhagwan Mahaveer Viklang Sahayata Samiti (BMVSS), a distributor of prosthetic devices based in India, produces a low cost prosthetic foot called the Jaipur Foot that exceeds the performance of most prosthetic feet commonly used in the developing world, and even some used in developed countries [3, 4]. However, the Jaipur Foot is handmade, which results in variable quality consistency between feet and higher cost of production than for mass-manufactured feet. The motivation of this work is to design a new prosthetic foot that maintains the performance and cost of the original Jaipur Foot but is mass-manufacturable. In order to do so, it is necessary to understand what it is about the mechanical design of the Jaipur Foot that yields its high biomechanical performance.

Despite many studies comparing different prosthetic feet, multiple literature reviews have reached the same conclusion: how the mechanical behaviour of a passive prosthetic foot affects the biomechanical functionality is not well understood [5, 6, 11, 14]. Despite being ten years old, these literature reviews still represent the state of the science, possibly because the focus of prosthetic design in academia has shifted from passive prosthetics to robotic prosthetics.

One metric, roll-over geometry, has stood out as a prominent design objective for passive prosthetic feet over the past decade. Roll-over geometry is defined as the path of the center of pressure along the bottom of the foot from heel strike to opposite heel strike in the moving reference frame defined by the ankle and the knee (the ankle-knee reference frame) [7]. Physiological roll-over geometries are similar for persons with a given leg length. These shapes have been shown to remain unchanged as walking speed, shoe heel height, and added torso weight are varied [8–10]. Some studies have suggested that prosthetic feet with roll-over geometries that mimic physiological roll-over geometries result in more symmetric gait [7] and higher metabolic efficiency while walking [1, 2].

However, our recent theoretical work has shown that roll-over geometry is not sufficient in characterizing prosthetic feet, as it does not fully describe lower leg kine-

matics. As a result, it is possible for two different prosthetic feet to have identical roll-over geometries, but very different lower leg kinematics during walking. In previous work, we proposed a novel prosthetic foot design objective, the Lower Leg Trajectory Error (LLTE†) [13]. This metric incorporates both the roll-over geometry of the foot and the orientation of the lower leg segment in the laboratory reference frame throughout a step, thus fully describing the lower leg kinematics.

Thus far, all work regarding LLTE† has been purely theoretical. The next step in moving towards using LLTE† in the design of commercial prosthetic limbs is to clinically test the validity of LLTE† as a design objective by building a prototype optimized for LLTE†. An initial prototype was built in 2015 [12], has been built. This prototype consisted of rotational ankle and metatarsal joints with constant rotational stiffnesses optimized for LLTE†. The joint stiffnesses were provided by linear extension springs offset from the ankle joint and compression springs offset from the metatarsal joint. While theoretically a very simple design, the resulting prototype had a mass of 2.06 kg, twice that of the Jaipur Foot, which is already heavier than most existing prosthetic feet.

The goal of this work is to produce a prototype prosthetic foot that can be used in a large scale gait analysis study to test the viability of LLTE† as a design objective for prosthetic feet. To do so, a new conceptual prosthetic foot architecture consisting of a rotational ankle joint and a cantilever beam forefoot is presented. The design variables of this new architecture, namely the rotational stiffness of the ankle and the bending stiffness of the forefoot, are optimized for LLTE†. The considerations in building a physical prototype based on this theoretical design are discussed, and the resulting prototype is presented. Qualitative feedback from preliminary testing is reported and discussed.

C.2 Prototype Concept and Optimization

The conceptual architecture is similar to the previous prototype with rotational joints at the ankle and the metatarsal, but rather than a metatarsal joint, the new proto-

type has a compliant cantilever beam forefoot, which eliminates the need for the linear compression springs at the metatarsal joint and consequently reduces the weight (Fig. C-1). The design variables available to be optimized for LLTE† are the ankle joint rotational stiffness, k_{ank}, the length of the rigid structure extending from the ankle-knee axis, d_{rigid}, and the forefoot beam bending stiffness, EI. In this work, the height of the ankle rotational joint, h, is a parameter fixed at 0.08 m. This height was chosen to best approximate the center of rotation of a physiological ankle joint based on published gait data [15].

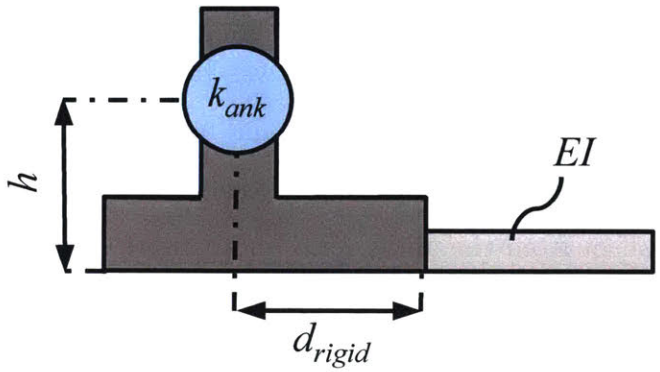

Figure C-1: Conceptual prosthetic foot architecture

C.2.1 Calculation of LLTE†

In order to calculate the LLTE†, a set of representative physiological gait data is required. The vertical and horizontal ground reaction forces, GRF_y and GRF_x respectively, and the instantaneous center of pressure along the ground, d_{cp}, are used as inputs to calculate the deformed shape of the foot/ankle complex througout stance phase. The center of pressure and all other spatial coordinates in the laboratory reference frame used in this work are measured from a reference point directly below the ankle when the bottom of the foot is in contact with the ground.

The LLTE† measures how well the resulting modeled lower leg kinematics match target physiological kinematic data. For this study, a set of published physiological gait data for a subject of body mass 56.7 kg was used. [15] The LLTE† is a root-

mean-square error comparing the trajectory of the lower leg segment of the modeled prototype to a target physiological trajectory, defined as

$$LLTE^{\dagger} \equiv \left[\frac{1}{N} \sum_{n=1}^{N} \left\{ \left(\frac{x_n - \hat{x}_n}{\hat{x}_{max} - \hat{x}_{min}} \right)^2 + \left(\frac{y_n - \hat{y}_n}{\hat{y}_{max} - \hat{y}_{min}} \right)^2 + \left(\frac{\theta_n - \hat{\theta}_n}{\hat{\theta}_{max} - \hat{\theta}_{min}} \right)^2 \right\} \right]^{\frac{1}{2}}, \tag{C.1}$$

where x and y are the horizontal and vertical positions of the ankle joint respectively and θ is the orientation of the ankle-knee axis with respect to the vertical. The variables $\hat{x}$, $\hat{y}$ and $\hat{\theta}$ refer to the physiological data. The error in each coordinate is normalized by the range of that coordinate in the physiological data over the portion of the step included in the analysis. The subscript n refers to each time interval, with total number of time intervals N. [13]

For a given set of design variables (that is, ankle stiffness and forefoot bending stiffness), the coordinates x, y and θ were calculated for each time interval using the published ground reaction forces and instantaneous centers of pressure as inputs. When the center of pressure is along the rigid structure, that is, $d_{cp} < d_{rigid}$ (Fig. C-2), the moment at the ankle joint is given by

$$M_{ank} = GRF_y \cdot d_{cp} + GRF_x \cdot h. \tag{C.2}$$

For a given ankle joint stiffness, k_{ank}, the resulting rotation at the ankle joint is

$$\theta_{ank} = \frac{M_{ank}}{k_{ank}}. \tag{C.3}$$

Because the bottom of the rigid structure of the foot must be in contact with the ground in order to not contradict the center of pressure location used as an input, the angle of the lower leg segment, θ, is equal to the ankle angle, θ_{ank}. The horizontal and vertical positions of the ankle are $x = 0$ and $y = h$ respectively for all times when

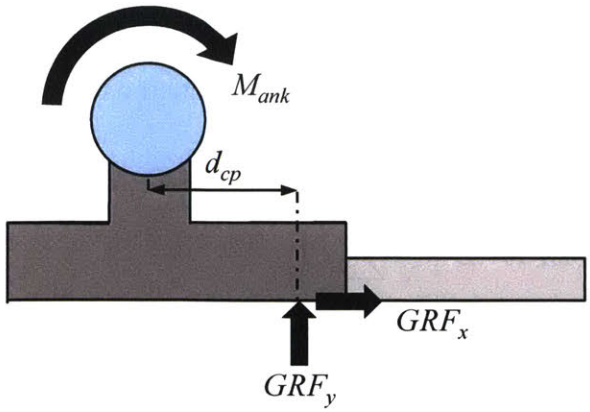

Figure C-2: Free body diagram showing calculation of ankle moment from ground reaction forces when center of pressure acts on rigid structure

the center of pressure is along the rigid portion of the foot.

When the center of pressure progresses beyond the rigid structure to the compliant beam, this calculation becomes more complex. In this case, the angle of deflection of the beam forefoot, or θ_{foot}, must also be calculated (Fig. C-3. To find θ_{foot}, the magnitude of the force acting transverse to the beam, F_{trans} , must be found. However, since the inputs to the model are the ground reaction forces in the laboratory reference frame, the magnitude of the transverse force cannot be found without knowing θ_{foot}. Hence the deformed shape of the beam under the ground reaction forces was calculated iteratively.

First, the load transverse to the beam was calculated assuming the beam did not deform at all, or $\theta_{foot} = 0$. Then

$$F_{trans} = GRF_y. \tag{C.4}$$

This transverse load was then used to calculate a second iterative value for θ_{foot}, by

$$\theta_{foot} = \frac{F_{trans}\left(d_{cp} - d_{rigid}\right)^2}{2EI}. \tag{C.5}$$

The new transverse load was then found with

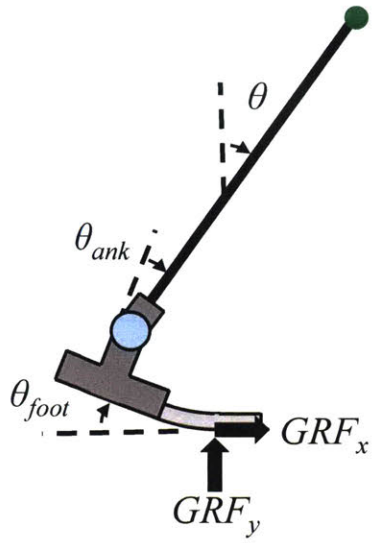

Figure C-3: Free body diagram for ground reaction forces acting on compliant beam forefoot

$$F_{trans} = GRF_y \cdot \cos\theta_{foot} + GRF_x \cdot \sin\theta_{foot}. \tag{C.6}$$

These calculations of θ_{foot} and F_{trans} were repeated using Eqns. (C.5) and (C.6) until subsequent values of θ_{foot} differed by less than 0.5 degrees.

It should be noted that eqn. (C.5) is only valid for small deflections for which $\theta_{foot} \approx \tan\theta_{foot}$. For particularly small beam bending stiffness values, this equation no longer accurately represents the physical beam when the ground reaction force acts at the end of the toe. However, in the range of bending stiffnesses, beam lengths, and transverse forces considered here, deflections are small and eqn. (C.5) is appropriate.

The moment about the ankle was then calculated with

$$M_{ank} = F_{trans} \cdot d_{cp} + F_{axial} \cdot h \tag{C.7}$$

where

$$F_{axial} = -GRF_y \cdot \sin\theta_{foot} + GRF_x \cdot \cos\theta_{foot}. \tag{C.8}$$

Equation (C.3) was used to find the ankle angle, θ_{ank}. The lower leg angle, θ, was

given by

$$\theta = \theta_{ank} + \theta_{foot}. \tag{C.9}$$

The horizontal and vertical coordinates of the ankle were calculated as

$$x = d_{cp} \cdot \left(1 - \cos\theta_{foot}\right) \tag{C.10}$$

and

$$y = d_{cp} \cdot \sin\theta_{foot} + h \cdot \cos\theta_{foot}. \tag{C.11}$$

Through eqns. (C.2) through (C.11), x, y, and θ were calculated for each time interval from foot flat to late stance. Using these coordinates, the LLTE† was calculated for the given set of design variable values.

C.2.2 Design Optimization

The design variables, k_{ank}, d_{rigid}, and EI, were optimized heuristically through grid sampling. Each design variable was systematically varied over a range of reasonable values. The LLTE† value was calculated for each possible combination of design variables. The set of design variables giving the lowest LLTE† value was taken to be the optimal design.

The minimum LLTE† value, 0.159, was calculated for k_{ank} = 6.1 N·m/deg, d_{rigid} = 0.08 m, and EI = 5.4 N·m^2. To depict the dependence of the LLTE† value on each of the design variables, Fig. C-4 shows the LLTE† values found for a slice of the design space for which d_{rigid} is held constant at the optimal value of 0.08 m.

The resulting lower leg trajectory is graphically compared to the target physiological lower leg trajectory in Fig. C-5. Each of the individual kinematic coordinates, x, y, and θ are plotted against the corresponding physiological coordinates in Fig. C-6.

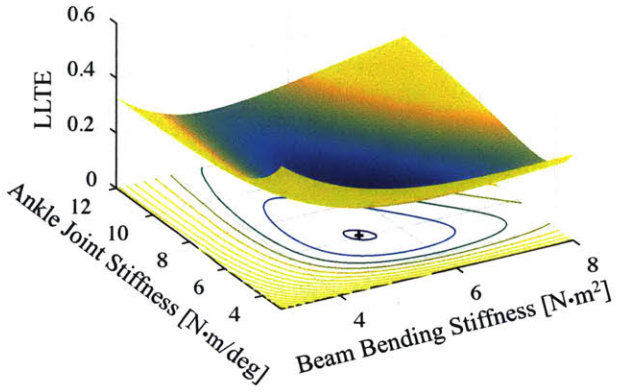

Figure C-4: LLTE† values for slice of design space for which d_{rigid} is held constant at $d_{rigid} = 0.08$ m

C.3 Mechanical Design

In order to clinically validate the theoretical work suggesting the LLTE† value as a design objective for prosthetic feet, it is necessary to design, build and test a prosthetic foot based on the optimal design found in the previous section. The goal is to design a proof-of-concept prototype as quickly as possible without spending time on details that are irrelevant in early-stage design, such as appearance, long-term durability, and mass-manufacturability. A solid model of the prototype designed for this purpose is shown in Fig. C-7. The rigid structural components were machined from delrin. The ankle joint rotates about a steel pin. Extension springs offset behind the ankle joint at a constant radius provide the ankle joint rotational stiffness. The compliant beam forefoot was made from nylon and was fixed to the rigid delrin structure with machine screws fastened directly into tapped holes in the delrin. At BMVSS, the standard method of attaching the prosthetic socket to the Jaipur Foot is to heat the plastic exoskeletal socket until it becomes pliable, then slide the socket over the ankle, which consists of a wooden block inside of the rubber exterior of the foot. Four radial wood screws secure the socket to the ankle. To allow technicians at BMVSS to use this same method of attachment in prototype testing, a wooden ankle block of similar size and shape to the Jaipur Foot ankle was mounted to the top of the delrin structure.

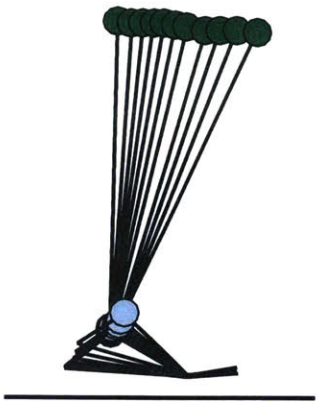

(a) Physiological Trajectory

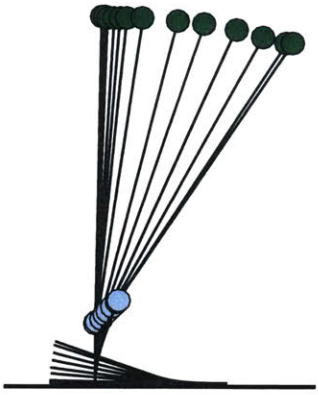

(b) Optimal Model Trajectory

Figure C-5: Graphical comparison of optimal foot design lower leg trajectory with physiological lower leg trajectory

After a wooden ankle block is used, it can be replaced so no cracking occurs around mounting holes from previous tests. The prototype as built has a mass of 1.24 g, which is approximately 40% less than the mass of the previous prototype. This reduction in mass is due to the new architecture, which no longer requires metal compression springs at the metatarsal joint nor a rigid toe structure.

C.3.1 Spring Selection and Considerations

For speed and ease of design, off-the-shelf springs were used to provide the ankle joint rotational stiffness. Based on the above analysis, the ankle joint required a rotational stiffness of 6.1 N·m/deg and at least 10 degrees of rotation before yield. Additionally, the entire mechanism needed to be as compact and light weight as possible such that it did not interfere with gait nor add significant mass not accounted for in the analysis. These requirements immediately preclude the use of torsion springs, as those springs of sufficient stiffness were far too bulky to fit within the approximate size and shape of a prosthetic foot. Linear compression springs were also considered, as they can be small and very stiff, but constraining the ends of the compression springs in such a way as to achieve constant rotational stiffness about the ankle joint throughout large rotations proved problematic. Thus linear extension springs were chosen.

The extension springs were mounted using pins passing through hooks at either

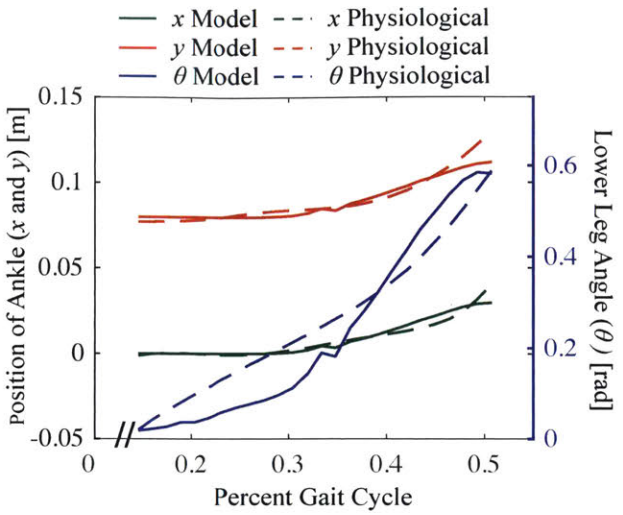

Figure C-6: Individual spatial coordinates of optimal foot design compared to physiological target values throughout stance phase

end, so as the ankle joint dorsiflexed, the hooks were free to rotate on the pin joints to avoid being over-constrained. The side of the springs rested along a constant radius cam. In this way, the extension force of the spring had a constant moment arm about the ankle joint even over large rotations, resulting in a constant rotational stiffness. The final spring configuration was selected to maximize range of motion with minimal total mass. Ultimately, three springs, each of linear stiffness 27846 N/m, were used in parallel, offset from the ankle joint by a radius of 0.065 m (Fig. C-8). In this configuration, the ankle could dorsiflex 14.8 degrees before reaching the manufacturer's recommended maximum extension. The total mass and width of all three springs were 144.8 g and 0.076 m respectively.

The springs were mounted at an angle rather than vertically, as was done in the earlier prototype, to reduce the total volume and, consequently, mass, of the structure required to support them.

C.3.2 Cantilever Beam Forefoot Design

To replicate approximate physiological foot geometry, the beam forefoot was chosen to be 0.064 m wide and 0.07 m long. Materials considered were Delrin, ABS, nylon,

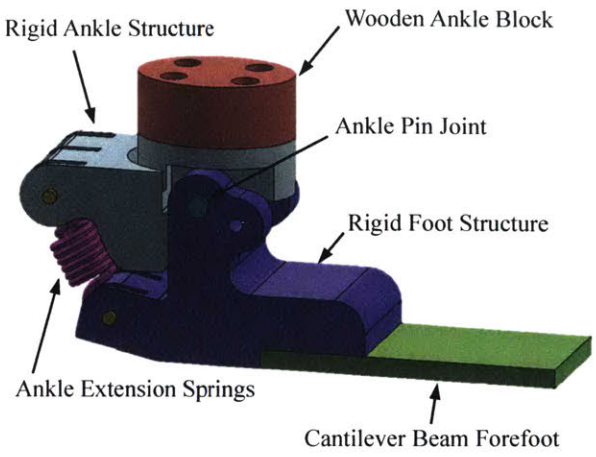

Figure C-7: Solid model of prototype designed based on LLTE† optimization

polycarbonate, aluminum and steel. To produce the specified beam bending stiffness $EI = 5.4$ N·m^2, the required thickness of the beam for each material was calculated. For those thicknesses, the maximum force that could be applied to the tip of the beam before yielding occured was calculated. The nylon beam could withstand the highest load before yielding. This result was not surprising, as nylon's high ratio of yield strength to Young's modulus makes it a particularly good flexural material. Thus the beam forefoot was constructed of nylon with thickness 0.008 m.

C.3.3 Preliminary Testing

The prototype was brought to India for an initial round of testing with our partners at BMVSS. The purpose of this testing was not yet to validate the theoretical LLTE† work, but rather to determine the suitability of this prototype for use in a larger-scale gait analysis study.

The prototype was fitted on three male subjects with unilateral transtibial amputations who primarily use the Jaipur Foot. Apart from the amputations, the subjects had no further pathologies. The subjects were asked to walk on flat ground using the prototype until they felt comfortable with it, at which point they were asked to walk up and down stairs and ramps. After 30 minutes to an hour using the prototype, the subjects were asked qualitatively what they liked and disliked about the prototype.

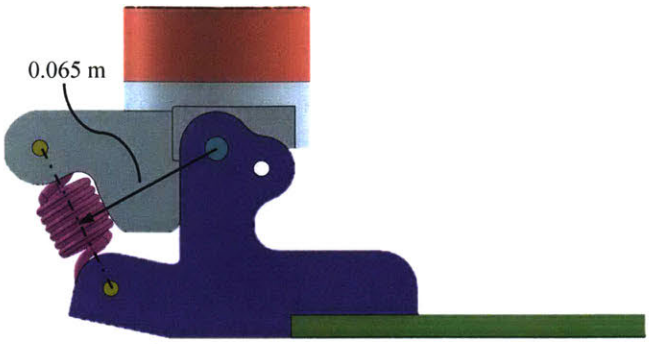

(a) Side View

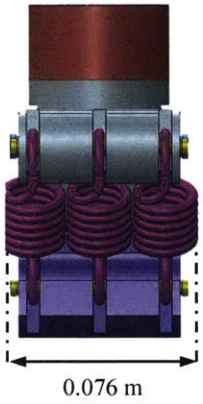

(b) Rear View

Figure C-8: Linear extension spring configuration used to produce constant ankle joint rotational stiffness of $k_{ank} = 6.1$ N· m/deg

The subjects liked the energy storage and return aspects of the foot relative to the Jaipur Foot, which is purely dissipative. Dislikes primarily focused on the appearance and the weight of the prototype. Despite a 40% reduction in mass relative to the previous prototype, the prototype was still too heavy, particularly in the region posterior to the ankle, to claim that the weight of the prototype did not negatively affect the user's gait, potentially negating the benefits of the optimized LLTE†. Because need for improvement was identified from the first three subjects, no further testing was necessary with this particular prototype. Further reduction in weight is required before proceeding with a larger scale gait analysis study to determine the validity of the theoretical work.

C.4 Discussion and Conclusion

As mentioned throughout this work, LLTE† remains a theoretical objective function for prosthetic foot design. Clinical validation is required to show whether it provides a means of connecting the mechanical behaviour of a prosthetic foot to biomechanical functionality when used in practice.

Calculation of LLTE† requires a set of ground reaction force and instantaneous center of pressure data as inputs and corresponding kinematic gait data as target outputs. In this study, a set of published physiological gait data for typical, unimpaired walking was used. The ground reaction forces used as inputs here are therefore different than what would be expected on the prototype, as it is well known that persons with amputations exhibit different gait characteristics than persons without amputations. However, it is also known that the gait of a person using a lower limb prosthesis is affected by the prosthesis itself. Thus rather than start with input data collected from persons with amputations that necessarily caries with it attributes of a different prosthetic foot, the physiological, unimpaired data is used as a starting point. The design of the prototype can then be refined through an iterative process. Once a foot is made based on unimpaired data, it can be tested on a group of individuals with amputations and the ground reaction forces measured. These measured ground reaction forces can then be used as inputs with the same set of target gait kinematic outputs to re-design the foot. This process can be repeated until the input ground reaction forces used to design the foot and the ground reaction forces observed in testing the foot converge.

Similarly, because the published gait data came from a single subject with body mass 56.7 kg, the optimal foot design is only optimal for persons of similar body mass. In order to validate LLTE† as a design objective for prosthetic feet, the prototype will have to be customized to fit the body mass and foot length of the subjects in the study. This customization can be done using the same method as described here with a different set of gait data as inputs.

This paper presented the theoretical optimization, physical design, and prelim-

inary testing of a prototype prosthetic foot to evaluate the effectiveness of Lower Leg Trajectory Error as a design objective. A conceptual foot architecture intended to reduce the weight of a previous prototype was presented. The calculation of the LLTE† was described, and the design variables, that is, the ankle stiffness, the length of the rigid structure, and the bending stiffness of the compliant beam forefoot, were optimized. The design with the minimum LLTE† value, 0.159, was found for $k_{ank} =$ 6.1 N·m/deg, $d_{rigid} = 0.08$ m, and $EI = 5.4$ N·m^2. A physical prototype that meets these specifications was presented. Preliminary testing revealed that, despite a significant weight reduction from the previous prototype, the new prototype is still too heavy to be used in a large-scale study to validate LLTE† as a design objective. Future work will focus on eliminating the use of heavy linear extension springs by designing integrated geometries that exhibit similar behavior through flexural elements.

THIS PAGE INTENTIONALLY LEFT BLANK

Bibliography

[1] Peter G Adamczyk, Steven H Collins, and Arthur D Kuo. The advantages of a rolling foot in human walking. *The Journal of Experimental Biology*, 209(Pt 20):3953–63, October 2006.

[2] Peter G Adamczyk and Arthur D Kuo. Mechanical and energetic consequences of rolling foot shape in human walking. *The Journal of experimental biology*, 216(Pt 14):2722–31, July 2013.

[3] A. P. Arya, A. Lees, H.C. Nirula, and L. Klenerman. A biomechanical comparison of the SACH, Seattle and Jaipur feet using ground reaction forces. *Prosthetics and Orthotics International*, 19:37–45, 1995.

[4] Bhagwan Mahaveer Viklang Sahayata Samiti. Jaipurfoot.org. http://www.jaipurfoot.org.

[5] Brian J. Hafner. Clinical Prescription and Use of Prosthtic Foot and Ankle Mechanisms: A Review of the Literature. *Journal of Prosthetics and Orthotics*, 17(4):S5–S11, 2005.

[6] Brian J. Hafner, Joan E. Sanders, Joseph Czerniecki, and John Fergason. Energy storage and return prostheses: does patient perception correlate with biomechanical analaysis? *Clinical Biomechanics*, 17(5):325–344, 2002.

[7] A. H. Hansen, D. S. Childress, and E. H. Knox. Prosthetic foot roll-over shapes with implications for alignment of trans-tibial prostheses. *Prosthetics and Orthotics International*, 24(3):205–215, January 2000.

[8] Andrew H Hansen and Dudley S Childress. Effects of shoe heel height on biologic rollover characteristics during walking. *Journal of Rehabilitation Research & Development*, 41(4):547–554, 2004.

[9] Andrew H. Hansen and Dudley S. Childress. Effects of adding weight to the torso on roll-over characteristics of walking. *The Journal of Rehabilitation Research and Development*, 42(3):381, 2005.

[10] Andrew H. Hansen, Dudley S. Childress, and Erick H. Knox. Roll-over shapes of human locomotor systems: effects of walking speed. *Clinical Biomechanics*, 19:407–414, 2004.

[11] C Hofstad, H Linde, J Limbeek, and Klaas Postema. Prescription of prosthetic ankle-foot mechanisms after lower limb amputation. *Cochrane Database Syst Rev*, 1, 2004.

[12] Kathryn M. Olesnavage and Amos G. Winter V. Design and qualitative testing of a prosthetic foot with rotational ankle and metatarsal joints to mimic physiological roll-over shape. In *ASME 2015 International Design Engineering Technical Conferences and Computers and Information in Engineering Conference*, August 2015.

[13] Kathryn M. Olesnavage and Amos G. Winter V. Lower leg trajectory error: A novel optimization parameter for designing passive prosthetic feet. In *IEEE International Conference on Rehabilitation Robotics (ICORR)*, pages 271–276, August 2015.

[14] Harmen van der Linde, Cheriel J Hofstad, Alexander CH Geurts, Klaas Postema, Jan HB Geertzen, and Jacques van Limbeek. A systematic literature review of the effect of different prosthetic components on human functioning with a lower-limb prosthesis. *Journal of rehabilitation research and development*, 41(4):555–570, 2004.

[15] David A. Winter. *Biomechanics and Motor Control of Human Movement.* John Wiley & Sons, Inc, fourth edition edition, 2009.